UDK 621.3:(53+54+621+66)(05)(497.1)=00 ISSN 0352-9045

INFORMACIJE MIDEM 1 ◦1996

Strokovno društvo za mikroelektroniko elektronske sestavne dele in materiale

Časopis za mikroelektroniko, elektronske sestavne dele in materiale
Časopis za mikroelektroniku, elektronske sastavne dijelove i materijale
Journal of Microelectronics, Electronic Components and Materials

INFORMACIJE MIDEM, LETNIK 26, ŠT. 1(77), LJUBLJANA, marec 1996

INŠTITUT ZA ELEKTRONIKO IN VAKUUMSKO TEHNIKO

INFORMACIJE MIDEM 1 ° 1996

INFORMACIJE MIDEM	LETNIK 26, ŠT. 1(77), LJUBLJANA,	MAREC 1996
INFORMACIJE MIDEM	GODINA 26, BR. 1(77), LJUBLJANA,	MART 1996
INFORMACIJE MIDEM	VOLUME 26, NO. 1(77), LJUBLJANA,	MARCH 1996

Izdaja trimesečno (marec, junij, september, december) Strokovno društvo za mikroelektroniko, elektronske sestavne dele in materiale.
Izdaja tromjesečno (mart, jun, septembar, decembar) Stručno društvo za mikroelektroniku, elektronske sastavne dijelove i materiale.
Published quarterly (march, june, september, december) by Society for Microelectronics, Electronic Components and Materials - MIDEM.

Naslov uredništva
Adresa redakcije
Headquarters
Uredništvo Informacije MIDEM
Elektrotehniška zveza Slovenije
Dunajska 10, 1000 Ljubljana, Slovenija
(0)61 - 316 886

Letna naročnina znaša 12.000,00 SIT, cena posamezne številke je 3000,00 SIT. Člani in sponzorji MIDEM prejemajo Informacije MIDEM brezplačno.
Godišnja pretplata iznosi 12.000,00 SIT, cijena pojedinog broja je 3000,00 SIT. Članovi i sponzori MIDEM primaju Informacije MIDEM besplatno.
Annual subscription rate is DEM 200, separate issue is DEM 50. MIDEM members and Society sponsors receive Informacije MIDEM for free.

Znanstveni svet za tehnične vede l je podal pozitivno mnenje o časopisu kot znanstveno strokovni reviji za mikroelektroniko, elektronske sestavne dele in materiale. Izdajo revije sofinanci rajo Ministrstvo za znanost in tehnologijo in sponzorji društva.
Scientific Council for Technical Sciences of Slovene Ministry of Science and Technology has recognized Informacije MIDEM as scientific Journal for microelectronics, electronic components and materials.
Publishing of the Journal is financed by Slovene Ministry of Science and Technology and by Society sponsors.

Znanstveno strokovne prispevke objavljene v Informacijah MIDEM zajemamo v:
* domačo bazo podatkov ISKRA SAIDC-el, kakor tudi
* v tujo bazo podatkov INSPEC

Prispevke iz revije zajema ISI® v naslednje svoje produkte: Sci Search®, Research Alert® in Materials Science Citation Index™

Scientific and professional papers published in Informacije MIDEM are assessed into:
* domestic data base ISKRA SAIDC-el and
* foreign data base INSPEC

The Journal is indexed by ISI® for Sci Search®, Research Alert® and Material Science Citation Index™

Po mnenju Ministrstva za informiranje št.23/300-92 šteje glasilo Informacije MIDEM med proizvode informativnega značaja, za katere se plačuje davek od prometa proizvodov po stopnji 5 %.

Grafična priprava in tisk	BIRO M, Ljubljana
Grafička priprema i štampa	
Printed by	
Naklada	1000 izvodov
Tiraž	1000 primjeraka
Circulation	1000 issues

UDK621.3:(53+54+621+66), ISSN0352-9045 Informacije MIDEM 26(1996)1, Ljubljana

Nadaljna internacionalizacija društva MIDEM in njegovih aktivnosti

Že v uvodniku prejšnje številke revije "Informacije MIDEM", 25(1995)4, sem napravil kratek presek dela društva MIDEM v letu 1995.

V tej številki bi rad dopolnil napisano še z nekaterimi novimi podatki, ki nam vzbujajo optimizem in potrjujejo našo idejo internacionalizacije društva, začrtano leta 1992.

Društvo MIDEM je mednarodno društvo ne samo zaradi tega, ker so člani organov društva tudi tuji državljani, temveč ker je mednarodno tudi njegovo članstvo. Več kot 32% naših članov prihaja iz drugih držav. Resda jih je največ iz sosednjih držav, vendar konferenca MIEL-SD in revija "Informacije MIDEM" pritegneta tudi strokovnjake iz oddaljenejših dežel, ki se ob tej priložnosti včlanijo v društvo.

Tudi začetni pesimizem glede prihodnosti konference MIEL-SD počasi plahni ob podatku, da število udeležencev in referatov iz leta v leto narašča in, da se tudi delež tujih referatov povečuje (leta 1993 24%, leta 1996 pa pričakujemo 40% delež tujih referatov).

Več dela smo vložili v popularizacijo konference in društva. Med drugim smo ob pomoči Dejana Križaja s Fakultete za elektrotehniko, Ljubljana, Laboratorij za elektronske elemente, koncem meseca aprila '96 postavili dve MIDEM strani na INTERNETU in tako predstavili svojo dejavnost globalnemu občinstvu.

Further Internationalisation of MIDEM Society and its Activities

In the last issue of the Journal "Informacije MIDEM", 25(1995)4, I presented the work of MIDEM Society in the year 1995. Now, I would like to add some fresh data which excite optimism and confirm our idea of Society internationalisation launched in 1992.

MIDEM Society is an international society not only because its bodies members are also foreigners but because about 32% of its members come from foreign countries. It is true that most of them are from neighbouring countries but participants of MIEL-SD Conferences, as well as contributors to our Journal "Informacije MIDEM" originate also from far away countries and become MIDEM members.

The pessimism present a few years ago regarding the future of MIEL-SD Conference is slowly melting away since the number of participants and papers from foreign countries is slowly increasing (in 1993 it was 24% and in 1996 we expect 40% foreign papers).

More work has been inputted in the presentation of the Society and its activities. Among other actions and with the help of Mr. Dejan Križaj, Faculty for Electrical Engineering, Ljubljana, Laboratory for Electron Devices, MIDEM Society has, since end of April '96, two pages on INTERNET which present our activities to global community.

Editor in Chief
Iztok Šorli

INTERNET ADDRESSES

1. Presentation of MIDEM Society and Journal "Informacije MIDEM":

http://pollux.fer.uni-lj.si/MIEL/MIDEM.htm

2. Presentation of the Conference MIEL-SD:

http://pollux.fer.uni-lj.si/MIEL/miel96.htm

3. Email can be sent to:

Iztok.Sorli@guest.arnes.si

DRIVER CIRCUIT FOR AN AUTOMOTIVE SMART POWER SYSTEM CHIP

Heinz Zitta, Siemens EZM, Villach, Austria

Key words: microelectronics, automotive electronics, smar power technology, semiconductor chips, system chips, reliable operation, electronic circuits, driver circuits, warning lamps

Abstract: A driver circuit is presented as part of a system chip fabricated in a smart power technology. In automotive applications like anti brake control systems or airbag control units any malfunctions, detected by internal diagnostic circuits, are reported to a warning lamp. The requirements for this lamp driver and the circuit realization are presented in detail. Special efforts are done to keep the driver circuit operational also under worst case supply voltage conditions.

Krmilna elektronika za inteligentno močnostno sistemsko integrirano vezje avtoelektronike

Ključne besede: mikroelektronika, elektronika avtomobilska, tehnologija močnostna inteligentna, čip-i polprevodniški, čip-i sistemski, delovanje zanesljivo, vezja elektronska, vezja gonilna, lučke opozorilne

Povzetek: V prispevku predstavim krmilno elektroniko kot del sistemskega integriranega vezja izdelanega v inteligentni močnostni tehnologiji. Pri uporabi v avtoelektroniki, npr. za nadzor delovanja ABS ali za nadzor delovanja sistema zračne blazine, mora biti vsaka napaka, ki jo odkrije notranje diagnostično vezje, signalizirana z opozorilno lučko. V tem prispevku natančno opišem zahteve, kakor tudi izvedbo elektronike za krmilnik lučke kot dela večjega sistemskega integriranega vezja. Posebno pozornost sem posvetil obnašanju krmilnega vezja pod najhujšimi pogoji delovanja napajalne napetosti.

1. INTRODUCTION

Today's suppliers of automotive electronic units are going to prefer a system-on-a-chip approach to achieve the ever increasing reliability requirements. Smart Power technologies make it possible to combine parts of the logic, the power drivers and the analog diagnostic functions on one chip. Special efforts are necessary to obtain the right diagnostic functions also under external failure conditions. A bad condition - from the point of view of the circuit designer - is the condition of broken supply wires. How to consider this restriction in designing a driver circuit for a warning lamp is described in detail.

2. SMART POWER TECHNOLOGY

The system chip is realized in a power BiCMOS Technology. The cross section of some devices is shown in fig. 1.

Based on a p^-substrat and a n^-doped epitaxial layer it offers a combination of a high voltage DMOS device and low voltage bipolar (npn and pnp) and CMOS devices. The current path in the power device is vertical but the drain connection is brought to the surface via a buried layer and sinkers, also called an updrain configuration. The low voltage p-channel and n-channel transistors allow the integration of medium complexity CMOS logic

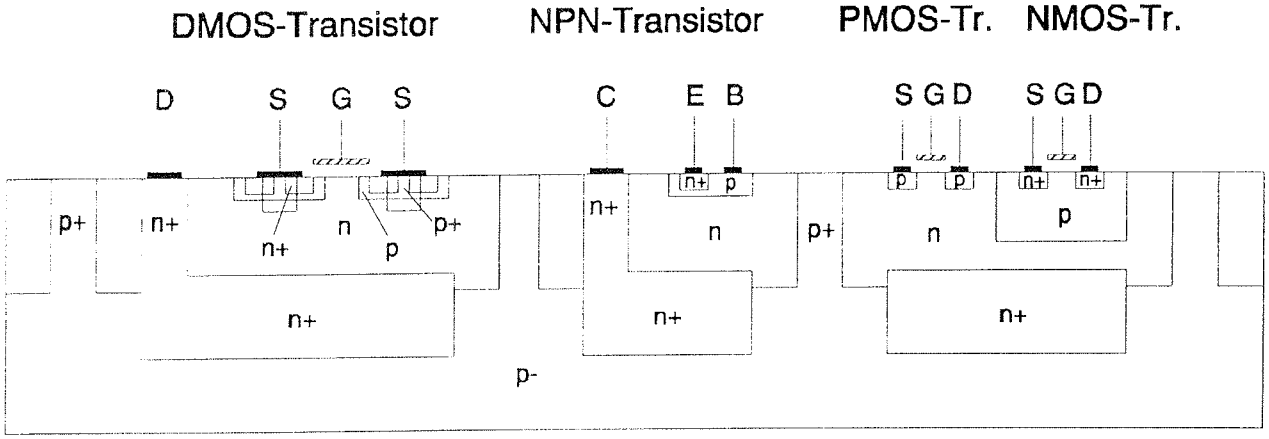

Fig. 1: Cross section of the Smart Power Technology

parts into the power switches. The bipolar transistors are provided for the analog circuits due to their better characteristics like noise, offset and drift behavior.

The use of this technology enables the system integration of the airbag power chip. The DMOS is used as power device to switch currents in the range of few amps, the low voltage CMOS components enable the realization of logic parts. The bipolar components are important for designing the analog functions where maximum precision is required.

3. BLOCK DIAGRAM OF AN AUTOMOTIVE SYSTEM CHIP

The typical configuration of an automotive system chip is shown in fig. 2. The smart power technology allows it to integrate all functions except the microprocessor on one chip. It includes power outputs to drive the application specific loads and analog diagnostic circuits which are responsible for testing the internal circuits and the external components. All diagnostic information are summed up and lead to an output which drives a lamp. This warning lamp is suited in the dashboard of the car. It is switched on for a short time when you start the car and then - if everything is okay - it will be switched off. In case of any error of the system this warning lamp will be switched on again. Because the driver circuit of this warning lamp has to do its job very reliably, it was chosen to be presented in more detail.

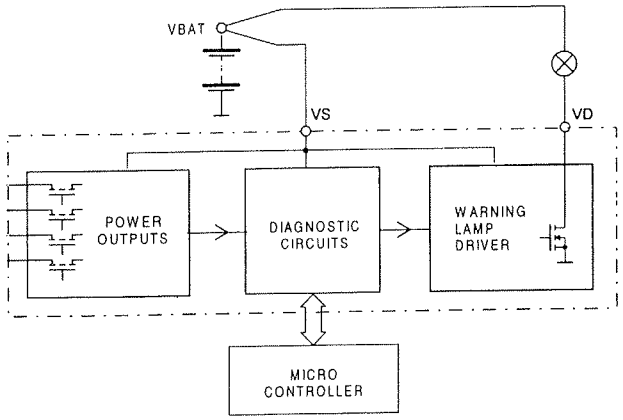

Fig. 2: Block diagram of a smart power system chip

loosing the battery connection (VS in fig.2) to the module should result in an activated lamp. The driver circuit itself has also to be short circuit protected. Therefore current limiting and overtemperature protection are required.

5. CIRCUIT REALIZATION

A block diagram of the lamp driver circuit is shown in Fig. 3. Under normal supply voltage conditions the load RL is fed by the voltage VBAT, whereas the logic and the gate driver circuits are supplied with VS. Now we assume the following error condition: The voltage VS is missing but the voltage VBAT exists. In that case the lamp should be switched on. This would report the error condition of the missing VS because all errors are reported by switching on the lamp - normally by the logic circuit. But the logic circuit is now missing its supply voltage! To achieve the desired function, the gate voltage has to be captured from VBAT via the load. It would be no problem when the DMOS is switched off. But the switched on DMOS does not provide a sufficient voltage VD at its drain to supply the circuits. The target is to develop a gate driver circuit which can manage this condition. This is done by two essential steps: First a charge pump is used to multiply the low voltage VD to an adequate level. And second a regulation circuit controls the saturation voltage VD in that way, that it will not drop below a minimum value which is necessary as operation voltage for the charge pump. Additionally the design of the overload protection circuit has to accept a low voltage VD as supply voltage.

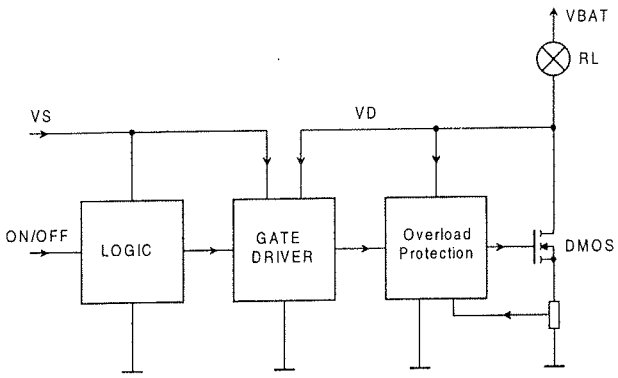

Fig. 3: Block diagram of the lamp driver circuit

4. REQUIREMENTS FOR THE LAMP DRIVER CIRCUIT

The purpose of the warning lamp is to report any malfunction of the electronic system to the car driver. The summary of the status from all internal diagnostic circuits is used as logic input for the lamp driver. In case of an error the lamp has to be switched on. Under normal supply voltage conditions this task is not a challenge to the circuit designer but it is the no-supply-voltage condition which results in a new circuit design:

A more detailed circuit diagram is shown in fig. 4. The gate voltage of the DMOS is supplied either via VS or via VCP, the output voltage of the charge pump. The input voltage of the charge pump is supplied from VD, the drain voltage of the power DMOS. A bias circuit, formed of the devices Q1 to Q4 generates a stabilized current IB which is mirrored to supply the charge pump and the regulation circuit. To keep the bias circuit operating, the voltage VD should not drop below the value of two VBE-voltages. The regulation part controls it in that way: The DMOS gate is charged by the current I8

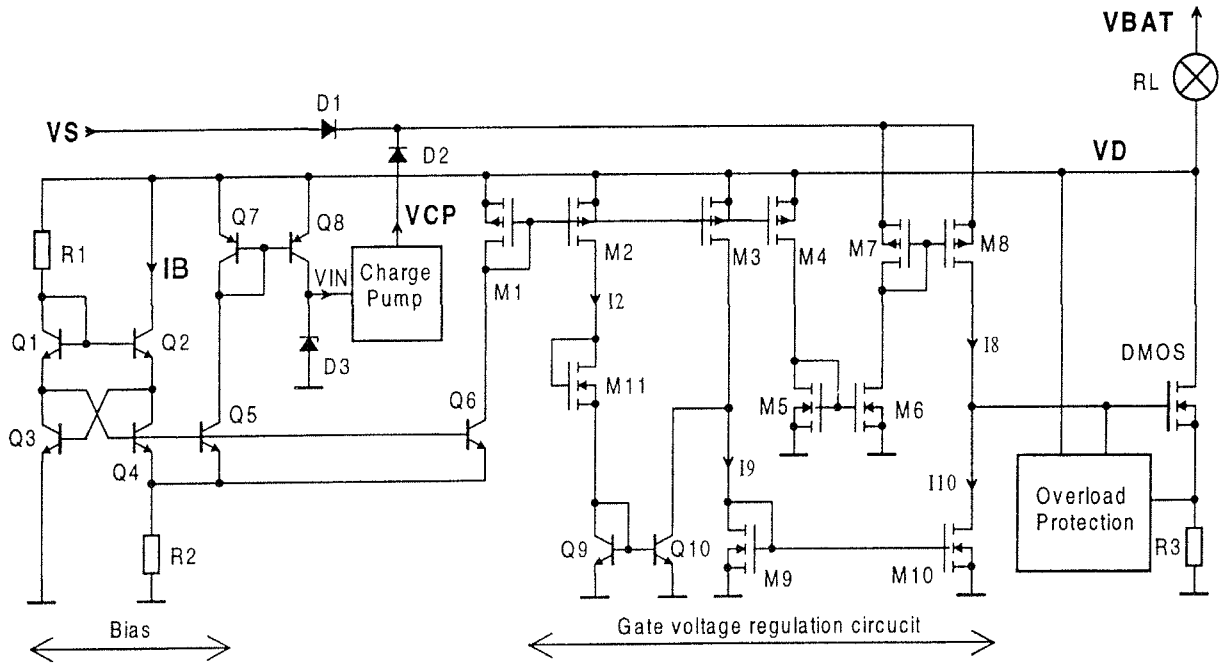

Fig. 4: Circuit diagram of the lamp driver circuit

and discharged by the current I10. The discharging current is cut off by means of Q10, so the DMOS will remain switched on. If the drain voltage VD decreases a point will be reached where the current I2 becomes zero. Then the current I9 and -correspondingly - I10 will increase. This leads to a state, where I8 is equal to I10 as a stable operating point. The relative huge gate capacitance of the DMOS acts as a sufficient loop compensation of this regulation circuit. The final voltage of VD is defined by the voltage drops of M11 and Q9. In practice it is about 2 V which is high enough to feed the bias circuit and the charge pump. On the other hand it is low enough to be accepted as a drain to source voltage drop of the DMOS.

The charge pump circuit is shown in fig. 5. To achieve the required gate voltage a multiple stage design was chosen. The five inverter stages are directly connected in a feedback loop as a ring oscillator, therefore no additional oscillator is necessary.

The overload protection circuit is shown in fig. 6. It provides current limiting and temperature protection of the DMOS. The bias generator is the same as shown in fig.4. The current I2 is defined by $I2 = \Delta VBE / R2$.
ΔVBE is given by comparing Q1 + Q4 with Q2 + Q3:
$\Delta VBE = Vt \cdot [\ln(AreaQ1) + \ln(AreaQ4) - \ln(AreaQ2) - \ln(AreaQ3)]$
$Vt = kt/q$ depends on the absolute temperature, so the bias circuit actually is a so called PTAT source, that means the current is **p**roportional **t**o the **a**bsolute **t**emperature. Adding the current mirror Q7, Q11 and the devices R4, Q14 completes the circuit to a temperature shutoff block. The voltage drop across R4 is increasing with temperature. Compared with the decreasing VBE-characteristic of the bipolar device Q14 it results in a well defined temperature switch off point.

Current limiting is the second task of the shown circuit. The current threshold is defined by the Δ VBE of Q15 and Q16, compared with the voltage drop on R3. The shunt resistor R3 is part of the metal interconnect layer,

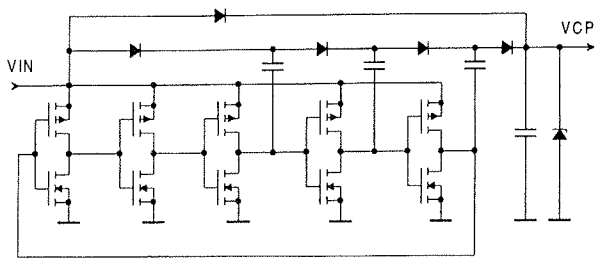

Fig. 5: Charge pump circuit

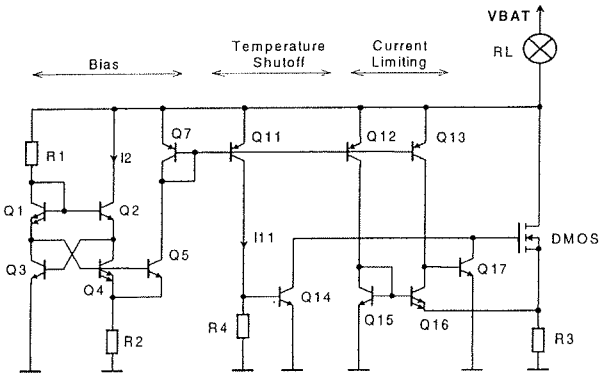

Fig. 6: Overload protection circuit

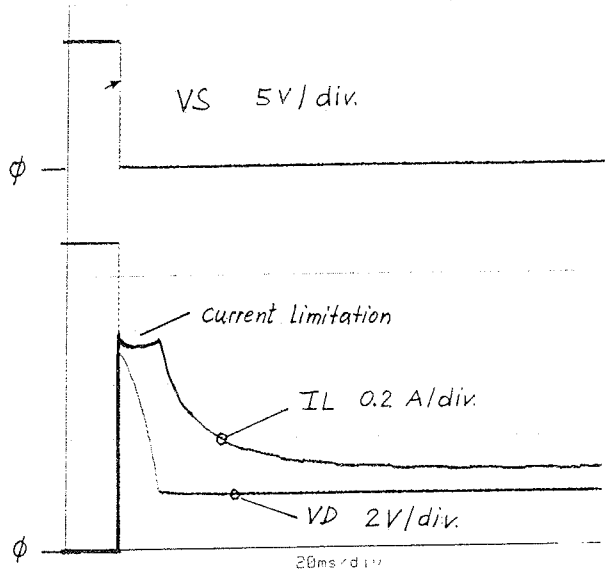

Fig. 7: Measuring result: VS drop from 12V to 0V results in switching on the lamp

this leads to a first order temperature compensation of the current threshold.

6. MEASUREMENT RESULTS

Measurement results are shown in fig. 7. When the supply voltage VS is interrupted, the lamp is turned on. For the first 20 ms the high inrush current of the lamp is limited, then the output voltage VD is stabilized to a value of 2 V.

CONCLUSION

A new lamp driver circuit was realized in a smart power system chip for automotive application. The requirements of reliable operation could be fulfilled also in a situation, where the chip itself has no supply voltage and only the lamp is supplied. This was done by using a charge pump to feed the gate of the power DMOS by its own drain voltage in the on-state. Additionally overload protection circuits were designed which work under very low supply voltage conditions.

Heinz Zitta
Siemens-Entwicklungszentrum für Mikroelektronik
Siemensstrasse 2, A-9500 Villach, Austria
Phone: + 43 42 42 305 360
Fax: +43 42 42 305 223

Prispelo (Arrived): 7.11.1995 Sprejeto (Accepted): 12.12.1995

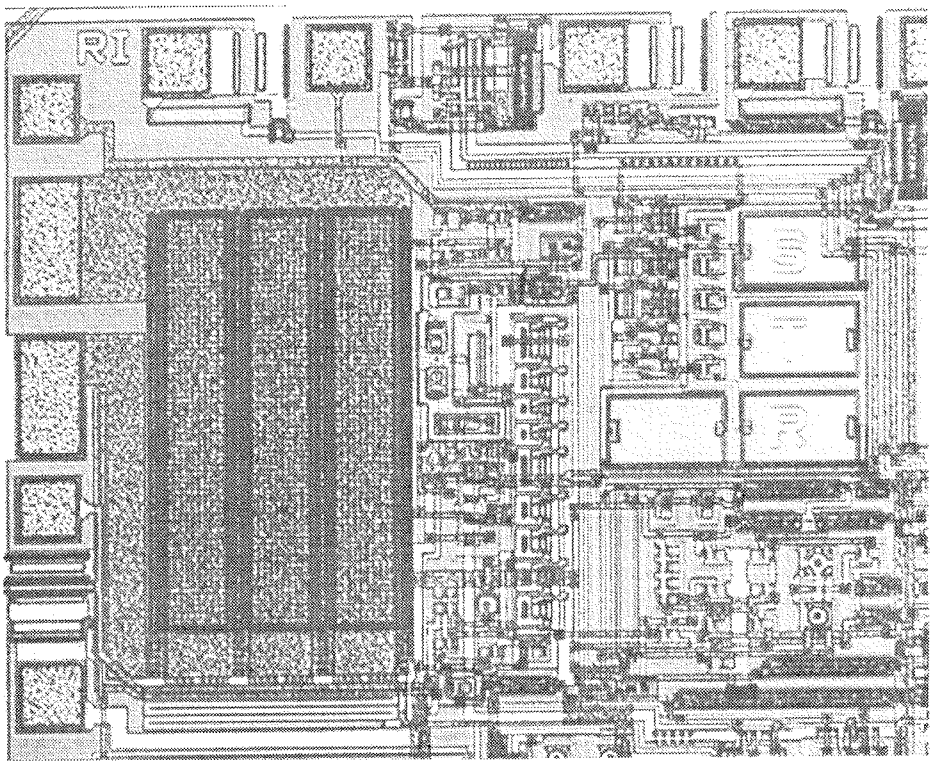

Fig. 8: Part of the chip showing driver circuit, area approx. 1.0x1.1 mm^2

THE CONTROL OF AN AC TO HF-AC RESONANT LINK CONVERTER

Miro Milanovič, Robert Kovačič, Franc Mihalič, Rudi Babič
University of Maribor,
Faculty of Electrical Engineering and Computer Science, Slovenia

Keywords: voltage converters, HF-AC AC resonant link converters, UPS, uninterruptible power supplies, DC-DC converters, circuit modelling, circuit analysis, injected-absorbed current method, pulse width modulation, analog control, resonant circuits, high efficiencies

Abstract: The term HF-AC Resonant Link Converters usually denotes a circuit, whose main part is a resonant tank circuit. The main goal of designers of such circuits is to reach a constant magnitude of output voltage with constant frequency and independence of load conditions. In this paper the possibility of maintenance of the constant HF-AC voltage on parallel resonant circuits (frequency 25 kHz) from main supply will be considered. In the family of AC to HF-AC Resonant Link Converters the proposed circuit is quite new. This goal has been reached by providing the energy from main supply by using the accordance between the serial and parallel resonance of the chosen circuit.

Analogna regulacija visokofrekvenčnega AC-AC resonančnega pretvornika

Ključne besede: pretvorniki napetostni, HF-AC AC pretvorniki s povezavo resonančno, UPS napajalniki brez prekinitve, DC-DC pretvorniki, modeliranje vezij, analize vezij, metoda toka injiciranega-absorbiranega, modulacija impulzno širinska, regulacija analogna, krogi resonančni, izkoristki visoki

Povzetek: Pretvorniki, ki so danes v široki uporabi, delujejo v stikalnem režimu ter preklapljajo pri polni napetosti in toku, se pogosto uporabljajo v mnogih aplikacijah, npr. UPS (viri za neprekinjeno napajanje), v reguliranih elektromotornih pogonih, DC/DC pretvornikih itd. S ciljem eliminacije nizkofrekvenčnih spektralnih komponent v izhodni napetosti sistema UPS, nizkofrekvenčnih motenj v momentu električnih motorjev in valovitosti v izhodni napetosti DC/DC pretvornikov, potrebujemo visokofrekvenčni napajalni vir. Takšen visokofrekvenčni vir pa ima zaradi dokaj velikih frekvenc delovanja znatne stikalne izgube. Problem rešujemo z vpeljavo resonančnih oz. kvaziresonančnih principov delovanja v obstoječe pretvornike. Pri uporabi omenjenega principa so mnogi avtorji predlagali vezja, ki v svojih strukturah vsebujejo dvosmerna stikala. V predlaganem vezju resonančnega pretvornika bodo za pretvorbo, ki jo izvede mrežni pretvornik, uporabljena enosmerna stikala. Pretvornik bo deloval s frekvenco 25kHz. Energija bo iz mrežnega dela posredovana paralelnemu resonančnemu krogu skozi serijski resonančni pojav. Ob prehodu napetosti in/ali toka skozi ničelno vrednost izklapljamo polprevodniška stikala v teh pretvornikih. Pretvorniki, zgrajeni na tem principu, se imenujejo "resonančni pretvorniki". S resonančnimi pretvorniki lahko dosežemo izkoristek pretvorbe nad 90%.

1. Introduction

Hard switch converter/inverter technique with high frequency switch is often utilised for many applications (UPS, Variable Speed Electrical Motor Drives, DC-DC Power Supply ect.). In order to get low harmonics contains in output voltage for UPS, low harmonics disturbance in torque of Electrical Motor Drive and low ripple in DC-DC supply units the high frequency is required. Unfortunately, on the contrary the converter/inverter switching losses increase enormously with higher frequency. Introducing resonant or quasi-resonant operation principle into known converters/inverters topology represents the possible solution of this problem. A lot of authors reported about the utility of such principles in wide at the area of Power Electronics /1, 2, 3/. The essential idea of our approach to resonant tank circuit problem is to provide the energy through serial resonant circuits into parallel resonant tank circuits in order to maintain the constant value of output voltage.

2. The novel circuit

The basic scheme for "evolution" of the proposed new circuits is shown in Fig. 1. The circuit represents a "half wave" configuration which is known from the rectifier's theory. Operation of such circuit is not too complicated. In steady state conditions (the parallel resonant circuits L_1 and C_1 operate and provide the energy to the resistor R_L), transistor Q_1 should be switched on when the parallel resonant link voltage crosses zero as shown in Fig. 5 (not necessary condition). Then L_{11} with elements of parallel resonant tank circuits L_1 and C_1 establishes serial resonant tank circuits. The current through transistor Q_1 is supposed to be in sinusoidal wave shape. When the current crosses zero, diode D_1 switches off and transistor Q_1 can be switched off as well. The soft switch operation is evident.

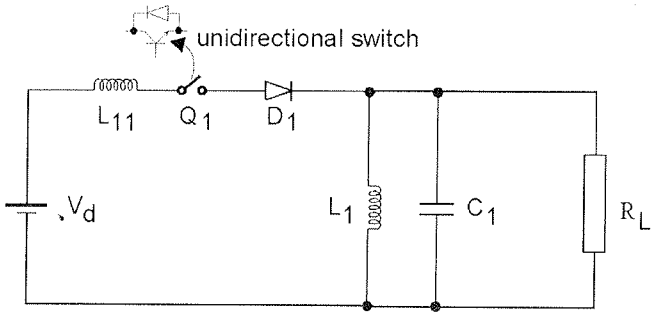

Fig. 1: The "half-wave" resonant link converter configuration

Operation of the circuit from Fig. 2 is quite similar. In that case the conducting losses are lower. In that circuit the energy is providing from DC supply to parallel resonant link in both half periods of AC high frequency voltage.

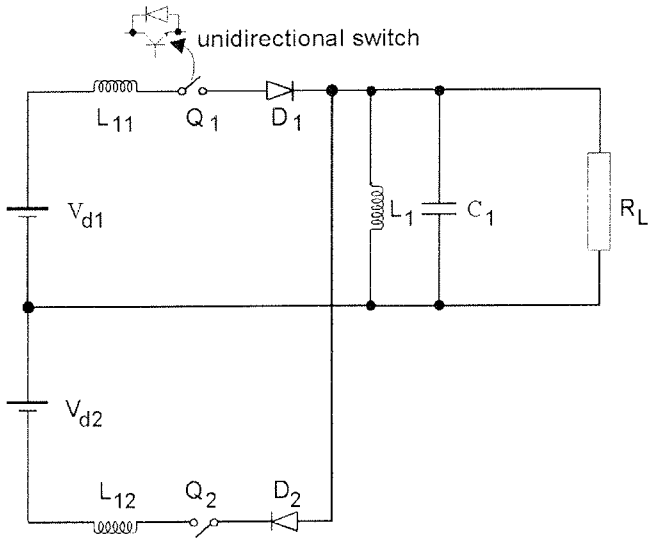

Fig. 2: The "full-wave" resonant link converter configuration

The 3rd circuit (Fig. 3) has been done like the last step of "evolution" of the first circuit (Fig. 1) which we would like to present in this paper. The voltage sources V_{d1} and V_{d2} have been simply replaced by diode bridge and main supply. The new circuit consists of a diode rectifier, two serial inductance (L_{11} and L_{22}), two transistors (Q_1 and Q_2) and two serial diodes which are not necessary for circuit operations because their functions can be taken over by diodes from rectifier bridge.

The converter which in first step operates like DC to HF Resonant Link Converter, in the last step becomes the converter which converts Three Phase Main supply into AC-HF voltage. For tests and operations the voltage of

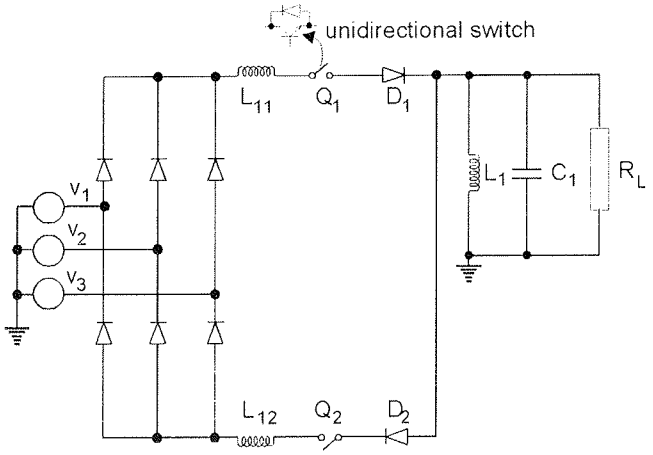

Fig. 3: The AC to HF-AC resonant link converter configuration

HF link, V_{out} = 1000 $V_{p\text{-}p}$, frequency, f_{out} = 22 kHz and P_{out} = 500 W has been chosen.

3. The start-up procedure

The most convenient way to analyse the start-up behaviour is to find out the equivalent circuit from circuit in Fig. 3. It is not difficult to see that the circuit in Fig. 1. represents that circuit. The circuit in Fig. 1 can be called a DC/(half wave) HF-AC resonant converter, because of the similarity in structure with AC/DC diode rectifier. The only difference between these two circuits is in wave shape of supply voltage. In regard to simplify analysis, the response of DC voltage will be discussed. The DC voltage on "+" terminal of diode bridge (Fig. 3) can be computed from the following equation.

$$V_d = \frac{3}{\pi}\hat{V}_1 \tag{1}$$

The original circuit (Fig. 1) will be described by a set of equations (2). These equations describe the behaviour of circuit in Fig. 3 as well. Let us suppose that the voltage V_d is constant and the step response of the circuit can be observed. The current responses are shown in Fig. 4.

The response where zero current crossing has been reached is very interesting because there is any free-wheeling diode needed which should correspond with the energy in inductance L_{11}. If the zero crossing condition trough L_{11} has not been reached there can be a voltage spike on the transistor Q_1 and the circuit can not operate.

$$\begin{aligned}
\frac{di_{L11}}{dt} &= \frac{1}{L_{11}}\left(V_d - v_C\right)\\
\frac{di_{L1}}{dt} &= \frac{1}{L_1}v_C\\
\frac{di_{L11}}{dt} &= \frac{1}{C}\left(i_{L11} - i_{L1} - \frac{1}{R}v_C\right)
\end{aligned} \tag{2}$$

The above system can be solved for two different time intervals. Equations (3), (4) and (5) represent the solution of system of equations (2) in time interval (t_0, t_1), (Fig. 5)

$$\begin{aligned}
i_{L11} = \frac{V_d}{\omega_{os}L_{11}}\Bigg[&\frac{L_{11}}{L_{11}+L_1}\omega_{os}t + \\
&\frac{L_{11}}{L_{11}+L_1}e^{-\frac{t}{2RC}}\sin(\omega_{os}t+\varphi)\Bigg] - \\
&I_{co}\frac{L_{11}}{L_{11}+L_1}\left[1-e^{-\frac{t}{2RC}}\cos(\omega_{os}t+\varphi)\right]
\end{aligned} \tag{3}$$

$$\begin{aligned}
i_{L1} = &\frac{V_d}{\omega_{os}L_{11}}e^{-\frac{t}{2RC}}\sin(\omega_{os}t+\varphi) \\
&+I_{co}e^{-\frac{t}{2RC}}\cos(\omega_{os}t+\varphi)
\end{aligned} \tag{4}$$

$$v_C = V_d \frac{L_{11}}{L_{11}+L_1}\left[1 - e^{-\frac{t}{2RC}}\cos(\omega_{os}t+\varphi)\right] + \frac{I_{co}}{\omega_{os}C} e^{-\frac{t}{2RC}} \sin(\omega_{os}t+\varphi) \quad (5)$$

and equations (6) and (7) represent the solutions of system of equations (2) in time interval (t_1,t_2) (Fig. 5):

$$i_{L1} = I_{C1} e^{-\frac{t}{2RC}} \cos(\omega_{op}t+\varphi) - V_d C \omega_{op} e^{-\frac{t}{2RC}} \sin(\omega_{op}t+\varphi) \quad (6)$$

$$v_C = V_d e^{-\frac{t}{2RC}} \cos(\omega_{op}t+\varphi) + \frac{I_{C1}}{\omega_{op}C} e^{-\frac{t}{2RC}} \sin(\omega_{op}t+\varphi) \quad (7)$$

where:

$$\omega_{os} = \frac{1}{\sqrt{L_N C}}, \quad L_N = \frac{L_{11}L_1}{L_{11}+L_1}, \quad \omega_{op} = \frac{1}{\sqrt{L_1 C}}$$

$$\varphi = \text{arctg}\left(\frac{Z_s}{R}\right), \quad Z_s = \sqrt{\frac{L_N}{C}}$$

If the appropriate value for L_{11} has been chosen, the current i_{L11} should not exceed the transistor current limit and the parallel resonant tank circuit gets enough energy and oscillation starts with its own parallel resonant frequency.

The current i_{L11} starts to flow when the switch Q_1 is ON. That current has a sinusoidal wave-shape because of the resonance behaviour of serial resonant tank circuit ($L_{11}//L_1$, C_1, R_L). When current crosses zero the diode D_1 switches OFF the serial resonant tank circuit. The parallel resonant tank circuit (L_1, C_1) relaxes itself on resistor R_L. When the output voltage v_C crosses zero the diode D_1 becomes switched ON (it has been supposed that triggering pulse on Q_1 is present all the time). The wave-shapes of currents i_{L11} are shown in Fig. 4.

The values of L_{11} and L_1 have been chosen with intention that the parallel resonant frequency must be 21 kHz, and the serial resonant frequency should assure the soft switching operation in start up procedure.

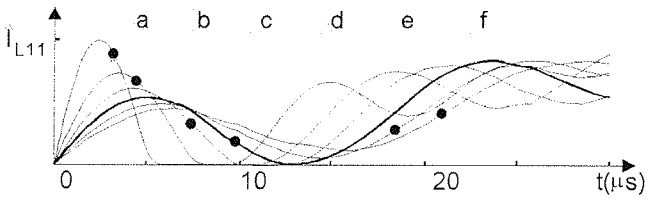

Fig. 4: The soft start analysis.

The wave forms of i_{L11} in Fig. 4 which are marked with "a, b, c, and d" enable the soft switching operation with respect to transistor's current limitation. In steady state there are no problems with soft switching operation because the HF AC link voltage is present. The results in Fig. 4 have been computed by using SPICE simulator.

4. The energy balance cosideration

Equations (3) to (7) which describe current i_{L11}, i_{L1} and v_C are very complex. Because of that the design procedure based on energy balance will be described in next lines.

4.1. The Load Requirements

Let us suppose the load is resistance whose power is denoted by P. The peak value of the output voltage is denoted by $\hat{V}_m$, the frequency of the output voltage is f_p and the peak value of the current through inductance L_{11} is denoted by $\hat{I}_m$. The energy which will supply the load for half of period of the output voltage can be expressed by the next formula:

$$W_{load} = P\frac{T}{2} \quad (8)$$

where $T = 1/f_p$.

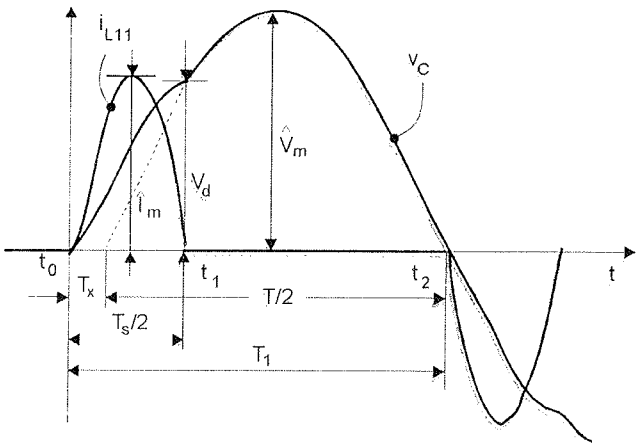

Fig. 5: The waveforms of current and voltage in resonant link converter

That amount of joules has to be stored in parallel resonant tank circuit and in ideal case the energy store in capacitor is:

$$W_C = \int_0^T v_C i_C = W_{load} \quad (9)$$

We can calculate the capacitance C_1, by using (4):

$$C = 2\frac{W_C}{\hat{V}_m^2} \quad (10)$$

The inductance L_1 has been calculated by using the expression:

$$L_1 = \frac{1}{4\pi^2 C f_p^2} \quad (11)$$

If the parallel resonant tank circuit has been relaxed (no power supply is connected on circuit), the resistor R_L would be connected on parallel resonant tank circuit. The energy which will be dissipated on the load, can be computed by formula:

$$W_{DISS} = P\left(\frac{T}{2} - \frac{T_s}{2}\right) \tag{12}$$

At the some time that amount of joules is exactly the quantity which has to be provided from DC power supply to parallel resonant tank circuit for each half of period of the output voltage (Fig. 5) in order to get constant output voltage on parallel resonant tank circuit. That yields:

$$W_{LN} = W_{DISS} \tag{13}$$

where W_{LN} describes the energy stored in serial equivalent inductance. This energy W_{LN} has been computed by using the expression:

$$W_{LN} = \int_0^t v_{LN} i_{LN} d\tau \tag{14}$$

For current which will be flown into serial equivalent resonant tank circuits a sinusoidal wave-shape has been supposed (Fig. 5). After time $t=T_S/2$ the energy flow has been stooped.

Expressions for inductor current and voltage yield from next formulas:

$$i_{LN} = \hat{I}_m \sin(\omega_s t) \tag{15}$$

$$v_{LN} = \omega_s \hat{I}_m L_N \cos(\omega_s t) \tag{16}$$

The equations (15) and (16) have been substituted into (14) and yields:

$$W_{LN} = L_N \frac{\hat{I}_m^2}{2} \tag{17}$$

From eq. (17), the equivalent inductance can be defined:

$$L_N = \frac{2W_{LN}}{\hat{I}_m^2} \tag{18}$$

Using (18) we can express the inductance L_{11}:

$$L_{11} = \frac{L_N L_1}{L_1 - L_N} \tag{19}$$

Such computed values for all elements of circuits (Fig. 3) has to be proofed by equations (3) to (7) in order to get soft switch behaviour for current i_{L11}. In the case when the soft switch operation has not been reached, it is necessary to change the ratio between inductance L_{11} and L_1, which means changing of ratio between energy W_{LN} and W_C.

4.2. The Power Supply Requirements

The above sections show the way of designing the elements of serial and parallel resonant tank circuit from load requirements. In many applications the DC power supply voltage has been forced by mean supply, eq. (1). On the other hand the peak value of current $\hat{I}_m$ has been proposed for energy balance consideration.

$$\hat{I}_m = f(V_d) \tag{20}$$

This two facts can not be considered together because of connection between that two quantities. The expression (10) has to be found in regard to get a small signal model of such converter as well /5/.

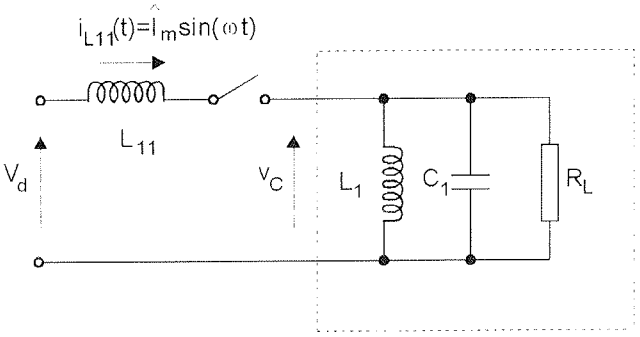

Fig. 6: The equivalent circuit for injected-absorbed current method

Let us suppose that the current i_{L11} and v_C have the wave-shape as shown in Fig. 5. The main current injected from L_{11} into parallel resonant tank circuit (L_1-C_1-R_L) is supposed to be sinusoidal.

$$i_{L11} = \hat{I}_m \sin(\omega_{os} t) \tag{21}$$

where ω_{os} is the serial resonant frequency.

On the other hand the derivative of inductance current i_{L11} should be described with the next set of equations:

$$\frac{di_{L11}}{dt} = \frac{1}{L_{11}}\left[V_d - V_d \sin(\omega_{os} t)\right] \tag{22}$$

$$\int_0^{\hat{I}_m} di_{L11} = \int_0^{T_s/4} \frac{1}{L_{11}}\left[V_d - V_d \sin(\omega_{os} t)\right] dt \tag{23}$$

Which gives us the expression for $\hat{I}_m$:

$$\hat{I}_m = \frac{T_s}{4L_{11}} V_d \left(1 - \frac{2}{\pi}\right) \tag{24}$$

The equation (14) connects the supply voltage V_d with the magnitude of inductance current $\hat{I}_m$.

5. The small signal model

According to the classification of analysing methods /5/, the injected-absorbed-current method belongs to the class of the simplest linear methods whose validity is limited to low-frequency, small-signal phenomena. The basic idea that leads to linearization is the introduction of the notation of average values of quantities of interest (usually voltages and currents). Their average values are determined by averaging over a period (duration T) of the switching frequency:

$$q_{av} = \frac{1}{T}\int_{t1}^{t2} q(t)dt \qquad (25)$$

where q represents any quantity of interest and t_1 represents the time at which the averaging process begins. The averaging eliminates the influence of the exact wave forms during the period of the switching frequency, on mathematical relationships among averaged quantities. The result is a dramatic simplification of mathematical expressions in the analysis. Fig. 7 shows the switching cell as a black box.

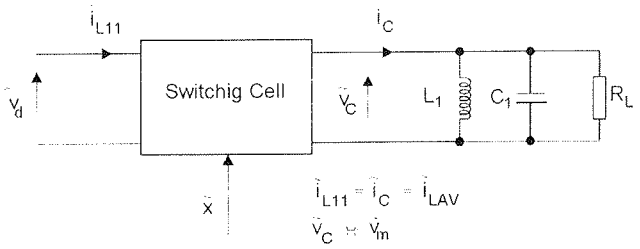

Fig. 7: The switching cell

Five quantities are marked at it's ports: the input voltage and current, the output voltage and current and a fifth quantity x, which is a controlled quantity. Assume now that the average values of the input current i_{L11} can be expressed as functions of the average value x of controlled quantity and the average values of the cell input voltages. The relations:

$$i_{LAV} = i_{LAV}(x, v_d) \qquad (26)$$

define these functions.

The average value of current i_{L11} will be denoted by i_{LAV}. From Fig. 5 and 6 follows the next expression:

$$i_{LAV} = \frac{2}{T}\int_0^{T_s/2} \frac{T_s V_d}{4L_{11}}\left(1-\frac{2}{\pi}\right)\sin(\omega_{os}t)dt = \frac{DV_d}{L_{11}(k+1)\omega_{os}}\left(1-\frac{2}{\pi}\right) \qquad (27)$$

In a linear model of the cell, a simple proportional relation among small quantities exists:

$$di_{LAV} = \frac{\partial i_{LAV}}{\partial D}dD + \frac{\partial i_{LAV}}{\partial v_d}dV_d = AdD + BdV_d \qquad (28)$$

Coefficients A and B are:

$$A = \frac{\partial i_{LAV}}{\partial D} = \frac{V_d}{L_{11}(k+1)\omega_{os}}\left(1-\frac{2}{\pi}\right)$$

$$B = \frac{\partial i_{LAV}}{\partial V_d} = \frac{D}{L_{11}(k+1)\omega_{os}}\left(1-\frac{2}{\pi}\right)$$

where $k = 2T_x/T$ (fig. 5).

Unfortunately there is no term to connect the small changing of average value of the input current with the peak value of the output voltage in eq. (28). An inaccurate method is published in /4/. The more accurate method requires that the average value of the output voltage on resonant tank circuit has to be introduced in analyses procedure. From Fig. 5 the half period average value of the output voltage can be evaluated:

$$v_{CAV} = \frac{1}{T_1}\int_0^{T_1} v_C(t)dt = \frac{1}{T_1}\left(\int_0^{T_s/2}\hat{V}_d\sin(\omega_{os}t)dt + \int_{T_s/2}^{T_1}\hat{V}_m\sin(\omega_{op}t+\varphi)dt\right) = \frac{2V_dD}{\pi(k+1)} + \frac{\hat{V}_m}{2\pi(k+1)}\left[4-\pi^2\left(2k^2+2kD+D^2\right)\right] \qquad (29)$$

where $\varphi = \omega_{op}T_x$, is a phase angle.

The total differential of the output average voltage was calculated by (30):

$$dv_{CAV} = \frac{\partial v_{CAV}}{\partial V_d}dV_d + \frac{\partial v_{CAV}}{\partial \hat{V}_m}d\hat{V}_m + \frac{\partial v_{CAV}}{\partial D}dD = DdV_d + Ed\hat{V}_m + FdD \qquad (30)$$

Where the coefficients D,E, and F are as follows:

$$D = \frac{\partial v_{CAV}}{\partial V_d} = \frac{2V_d}{\pi(k+1)}$$

$$E = \frac{\partial v_{CAV}}{\partial \hat{V}_m} = \frac{1}{2\pi(k+1)}\left(4-\pi^2\left(2k^2+2kD-D^2\right)\right)$$

$$F = \frac{\partial v_{CAV}}{\partial D} = \frac{2V_d}{\pi(k+1)} - \frac{\hat{V}_m\pi}{(k+1)}(k+D)$$

Instead of diferential quantities dx the small perturbations $\tilde{x}$ has been introduced.

In Fig. 8 the connection between the changing of average current i_{LAV} and it's response - changing of the output voltage v_{CAV} is shown wich means that there is connection between the small perturbations as well.

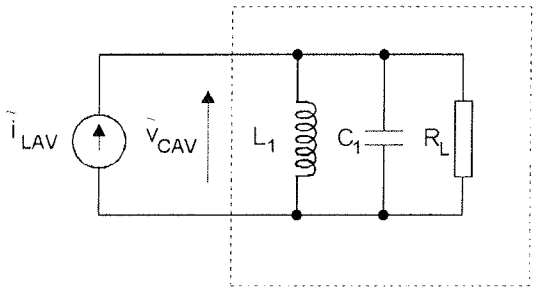

Fig. 8: The Parallel resonant circuit excited by current generator instead of voltage source, serial inductance and semiconductor switch

The voltage on the parallel resonance tank circuit is:

$$\tilde{v}_{CAV}(s) = \frac{sL_{11}}{s^2L_{11}C + s\left(\frac{L_{11}}{R}\right)+1}\tilde{i}_{AV}(s) = Z(s)\tilde{i}_{AV}(s) \quad (31)$$

After taking the Laplace transform of eq. (28) and (30) and eq. (28) into (31), regarding to eliminate $\tilde{I}_{LAV}$ and $\tilde{v}_{CAV}$, we get the following equation:

$$\tilde{v}_m = \frac{1}{E}\left[(A\tilde{d} + B\tilde{v}_d)Z(s) - D\tilde{v}_d - F\tilde{d}\right] \quad (32)$$

The transfer function $\frac{\tilde{v}_m(s)}{\tilde{d}(s)}$ was calculated by using eq. (32) with presumption that $\tilde{v}_d = 0$, which yields:

$$\frac{\tilde{v}_m(s)}{d(s)} = -\frac{1}{E}\frac{FL_1Cs^2 + s\left(\frac{L_1}{R} - AL_1\right)+1}{s^2L_1C + s\left(\frac{L_1}{R}\right)+1} \quad (33)$$

From eq. (33) the magnitude and phase of the transfer function can be computed. Fig. 10 (a), (b) show the magnitude and phase frequency responses.

The control object (Fig. 9) consist of PWM block as well. A frequency responce of PWM was published in /4/.

From eq. (34) the magnitude and phase of the PWM transfer function can be computed. The frequency response of PWM and of whole object are shown in Fig. 10 (c),(d) and (e),(f) respectively. A design of control parameter has been done in frequency domain.

$$\frac{\tilde{d}(s)}{\tilde{u}_{kr}(s)} = \frac{K}{\hat{V}_m}\frac{1}{sT_s+1} \quad (34)$$

where $K = \frac{1}{2\pi}\cos^{-1}\left(-\frac{V_d}{\hat{V}_m}\right)\frac{T}{T_x} - 1.$

5. The experimental results

The experimental results confirm our theoretical model of the AC to HF-AC Resonant Link Converter where a control of the peak value of the high frequency output voltage was achieved. The proposed control scheme is described in Fig. 9.

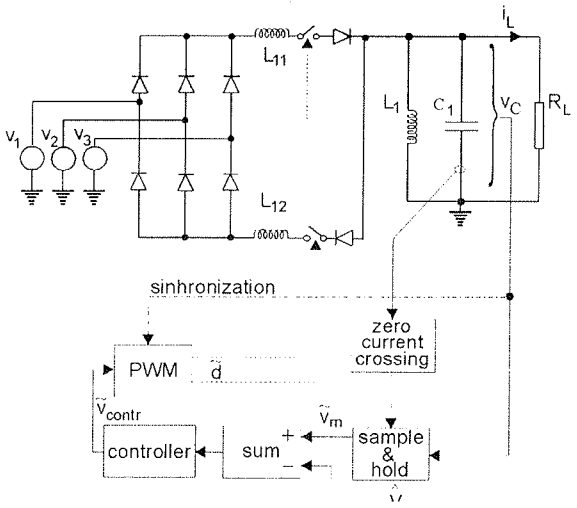

Fig. 9: The control sheme

The S&H circuit is used instead of the peak detector. The capacitor current i_C has a delay versus voltage v_C exactly 90^0 el. If the voltage is sampled in that time instant (when the current i_C crosses zero), the peak value of voltage v_C will be measured. That simple phenomena helped, that there are any filter in measuring circuit. The delay will be one period of the output voltage.

6. Conclusion

The main idea which has been discussed in this article is providing the energy through serial resonant tank circuit into parallel resonant tank circuit. By substitution the diode rectifier and main supply instead of DC voltage the "new" circuit was introduced. In order to use snubberless circuit the start up problem has to be solved by manipulations with values of L_{11} and L_1. The main effort has been done at the efficiency analysis and consequently the efficiency increases up to 92%. There are no switching losses, but there are core and copper losses in inductance and conducting losses in transistors and diodes. With introduction of the Injected-Absorbed-Current method of analysis the linearized transfer function has been developed for AC to /HF-AC resonant link converter.

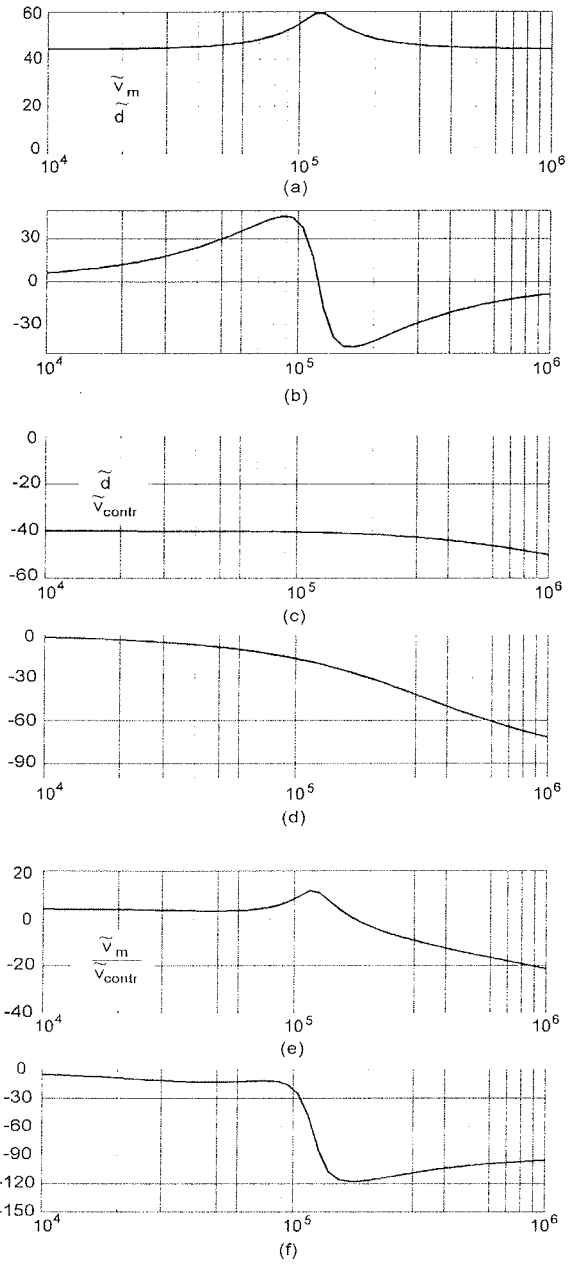

Fig. 10: The frequency responses

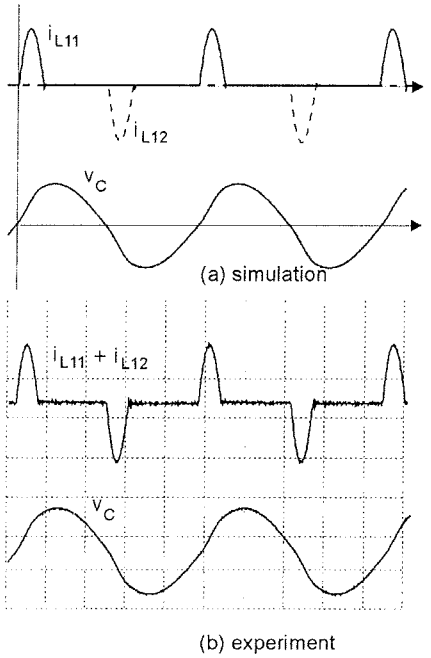

Fig.11: (a) simulation results; currents i_{L11}, i_{L12} and voltage v_C, (b) experimental results i_{L1},i_{L11} (1 A/div) and voltage v_C (50 V/div), time axis 10 µs/div

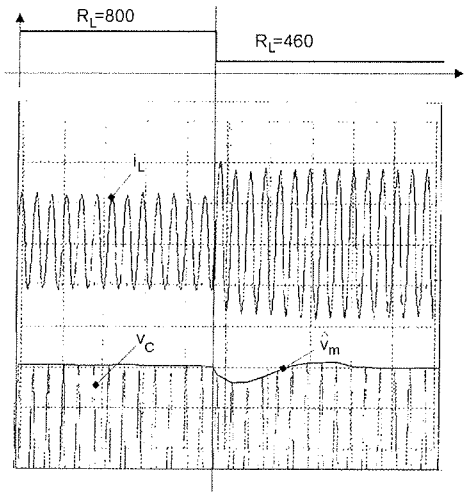

Fig 12: The experimental results: i_L, x-axis 100 µs/div, y-axis 0.2 A/div, v_C, V_{p-p}=300 V, x-axis 100 µs/div, y-axis 20V/div.

References

/1/ P.K. Sood, T.A. Lipo, "Power Conversion Distribution System Using a Resonant High Frequency AC Link", IEEE IAS Trans., vol. 24, pp. 586-596, March/April 1988.

/2/ D.M. Divan, "The Resonant Link Inverter, a New Concept in Power Conversion", IEEE-IAS Annual Meeting Conf. Rec. 1986 pp. 648-656.

/3/ S.K. Sul, T.A. Lipo, "Design and Performance of a High Frequency Link Induction Motor Drive Operating at Unity Power Factor", IEEE IAS Annual Meeting, Proc., pp. 308-313, Oct. 1988.

/4/ M. Milanovič, D. Zadravec, A. Hren, F. Mihalič, "DC to HF-AC Resonant Link Converter by Using Serial and Parallel Resonance", IEEE PEDS Conference, Singapore Feb. 1995.

/5/ A.S. Kislovski, R. Redl, N.O. Sokal, Dinamic Analysis of Switching-Mode DC/DC Converters, Van Nostrand Reinhold, New York 1991.

izr.prof. dr. Miro Milanovič
Robert Kovačič, dipl.ing.
mag. Franc Mihalič, dipl.ing.
doc.dr. Rudi Babič
University of Maribor
Faculty of Electrical Engineering and Computer Science
Smetanova 17
2000 Maribor
tel.: +386 62 221-112
fax: +386 62 273-578

Prispelo (Arrived): 01.02.1996 Sprejeto (Accepted): 27.02.1996

TANKOPLASTNI KAPACITIVNI SENZOR RELATIVNE VLAŽNOSTI

L.I. Belič, K. Požun
Inštitut za elektroniko in vakuumsko tehniko, Ljubljana, Slovenija

Ključne besede: merjenje vlage, senzorji vlage organski, senzorji kapacitivni, vlažnost relativna, plasti tanke,nanašanje plasti tankih, elektrode prepustne za paro vodno, časi odzivni, karakteristike senzorjev, polietersulfon snov, merjenje debelin plasti tankih

Povzetek: Pospešene raziskave na področju merjenja zračne vlage so pripeljale do zamenjave mehanskih detektorjev s senzorji, ki v odvisnosti od zračne vlage spreminjajo svoje električne karakteristike in so zato primerni za vgradnjo v elektronske merilnike. V grobem ločimo uporovne in kapacitivne senzorje. Kot material za izdelavo senzorjev uporabljajo različne soli, v zadnjem času pa predvsem keramične in polimerne materiale.

V delu predstavljamo kapacitivni polimerni senzor vlage. Glavne prednosti takega senzorja so majhne dimenzije, velika občutljivost, kratek reakcijski čas, majhen temperaturni koeficient in skoraj zanemarljiv vpliv pretoka zraka na meritev. Točnost meritev, ki jo lahko dosežemo z omenjenim tipom senzorja, znaša ±1% relativne vlage.

Ena od bistvenih lastnosti tankoplastnega kapacitivnega senzorja je kratek odzivni čas. Podrobneje bomo opisali hitrost odziva senzorja v odvisnosti od različno naparjene zgornje elektrode.

Capacitive Thin Film Relative Humidity Sensor

Keywords: humidity measurement, humidity sensors, capacitive sensors, relative humidity, thin films, thin film deposition, water vapour permeable electrodes, response times, characteristic of sensors, polyethersulphone substance, thickness measurements of thin films

Abstract: The rapid research in the field of humidity measurements enabled the replacement of the mechanical humidity sensors with electrical sensors where the change of relative air humidity influences the sensor electrical properties. Such sensors are suitable for use in various electronically supported applications. Humidity sensors can be divided into two major categories - resistive and capacitive sensors. As the humidity sensors active substances different salts were most often used. Nowadays the different ceramic and polymer materials are used instead.

The article describes capacitive relative humidity sensors with polymer dielectric material.

Such sensors can be produced very small and sensitive. They have short response time, very small temperature coefficient and the capacitance is almost independent on the air flux. The accuracy of the relative humidity measurements is within ±1%.

One of the most important properties of the relative humidity sensor is its very short response time. The response time as the function of the different upper electrode sputtering mode is presented.

UVOD

Znanih je več načinov merjenja relativne vlažnosti: meritve mehanskih sprememb, psihrometrične meritve in meritve spremembe električnih lastnosti kot sta sprememba upornosti in kapacitivnosti /1-4/.

V kapacitivnem tankoplastnem senzorju relativne vlage predstavlja osnovo za določanje vlage sprememba lastnosti tanke polimerne plasti pri interakciji z vodno paro. Pri interakciji vodne pare s polimerom prihaja do kombinacije mehanskih, kemičnih in električnih pojavov. Adsorpcija vodnih molekul in vezava vodnih molekul preko vodikovih vezi na polimer povzroči spremembo dielektrične konstante. Nastala sprememba kapacitivnosti senzorja je v idealnem primeru odvisna samo od količine adsorbirane vodne pare. Senzor vlage izkorišča nekaj desetkrat večjo relativno dielektrično konstanto vode, ki je cca 80 v primerjavi z relativno dielektrično konstanto uporabljenega polimera, ki znaša med 3-4.

Osnovna lastnost kondenzatorja in v našem primeru senzorja relativne vlažnosti, ki jo izkoriščamo, je kapacitivnost, določena s preprosto linearno zvezo $C = C_0\varepsilon_r$ je z geometrijo določen koeficient, ε_r je relativna dielektričnost snovi med elektrodama.

Mehanizem vezave adsorbiranih vodnih molekul na polimer omogočajo šibke vodikove vezi med molekulami vode in značilnimi skupinami na površini polimera. Čim večje je število aktivnih mest, na katere se vežejo vodikove vezi, tem bolj strma je adsorpcijska izoterma.

EKSPERIMENTALNI DEL

Naš tankoplastni polimerni kapacitivni senzor relativne vlažnosti zraka deluje v temperaturnem območju od 0-100°C, področje relativne vlažnosti RH pa med 0 in 100% relativne vlage.

Osnovo senzorja predstavlja steklena podlaga. Na dobro očiščeno podlago skozi maske v visokem vakuumu naparimo spodnji elektrodi (NiCr). Nato nanesemo plast polimera.

Uporabljamo polimer na osnovi polietilen sulfona, ki je stabilen in omogoča zgoraj omenjene pogoje delovanja

senzorja. Velik problem predstavlja nanos polimerne plasti. Plast mora biti tanka (1 μm), enakomerno debela, težava pa je tudi v ponovljivosti nanosa. Minimalna debelina polimerne plasti je omejena z zahtevo po primarni prebojni napetosti senzorske strukture.

Pred nanosom vrhnje elektrode polimerni film aktiviramo v rahlo oksidativni atmosferi za dosego boljše adhezije med obema plastema. Hitrost nanašanja plasti kontroliramo s kvarčno tehtnico, debelino nanosa vrhnje elektrode merimo z mehanskim merilnikom višine stopnice. Zgornjo ektrodo nanašamo pod različnimi koti, in tako dosežemo različno morfologijo elektrode.

Izdelane senzorje najprej umerimo z uporabo kalibrov nasičenih raztopin po DIN 5008 /5/ za umeritve senzorjev vlage in umerjanje merilnikov vlage. Umerjenim senzorjem izmerimo električne lastnosti: kapacitivnost, izgubni kot, hitrost odziva in impedanco pri frekvenci 10 kHz, z RCL merilnikom Promax MZ- 705.

REZULTATI IN DISKUSIJA

Večplastno senzorsko strukturo občutljivo na zračno vlago sestavljata dve elektrodi na steklenem nosilcu z vtaljenimi provodi (sl.1).

Senzorska struktura (plast polimera in elektrodi) tvorijo dva serijsko vezana kondenzatorja (sl.1a).

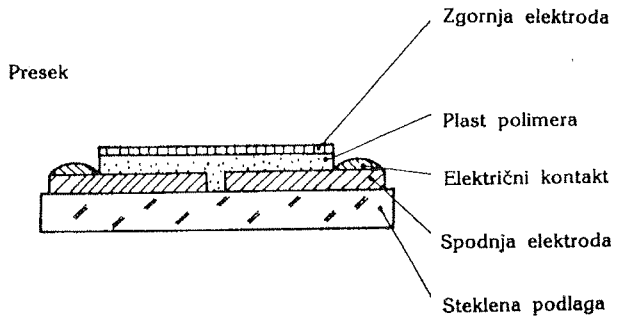

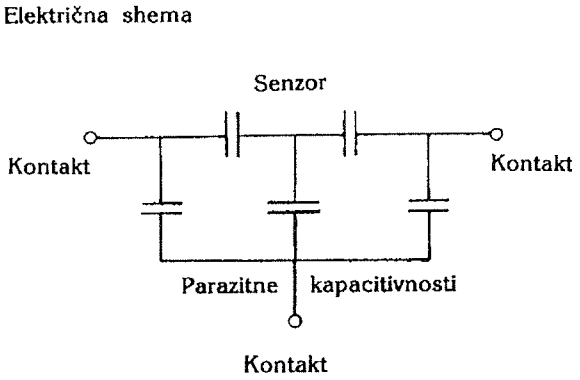

1a

Slika 1: Shematski prikaz tankoplastnega kapacitivnega senzorja relativne vlažnosti zraka, 1a) električna shema senzorja

Kondenzator torej sestavljata dve galvansko ločeni elektrodi in dielektrik, ki zapolnjuje prostor med njima. Uporabljen polieteresulfon (PES) ima naslednjo strukturno formulo /6/:

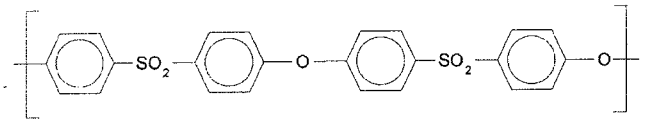

Molekule vode se z vodikovo vezjo vežejo na SO_2 (sulfonsko) skupino. Možna, a manj verjetna je vezava tudi na -O- skupino.

Na sliki 2 je SEM posnetek površine polimera. Meritve hrapavosti polimerne plasti so pokazale, da hrapavost zelo niha. Celotna debelina polimera je 1000 nm, hrapavost polimera, izmerjena z mehanskim merilnikom višine stopnice TENCOR Alfa Step 100, pa odstopa tudi od 0.1 do 0.3 μm. To pomanjkljivost smo delno odpravili s spremenjenim sušenjem polimera.

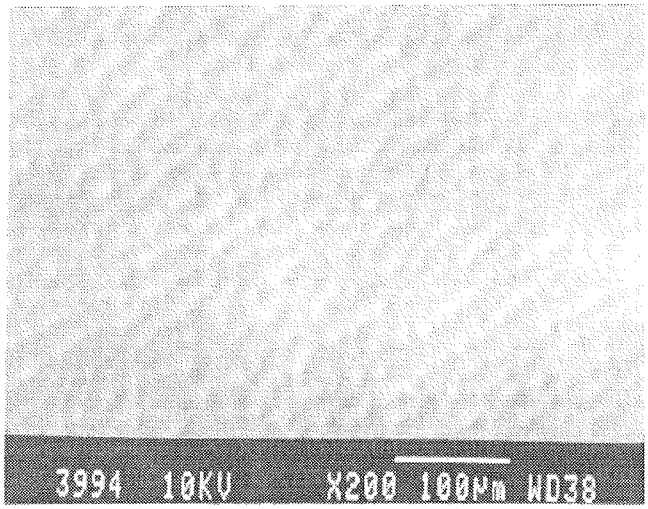

Slika 2: SEM posnetek površine polimera, povečava 200X.

Zveza med kapacitivnostjo in relativno vlago pri konstantni temperaturi mora biti pri senzorju vlage čim bolj linearna. Na sliki 3 je prikazana izmerjena histereza, ki nastane med naraščanjem relativne vlažnosti - krivulja a in pri njenem padanju b. Nastala histereza je minimalna, kar je pri senzorju vlage zaželeno. Spremembo kapacitivnosti senzorja v območju 0-98% relativne vlage smo določali v nasičenih solnih raztopinah. Parni tlak vodne pare je pri uporabljenih nasičenih raztopinah znan in konstanten. Meritve so potekale pri konstantni temperaturi 23°C.

Ena bistvenih lastnosti senzorja je čim krajši odzivni čas.

Za doseganje zadostne hitrosti odziva senzorske strukture je potrebna primerna prepustnost vrhnje elektrode za vodno paro. Vrhnja elektroda mora poleg prepustnosti (je porozna) imeti tudi dovolj visoko električno prevodnost, obenem pa je treba zagotoviti primerno

majhne notranje napetosti in zadostno elastičnost, da pri močnejšem nasičenju polimera ne pride do porušitve spoja polimer - kovina.

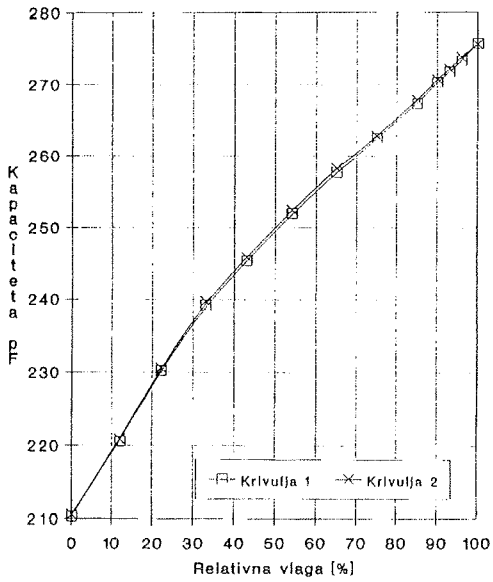

Slika 3: Sprememba kapacitivnosti senzorja vlage v odvisnosti od relativne vlažnosti. Krivulja 1 je bila posneta med naraščanjem vlage, krivulja 2 med njenim padanjem. Temperatura je bila konstantna 23°C.

Depozicija vrhnje elektrode poteka z naparevanjem pri različnih kotih. Kot je definiran kot kot med normalo substrata in normalo uporovne ladjice.

Elektrodo naparevamo v vakuumskem sistemu, ki ga izčrpamo do 10^{-6} mbara. NiCr (80-20) elektroda mora biti debela cca 100 nm. Maso naparjene plasti določimo s kvarčno tehtnico. V sistemu istočasno naparevamo NiCr plast tudi na referenčni stekleni substrat, ki ga uporabimo za merjenje debeline naparjene plasti. Zgornjo elektrodo smo naparevali pod kotom 0, 30, 45, 60 in 75°.

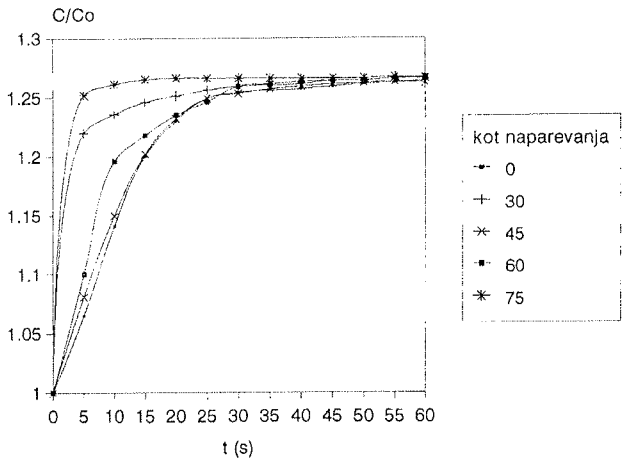

Slika 4: Prikaz odzivnega časa v odvisnosti od kota naparevanja zgornje elektrode

Različen kot nanašanja pomeni različno gostoto oz. poroznost elektrode in pri enakih časih naparevanja tudi različno debelino. Kako pa se kot nanašanja odrazi na hitrosti spremembe kapacitivnosti senzorja prikazuje slika 4. Najpočasneje se spreminja kapacitivnost v primeru, ko je kot naparevanja 0°, najhitreje pa, ko je kot naparevanja 75°.

Vzrok takemu obnašanju senzorja je prav gotovo večja poroznost elektrode, ki omogoči hitrejši dostop vodne pare do dielektrika. Do podobnih rezultatov so prišli tudi drugi avtorji /7/.

Potrditev, da je elektroda naparjena pod kotom 75° bolj porozna, kot kadar je naparjena pod manjšim kotom je tudi diagram na sliki 5.

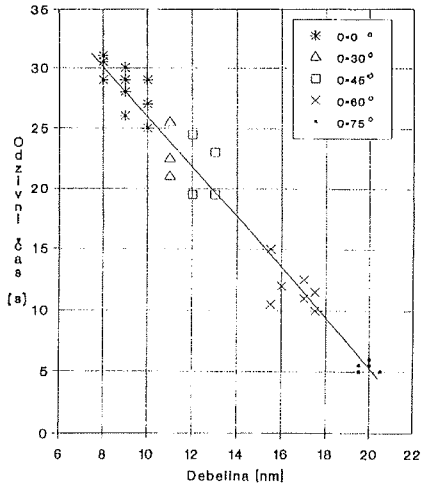

Slika 5: Diagram odvisnosti odzivnega časa v povezavi z debelino zgornje elektrode

Diagram prikazuje povezavo med odzivnim časom in debelino posameznih elektrod. Posebej je treba poudariti, da je bila masa pri vseh elektrodah konstantna. Ker je debelina elektrod pri enaki masi različna, to pomeni, da je gostota elektrod različna. Najdebelejša elektroda je najbolj porozna, dostop vodne pare do polimera je najlažji, odzivni čas pa je najkrajši.

SKLEPI

Razvili smo kapacitivni senzor relativne vlažnosti, ki ima skoraj linearno povezavo med kapacitivnostjo in relativno vlago.

Uspelo nam je narediti porozno vrhnjo elektrodo, ki omogoča hiter dostop zračne vlage in zato hiter odziv senzorja.

Porozna elektroda je posledica naparevanje pod kotom 75°.

Težave pri senzorju predstavlja polimerna plast, predvsem hrapava površina in ponovljivost nanosa.

Senzor relativne vlažnosti je na tržišču dostopen samo skupaj z merilno elektroniko. Na IEVT se posebna

skupina ukvarja z razvojem elektronike za RH merilnik. S to skupino tesno sodelujemo.

ZAHVALA

Delo je bilo opravljeno s finančno podporo Ministrstva za znanost in tehnologijo Slovenije, za kar se jim iskreno zahvaljujemo.

Zahvaljujemo se Kemijskemu inštitutu, sodelavcem Laboratorija za impendančno spektroskopijo za opravljene meritve in koristne nasvete.

LITERATURA

/1/ S.Takeda, Capacitive Humidity Element Using Polystiren Thin Films Formed by Plasma Polimerization, Japanese J. of Applied Physics, Vol.20, No7, (1981) 1291

/2/ Y. Maehashi, New Humidity Sensors Offer Reliable Performance JEE, Sensors and Application Technology, (1993) 28

/3/ G. Gerlach, K. Sager, A piezoresistive humidity sensors, Sensore and Actuators A, 43 (1994) 181

/4/ Chang-Dong Feng, H. Wang, S. Sun et al., Humidity Sensing Properties of Acetalized Polyvinil Alcohol Films, 188th Electrochemical Society Meeting, Vol. 95-2, (1995) 1577

/5/ Standard DIN 5008, Konstantklimate über Wassrigen Losungen Teil 1, Teil 2, Februar 1981

/6/ H.F. Merck, N.M. Bikales, C.G. Overberger, G. Menges, Encyklopedia of Polymer Science and Engineering, Se. Ed., Vol. 13, Yohn Wiley & Sons, New York, (1986) 196

/7/ S.Takeda, High response humidity sensors with plasma polymerized organic film, Vacuum, Vol. 41, No. 7-9, (1990) 1769

dr. Lidija I. Belič,dipl ing.
Karol Požun, dipl.ing.
IEVT Teslova 30
1000 Ljubljana, Slovenija
tel.: +386 (0)61 126 45 84
fax: +386 (0)61 126 45 78

Prispelo (Arrived): 20.02.1996 *Sprejeto (Accepted): 18.03.1996*

OUTGASSING PROPERTIES OF Au ELECTROPLATED CONTACT MATERIAL ARGELEC 181 FOR USE IN HERMETIC RELAYS

L. Koller, M. Jenko*, S. Vrhovec and B. Praček,
Institute for Electronics and Vacuum Technics, Ljubljana, Slovenia
* Institute of Metals and Technologies, Ljubljana, Slovenia

Keywords: electronic components, miniature relays, hermetical relays, electrical contacts, gold electroplating, cleaning of contact surfaces, vacuum outgassing, degrees of outgassing, AES, Auger electron spectroscopy

Abstract: The purpose of our study was to establish the degree of outgassing of gold plated material (produced with the use of citrate and phosphate electrolytes) still permitting the use of that material in hermetic relays. Systematic investigations of vacuum outgassing of Au electroplated Argelec 181 alloy are performed by Auger Electron Spectrometer which was additionally equipped with quadrupole mass spectrometer. The AES depth profile analysis revealed that the oxide layer on the Au electroplated Argelec 181 alloy is negligible and this is the reason for very low outgassing rate.

Razplinjevalne lastnosti elektrokemijsko pozlačenega kontaktnega materiala ARGELEC 181 za hermetične releje

Ključne besede: deli sestavni elektronski, releji miniaturni, releji hermetični, kontakti električni, zlatenje elektrokemično, čiščenje površin kontaktov, razplinjevanje vakuumsko, stopnje razplinjevanja, AES Augerjeva spektroskopija elektronska

Povzetek: Namen našega dela je bil določiti stopnjo razplinjevanja pozlačenega kontaktnega materiala, ki še dovoljuje njegovo uporabo za hermetične releje. Zlata kontaktna površina na osnovnem materialu Argelec 181 je bila nanešena v Au-citratni in Au-fosfatni kopeli. Pri sistematičnih raziskavah vakuumskega razplinjevanja elektrokemijsko pozlačene kontaktne zlitine Argelec 181 smo uporabili Augerjev elektronski spektrometer (AES), dodatno opremljen s kvadrupolnim masnim spektrometrom. AES globinska profilna analiza je pokazala, da je oksidna površinska prevleka na merjencu zanemarljiva, kar je tudi vzrok za zelo nizko stopnjo razplinjevanja.

Introduction

Recently, the properties of the outgassed material used for the hermetically encapsulated electronic parts draw much attention of the scientific community. One of the main serious causes of failure of electronic components is the film made from the contaminating products on the surface of electric contacts. Effects of a film are the increasing of the contact resistance and the decreasing of the electronic components reliability. The most common types of contamination are oxide and corrosion products, particulates, films formed by thermal diffusion processes, debris produced by mechanical wear and fretting, outgassing and condensation of contact surfaces. Contamination of the gold layer deposited on the contact alloy depends also on the electroplating process technology. The gold electroplated contact layers used in hermetic relays are very important because they act in decreasing the contact resistance and increasing the lifetime.

Experimental

Citrate and phosphate electrolytes (Kemijska tovarna Podnart) were used for electroplating /1,2,3,4/ of contact alloy Argelec 181 (Ag with 0.3 % of Mg). In both cases the thickness of the obtained Au layers was 0.5 μm. The citrate electrolyte as well as the phosphate one was found suitable for the electric currents up to 20 A and did not cause the contact sticking. To examine the degree of contamination and the surface structure of the gold layer obtained with the use of the two different baths the Auger Electron Spectroscopy (AES) was used. The PHI Spectrometer SAM, model 545A was used for the AES analysis. Experiment parameters were: static electron beam of 3 keV, 0.5 μA, 40 μm in diameter at an incident angle of 47° and the ion sputtering rate of Ni/Cr was 10 nm/min.

The surface with the dimension of 5mm x 5mm was etched by two ion guns (3 keV Ar^+). Figures 1 and 2 show profile diagrams where the contamination layer thickness obtained from the ion etching parameters is plotted against the concentration of the elements. The both types of gold electroplated surfaces were outgassed /5,6,7,8/ for several hours in high vacuum of $1x10^{-6}$ mbar at the temperature 135°C. The experimental high vacuum system used for our study was developed and built at the Institute for Electronics and Vacuum Technics. Outgassing products were analysed by the quadrupole mass spectrometer LEISK 1000M.

Results and discussion

The profile diagram (Fig. 1) shows the concentration profile of the surface gold layer deposited to the contact material Argelec 181 using phosphate electrolyte bath. It can be seen that the surface gold layer is covered with the very thin contamination film (~ 5 nm) formed of carbon containing traces of calcium and oxygen. Below

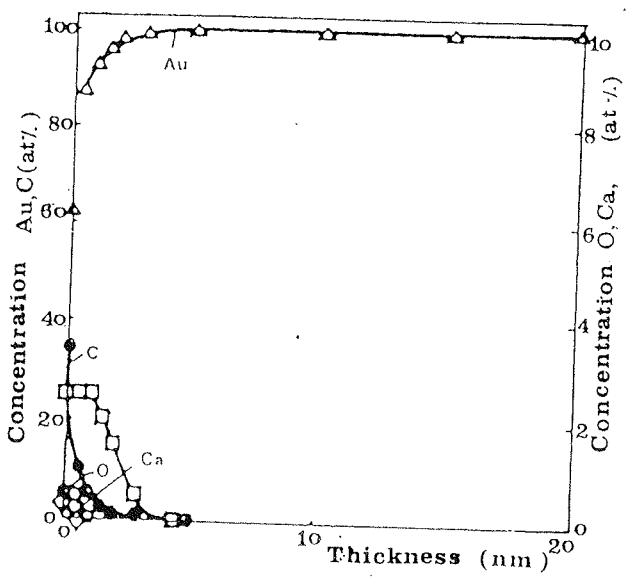

Fig. 1: Profile diagram of the gold surface layer (0.5 μm Au) deposited from the phosphate electrolyte.

this a high peak typical for Au is detected. The next profile diagram (Fig. 2) deals with the gold deposit from the citrate electrolyte. The surface contamination film has the thickness of about 2 nm and contains twice less

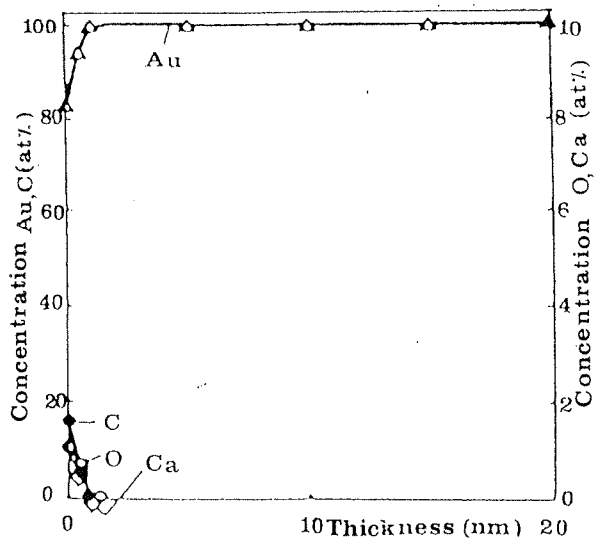

Fig. 2: Profile diagram of the gold surface layer (0.5 μm Au) deposited from the citrate electrolyte.

carbon than the former but greater concentrations of calcium and oxygen. Again, the gold layer below the contamination film is very clear. Then the analysis of gases outgassed from the samples of gold electroplated contact alloy obtained with the use of two different baths (citrate and phosphate electrolyte) was performed. Samples were heated in the experimental device shown in Fig. 3, 4, 5 and 6. After 24 hours heating at 135°C it was evident hat carbon, oxygen, water vapour and the remainings of the cleaning agents (ethanol and isopropyl alcohol) which have been adsorbed on

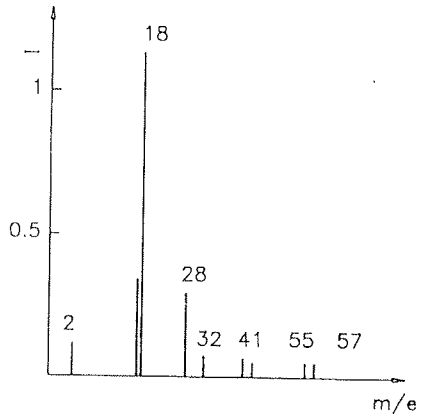

Fig. 3: Mass spectrum of the outgassed empty chamber (150°C, 24 hours of outgassing).

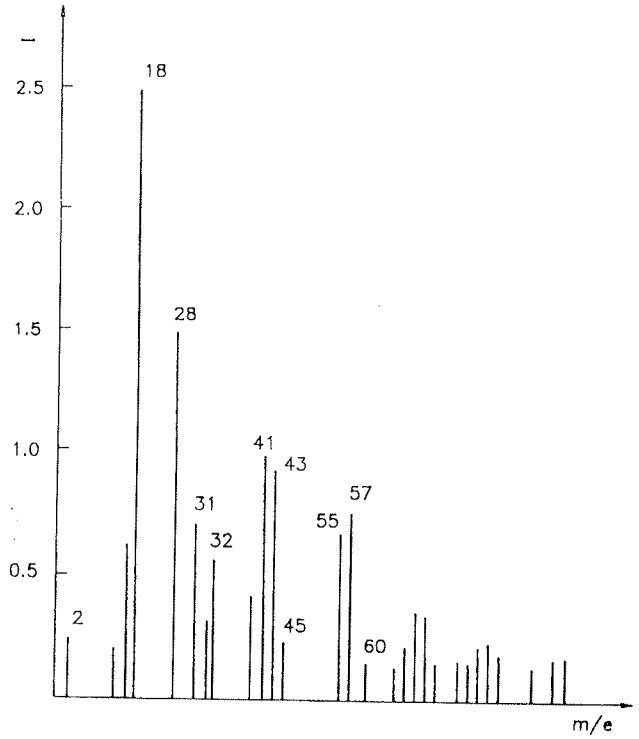

Fig. 4: Mass spectrum of the outgassing products from the electrochemically gold plated (citrate and phosphate electrolyte) contact alloy Argelec 181 (135°C, 1x10^{-6} mbar) after 30 minutes of outgassing.

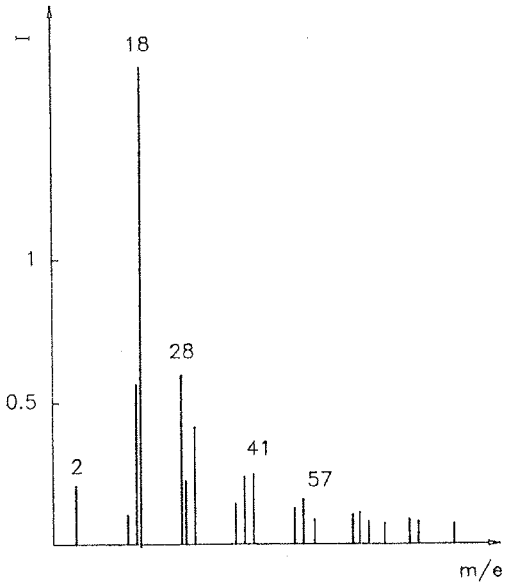

Fig. 5: Mass spectrum of the outgassing products from the electrochemically gold plated (citrate electrolyte) contact alloy Argelec 181 (135°C, 1x10^{-6} mbar) after 24 hours of outgassing.

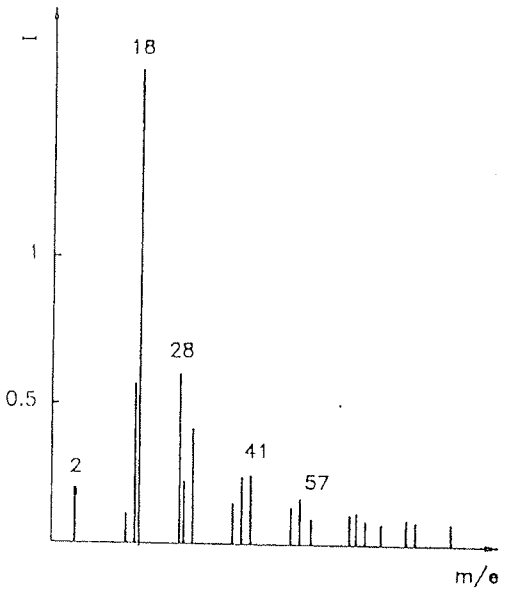

Fig. 6: Mass spectrum of the outgassing products from the electrochemically gold plated (phosphate electrolyte) contact alloy Argelec 181 (135°C, 1x10^{-6} mbar) after 24 hours of outgassing.

he surface were completely outgassed. The comparison between the spectra of two outgassed samples and the spectrum of the background - empty chamber (Fig. 3, 5 and 6) proves that. The degree of outgassing for hydrogen was then calculated and compared with the value obtained from the spectra (Fig. 3, 4, 5, 6). The ratio between the hydrogen peaks after outgassing (background subtracted) was f=0.1 for the gold layer from citrate and phosphate bath which is in agreement with the theoretically obtained value being equal to 0.067.

Conclusions

With the AES analysis we established that the contamination of the surface gold layers electroplated on the contact material Argelec 181 is strongly dependent on the technological process.

The degree of surface contamination is greater for the gold layer made with the use of phosphate electrolyte than for the other one. The inner gold layer is very pure in both technologies used.

The degree of outgassing (f) for hydrogen from the gold electroplated contact alloy Argelec 181 (Ag with 0.3% of Mg) from the citrate and phosphate electrolyte is low (about 0.1) which is in good agreement with the theoretically obtained value 0.067.

The contact alloy Argelec 181 electrochemically covered with the gold layer of the thickness of 0.5 μm after outgassing (135°, 24 hours, 1x10^{-6} mbar) is found to be a suitable contact material for use in electronic parts.

References

/1/ M. Hansen, Constitution of Binary Alloys, 2nd ed. (Mc Graw Hill, New York, 1958).

/2/ M. Gojo, 11. jug. simpozij o elektrokemiji, Rovinj (1989), p. 127.

/3/ Qualitetsprüfung galvanischer Überzeuge, (Sammelband, Nürnberg, 1990).

/4/ R. Sard, Properties of Electrodeposits, their Measurement and Significance, (Princeton, New Jersey, 1989).

/5/ L. Koller, R. Zavašnik and M. Jenko, Vacuum 43(1992)741.

/6/ L. Koller, M. Jenko, B. Praček and S. Spruk, Vacuum 44 (1993) 441.

/7/ L. Koller, M. Jenko, S. Spruk, B. Praček and S. Vrhovec, Vacuum 46 (1995) 827.

/8/ N. Yushimura, T. Sato, S. Adachi and T. Kanezawa, J. Vac. Sci.Technol. A8 (1990) 924.

L. Koller, dipl. ing.
S. Vrhovec
B. Praček, dipl.ing.
Institute for Electronics and Vacuum Technique
Teslova 30, 1000 Ljubljana, Slovenia
tel.: +386 (0)61 126 45 84
fax: +386 (0)61 126 45 78
Dr. M. Jenko, dipl. ing.
Institute of Metals and Technologies
Lepi pot 11, 1000 Ljubljana, Slovenia

Prispelo (Arrived): 09.01.1996 *Sprejeto (Accepted): 20.02.1996*

ELECTRICAL PROPERTIES OF A PASSIVE LAYER ON LITHIUM MEASURED IN ABSENCE OF LIQUID ELECTROLYTE

Miran Gaberšček, Darja Kek and Stane Pejovnik
National Institute of Chemistry, Ljubljana, Slovenia

Keywords: surface protection, pasivation, passive layers, passive films on lithium, LiCl, lithium chloride, thin films, $SOCl_2$, thionyl chloride, electrical properties, measurements of electrical properties, ionic conductors, layer porosity, impedance spectroscopy, electrical transport of mobile particles, equivalent circuits

Abstract: Electrical properties of a passive film formed on lithium in thionyl chloride are measured using impedance spectroscopy. Unlike in all previous investigations published in literature the measuring cells did not include liquid solution. In modelling of the measured impedance spectra the presence of poor electrical contact between the passive film and counter electrode, as well as the passive film porosity, were taken into account. The parameters of electrical transport across the passive film are compared with the corresponding literature data.

Električne lastnosti pasivne plasti na litiju, izmerjene v odsotnosti tekočega elektrolita

Ključne besede: zaščita površin, pasivacija, plasti pasivne, plasti pasivne na litiju, LiCl klorid litijev, plasti tanke, $SOCl_2$ tionil klorid, lastnosti električne, meritve lastnosti električnih, prevodniki ionski, poroznost plasti, spektroskopija impedančna, transport električni delcev gibljivih, vezja ekvivalentna

Povzetek: Električne lastnosti pasivnega filma, ki se tvori na litiju v prisotnosti tionil klorida, smo merili z impedančno spektroskopijo. Bistvena razlika glede na objavljene meritve v literaturi je, da merjeni sistem ni vseboval tekočega elektrolita. Pri modeliranju izmerjenih impedančnih spektrov smo tudi upoštevali slab električni kontakt med pasivnim filmom in pomožno elektrodo ter poroznost pasivnega filma. Tako dobljene parametre električnega transporta smo primerjali z ustreznimi podatki, objavljenimi v literaturi.

INTRODUCTION

If in contact with terrestrial environment most metallic surfaces are transformed into oxides and/or salts /1/. In cases when the newly formed surface layer prevents the underlying metal from further decay, the system is regarded passivated, the corresponding phenomenon is referred to as passivation and the thin surface layer as a passive layer (or passive film).

The electrical properties of the passive layers formed on lithium in aprotic media have exclusively been studied in systems in which the passive film was in contact with a liquid electrolyte. As lithium passive layers usually include a significant degree of porosity, such measurements only provide information about the combined electrical properties of the liquid electrolyte in layer's pores and those of the solid skeleton of the passive layer (Fig. 1a). As in most cases the pore geometry is not known, nothing can be said about the electrical properties of individual components, especially of the solid part of the passive layer. In this paper we present a technique which allows for direct measurements of the electrical properties of the solid part of the passive film formed on lithium in contact with thionyl chloride ($SOCl_2$). This passive film is polycrystalline LiCl with some inclusions of aluminium and sulphur compounds. The liquid electrolyte is removed from the system and a solid counter electrode is employed instead (Fig. 1b). The electrical properties of such an all-solid-state system are measured using the impedance spectroscopy and the results are interpreted taking into account both the porosity of the film as well as the poor contact between the passive layer and the solid counter electrode.

EXPERIMENTAL

Electrolyte: A 1.5 M $LiAlCl_4/SOCl_2$ electrolyte solution was used. $SOCl_2$ was purified by fractional distillation under an argon atmosphere. $AlCl_3$ (99,99%) was used, as obtained from Aldrich. LiCl (p. a.) from Kemika Zagreb was dried at 175°C under a vacuum for 72h. A 1.5 M solution of $LiAlCl_4/SOCl_2$ was prepared in an argon-filled dry box by slowly adding $AlCl_3$ to $SOCl_2$ in order to avoid heating, and then slowly adding LiCl in slight excess.
The water content of the electrolyte as found by IR spectroscopy was less than 10 ppm.

Materials: Thin LiCl films were prepared in two ways:
a) by immersion and spontaneous passivation of metallic lithium in a 1.5 M solution of $LiAlCl_4/SOCl_2$. Lithium was stored in the electrolyte for 14 days at 50°C, forming a passive layer of thickness of approx. 80 μm on the surface of the lithium metal. After this treatment the passivated surface was dried for at least two days in Ar atmosphere to remove all liquid electrolyte.

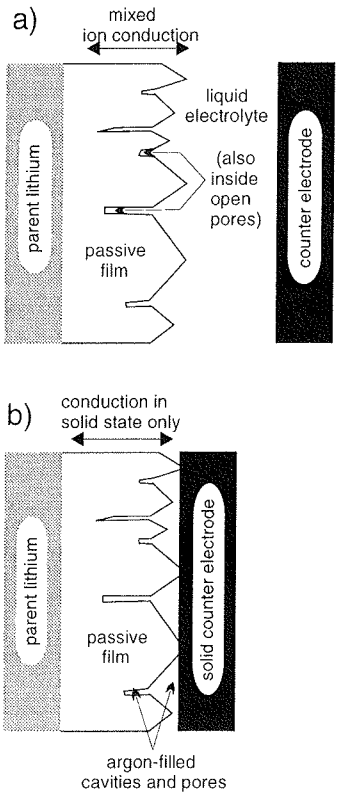

Fig. 1: Cell configurations used to study the electrical properties of passive films on lithium; a) commonly used cells, b) cell configuration used in the present study.

b) by evaporation from a LiCl substrate at a pressure of 10^{-4} mbar at 500°C to 550°C on a polished platinum sheet.

Electrodes: Electronic contacts were made using a conductive carbon cement (CCC) (Neubauer Chemikalien), a conductive silver paint (CSP) (GC Electronic), and a platinum sheet. Ionic contact was made by pressing a sheet of metallic Li against the film surface using a spring contact.

Using the described materials and electrodes the following types of cells were constructed:

a) ionic contacts:
- Li/passive film LiCl/Li; system A
- Li/passive film LiCl/Li/Li_3N; system B

b) mixed ionic and electronic contacts:
- Pt/thin film LiCl/Li; system C
- Li/passive film LiCl/CC; system D

Li_3N in system B was prepared by keeping Li/LiCl/Li cells in an argon atmosphere with up to ca 1% of N_2 but with only traces of O_2 and moisture - less than 5 ppm for several days.

Measurements: Impedance measurements were performed using a Solartron 1250 Frequency Response Analyzer (65000 Hz to 0.01 Hz) combined with a 1286 Electrochemical Interface and a Hewlett-Packard 4284A LCR Meter (1 MHz to 20 Hz). The impedance response was measured at variable DC voltage bias (-2 to +2V).

All measurements and cell preparations were performed in an argon-filled dry box facility.

RESULTS AND DISCUSSION

The shape of impedance response of the Li(parent electrode)/passive film/solid counter electrode system measured in the frequency range from 65000Hz-0.01Hz system may be divided in two cases (Fig.2):

a) if the solid counter electrode is metallic lithium, a slightly depressed arc is observed in the whole frequency range (Fig. 2a),

b) in all other cases a low-frequency tail in addition to the depressed high-frequency arc is observed (Fig. 2b).

Such behaviour may be explained in the following way: the high-frequency arc represents the response due to migration of lithium vacancies in the bulk passive film while the low-frequency tail is due to diffusion of mobile particles (lithium vacancies + the corresponding positively charged carriers) inside the passive film towards the passive film/counter electrode interface. Obviously, if both electrodes consist of metallic lithium the diffusion process is not observed (Fig. 2a). This means that the

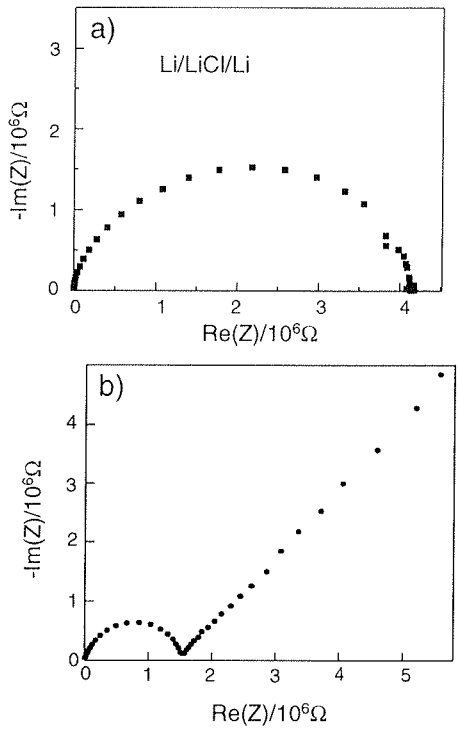

Fig. 2: Typical shape of the impedance response for a) symmetrical Li/passive film/Li cells, b) asymmetrical Li/passive film/solid counter electrode where "solid counter electrode" denotes the following electrodes: platinum, conductive carbon cement, and stainless steel.

impedance of the lithium/passive film interface is very low which prevents the mobile carriers from accumulation at that interface and diffusion is negligible. Conversely, in other systems the measured impedance of the passive film/solid counter electrode interface is high enough to allow for the accumulation of charge carriers and the diffusion process is observed (Fig. 2b).

The fact that the high-frequency arc is depressed (i.e. its centre lies below the real axis) implies that more than just one relaxation process take place within the passive film. Indeed, as shown in Fig. 3, one needs at least 2 RQ terms in order to get a satisfactory fit of a typical measurement. Here R represents the resistance and Q the so-called CPE (constant phase element) defined as

$$Q = \frac{R^{1-\alpha}}{(j\omega C)^{\alpha}} \qquad (1)$$

where $j=\sqrt{-1}$, ω is the angular frequency of the excitation signal, C is the capacitance and a is a parameter related to distribution of relaxation times. Analysis of many measured impedance responses have shown /2/ that one of the RQ terms probably represents the response of solid skeleton of the passive film while the other is most likely due to a combined effect of i) passive film pores and ii) the poor physical contact at the passive film/solid electrode interface on the impedance response of the system. Building up a simplified model simulating the electrical properties of the system (Fig.4) it was possible to show /2/ that the actual contact area between the passive film and the solid electrode was as low as 2-15% of the geometrical area of the contact. The reason for this is the high surface roughness of the passive film which prevents the solid electrode - unlike in the case of liquid electrolyte systems - from coming into intimate contact with the passive film surface. The second important result of analyses with the model in Fig.4 is the calculated value of average passive film thickness which lies in the range from 70 to 90 μm. This range agrees well with the values observed using the scanning electron microscopy (20-60 μm) and hence confirms the relevance of the proposed model. Finally, the model gives average values of conductivity of the solid skeleton of the passive film which at 25°C has a value of ca 10^{-9} Scm^{-1}. This is ca 100 times less than the average passive film conductivity found in liquid electrolyte systems /3/. A rough estimation based on the assumption of cylinder-shaped pores, and taking into account that the conductivity of liquid electrolyte is 10^{-2} Scm^{-1}, shows that in average the film porosity is ca 10^{-7} (i.e. the ratio between the cross-section area of pores and the geometrical cross-section area). Expressed in another way this means that if an average cubic single crystal has a base of 10μm, a typical pore diameter would be ca 3.5 nm. Due to difficult handling and chemical reactivity of the systems involving metallic lithium the latter result cannot be verified using, for example, SEM observations.

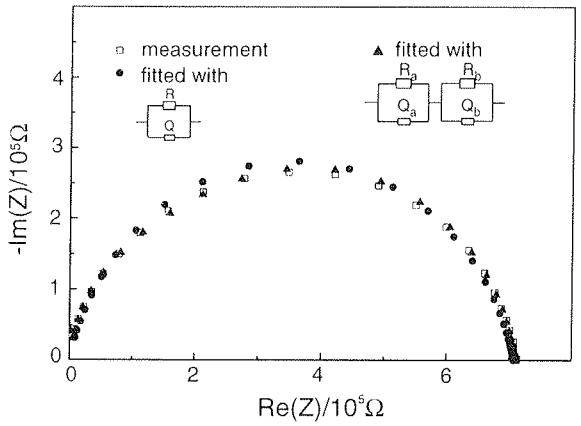

Fig. 3: Measured impedance spectrum fitted with two different equivalent circuits.

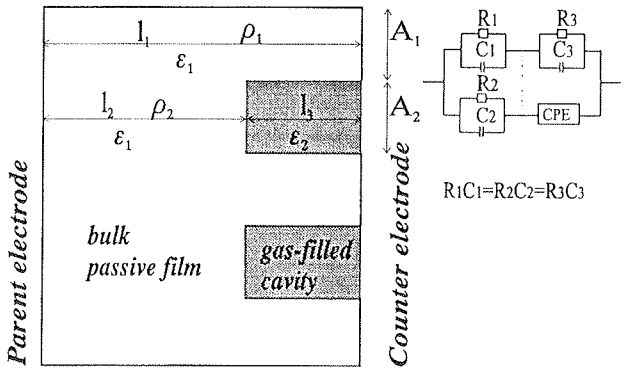

Fig. 4: Schematics of a model taking into account the poor contact at the passive film/counter electrode interface and/or film porosity.

Impedance response as a function of DC voltage bias:

Measurements of impedance response at variable DC voltage bias (e.g. 0 to ± 2 V) usually serve to distinguish between the contribution of bulk and interfacial response. Typical results are shown in Fig. 5. As expected, the high-frequency arc does not change with bias (Fig. 5 a) while the shape and magnitude of the low-frequency tail show significant dependence on DC voltage bias (Fig.5 b, c). The changes in the low-frequency response are ascribed to deposition (or dissolution) of metallic lithium at the passive film/solid counter electrode interface. For example, if the lithium electrode is biased positively, lithium ions are transferred from this electrode to the counter solid electrode where they are deposited as metallic lithium (Fig. 6 a). Gradually the surface of counter electrode covers completely with metallic lithium which, in terms of the impedance response, means that the low-frequency tail almost disappears (Fig. 5, b - triangles) compare with Fig. 1, curve A). If the deposition of metallic lithium continues, it may

happen that also the magnitude of high-frequency arc slightly reduces (Fig. 5, c). This result may be explained by taking into account the hypothesis developed for liquid electrolyte systems /3/, viz. that the further deposition of lithium occurs preferentially at grain boundaries which results in the dendritic growth shown in Fig. 6 b. When the dendrites have penetrated deeply enough into the bulk passive film the effective distance between both electrodes is considerably reduced which, in turn, is reflected in the size of the high-frequency arc.

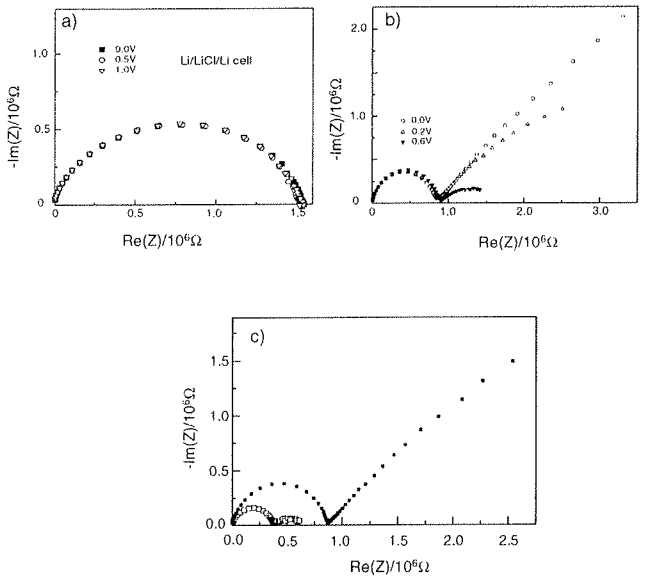

Fig. 5: The influence of dc voltage bias on impedance spectra of the investigated systems: a) symmetrical cell, b) asymmetrical cells in cases when Li is deposited at the counter electrode as shown in Fig. 6a, c) asymmetrical cells in cases when Li is deposited at the counter electrode as shown in Fig. 6b.

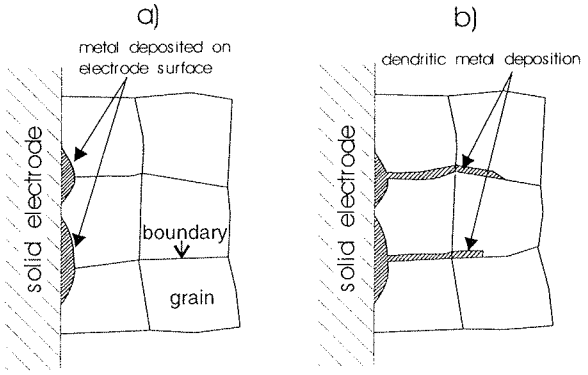

Fig. 6: a) deposition of metallic lithium in the first stage of dc voltage application, b) deposition of Li at after prolonged application of dc voltage.

Impedance response as a function of temperature:

Impedance response was measured as function of temperature in the range from 25 to 150°C. Using the model presented in Fig. 4, Arrhenius graph showing temperature dependence of passive film conductivity was constructed (Fig. 7). The activation enthalpy for lithium ion (or vacancy) conductivity was found to be 0.65±0.05 eV. This is 0.24 higher than the value obtained by Haven /4/ for LiCl single crystal in the temperature range 300°C to 450°C. The difference may be due to three reasons:

a) in our case the activation enthalpy has additional term due to extrinsic conductivity;

b) there may be an additional term due to the formation of associates or imperfections /5/;

c) conduction along grain boundaries of LiCl may be activated in a different way as the conduction in LiCl single crystals.

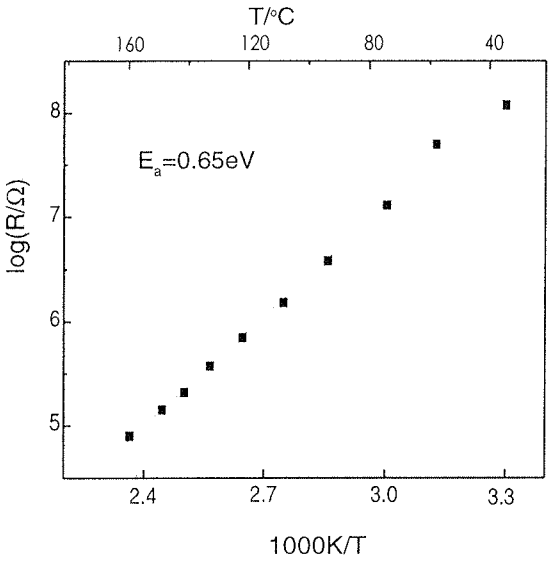

Fig. 7: Arrhenius plot showing temperature dependence of passive film conductivity.

CONCLUSIONS

The electrical properties of the passive film formed on lithium in thionyl chloride were studied in cells where the liquid electrode was replaced by solid electrodes of different types. Using a simple model describing the electrical properties of the systems under investigation the following results were obtained:

1. The conductivity of the solid part of the passive film was found to be ca 10^{-9} Scm^{-1}, which is ca two orders of magnitude lower than in systems including liquid electrolyte. The ratio between the cross-section area of pores and the solid part of the film was ca 10^{-7}.

2. If the lithium electrode was biased positively, the deposition of metallic lithium on the counter solid electrode was observed as a pronounced change in the low-frequency part of impedance spectra. Further deposition led to changes in the high-frequency arc as well, which was ascribed to the dendritic growth of metallic lithium into the bulk passive film.
3. The activation enthalpy for lithium ion (or vacancy) conductivity in the temperature range 25 to 150°C was found to be 0.65±0.05 eV.

ACKNOWLEDGEMENT

The financial support from The Ministry of Science and Technology of Slovenia is fully acknowledged.

REFERENCES

/1/ V. Brusic, in Corrosion Chemistry, Eds G.R. Brubaker and P.B.P. Phipps, American Chemical Society, Washington, D.C., 1979, pp. 153-184

/2/ D. Kek, M. Gaberšček, S. Pejovnik, J. Electrochem Soc., in press

/3/ E. Peled, in "Lithium Batteries", Ed J. P. Gabano, Chap. 3, Academic Press, Inc., (1983)

/4/ Y. Haven, RECUEIL, Vol. 69, (1950), 1471

/5/ A. Kroeger, in The Chemistry of Imperfect Crystals, Elsevier, New York, 1974

dr. Miran Gaberšček, dipl. ing.,
mag. Darja Kek, dipl. ing.,
prof. dr. Stane Pejovnik, dipl. ing.,
Kemijski inštitut,
Hajdrihova 19
1115 Ljubljana, Slovenija
tel.: +386 61 1760 200
fax: +386 61 1259 244

Prispelo (Arrived): 12.03.1996 *Sprejeto (Accepted): 18.03.1996*

KONFIGURACIJA MERILNEGA SISTEMA ZA ANALIZO MIKROVALOVNIH DIELEKTRIČNIH LASTNOSTI IN NJEN VPLIV NA NATANČNOST MERITVE

M. Valant, D. Suvorov, S. Maček
Institut "Jožef Stefan", Univerza v Ljubljani, Ljubljana, Slovenija

Ključne besede: sistemi merilni, resonatorji dielektrični, metode resonatorjev votlinskih refleksijske, lastnosti dielektrične, lastnosti mikrovalovne, napake merilne, frekvence resonačne

Povzetek: Postavljen merilni sistem za določevanje mikrovalovnih dielektričnih lastnosti temelji na refleksijski metodi votlinskega resonatorja. Raziskali smo odvisnost izmerjenih resonančnih frekvenc in faktorjev kvalitete od dimenzij testnih votlinskih resonatorjev. V primerih, ko je bila $TE_{01\delta}$ najnižja resonanca sistema, smo izmerili znatno nižje faktorje kvalitete (do 10%). Pri tem smo opazili tudi premik resonančne frekvence dielektričnega resonatorja k nižjim vrednostim. Meritve so bile natančnejše v primerih, ko smo uporabili večje testne votlinske resonatorje. Razvili smo tudi numerično metodo za izračun lastnih frekvenc votlinskega resonatorja z vstavljenim dielektrikom.

Configuration of the Measurement System for the Analysis of Microwave Dielectric Properties and its Influence on Accuracy of Measurement

Keywords: measuring systems, dielectric resonators, reflection resonant cavity methods, dielectric properties, microwave properties, measurement errors, resonant frequencies

Abstract: The main problem in the determination of the Q-value at the resonant condition arises due to the existence of the external EM field, which could penetrate into the conducting walls of the resonant cavity (skin effect). This causes a reduction of the measured Q-value. Therefore, to obtain the unloaded Q-value the resonant cavity should be large enough to avoid the skin effect. However, by increasing the size of the resonant cavity the resonant modes of the cavity shift to lower frequencies. This could cause the $TE_{01\delta}$ dielectric resonator mode to overlap with or to be mistaken for the resonant cavity modes. Usually the measurements are performed with a resonant cavity up to three or four times larger than the dielectric resonator. At permittivities of the dielectric resonator higher than approximately 20 this assure that the position of the $TE_{01\delta}$ dielectric resonator mode is below the first resonant cavity mode (TM_{010}).

Measurement system for determination of microwave dielectric properties was constructed employing the reflection resonant cavity method. The dependence of the measured resonant frequency and Q-value on the resonant cavity dimensions was determined. We noticed a significant reduction in the Q-value (up to 10%) if it is measured below the TM_{010} resonant cavity mode. Also the resonant frequency was slightly shifted toward the higher values due to the tuning effect. Measured Q-values were higher and therefore closer to unloaded Q-value when we used larger cavities. Numerical procedure for the determination of the resonant modes of the resonant cavity containing inserted dielectrics was also developed

Uvod

Pomembna prelomnica pri razvoju brezžične komunikacijske tehnologije je uvedba zmogljivih *mrežnih analizatorjev*, kar je, ob hkratnem razvoju računalniške tehnike, omogočilo simulacijo, analizo ter testiranje modelov. Eksperimentalno je bilo ugotovljeno in opisano /1/, kako se elektromagnetno polje resonančnih rodov sklaplja in razširja v medijih različnih dimenzij in različnih električnih lastnosti. Na osnovi takšnih spoznanj je postalo oblikovanje, testiranje in optimizacija mikrovalovnih vezij hitro in zanesljivo. Ob tem je bilo razvitih tudi nekaj novih, hitro izvedljivih in dokaj natančnih metod za karakterizacijo mikrovalovnih dielektričnih lastnosti materialov.

Analiza resonančnih karakteristik, ki so odvisne predvsem od oblike in dielektričnih lastnosti vzorcev, predstavlja osnovo večine merilnih metod za določevanje mikrovalovnih dielektričnih lastnosti materialov. Kompleksno vrednost dielektričnosti je teoretično mogoče izračunati le iz dimenzij vzorca, resonančne frekvence in širine resonančnega odziva, vendar je v praksi takšen izračun praviloma nenatančen. Temeljni razlog je v večini primerov enak. Elektromagnetno (EM) polje dielektričnega resonatorja je namreč moteno zaradi bližine prevodnih sten, nosilca, sklopitvenih zank itd. Motnje EM polja povzročajo premik resonančne frekvence k višjim vrednostim ter širitev resonančnega odziva.

Ker do sedaj še ni izvedena standardizacija merilnega sistema za določevanje mikrovalovnih dielektričnih lastnosti, obstajajo različne merilne metode, katerih rezultati med seboj niso vedno neposredno primerljivi. Konfiguracije merilnih sklopov se med seboj razlikujejo, zato je potrebno izbrati primerno metodo glede na

namembnost meritve, naravo vzorcev ter zahtevano natančnost. Na sliki 1 so prikazane nekatere najpogosteje uporabljane konfiguracije testnih sklopov.

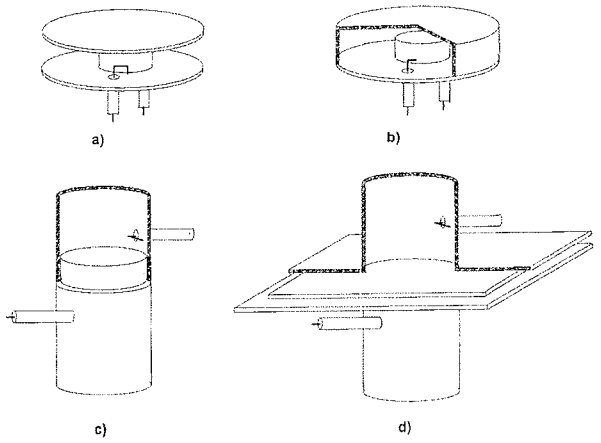

Slika 1: Nekatere najpogostejše konfiguracije testnih merilnih sklopov za določevanje mikrovalovnih dielektričnih lastnosti: a) Courtney-ev dielektrometer /2,3,4/, b) zaprti radialni dielektrometer /5/, c) Cohn-ov dielektrometer /6/ in d) merilni sklop za določevanje lastnosti substratov /7/

Pri merilnih sklopih, prikazanih na sliki 1, prihaja do napak pri merjenju dielektričnosti zaradi neidealnega stika med vzorcem in prevodno steno sklopa. Na takšnem stiku se namreč pojavijo zračne reže z znatno nižjo dielektričnostjo od dielektričnosti merjenega vzorca. Zaradi tega izmerimo prenizke dielektričnosti vzorcem, še posebej v primeru, ko je pri analiziranem rodu električna komponenta pravokotna na stično površino. Napako meritve lahko znatno zmanjšamo, če analiziramo resonančni odziv rodu, za katerega velja $E \cdot \underline{n} = 0$ na meji med vzorcem in steno merilnega sklopa. V primeru Courtney-evega dielektrometra /2-4/ to velja za $TE_{01}\delta$ rod, pri katerem ima električno polje le azimutalno komponento.

Uporabnost omenjenih metod omejuje dejstvo, da je določevanje faktorja kvalitete zelo zahtevno ter v večini primerov precej nenatančno. Zaradi bližine prevodnih sten se pojavijo precejšnje zunanje izgube, ki so posledica indukcije električnega toka v stenah ("skin effect"). Deloma lahko napako popravimo s preračunom na osnovi meritve dvakrat večjega vzorca iz istega materiala /4/, kar pa je zelo nepraktično, saj potrebujemo dva vzorca, meritev se časovno podaljša, ob tem pa tudi takšen pristop ne zagotavlja zahtevane natančnosti.

Tehnične karakteristike postavljenega merilnega sistema

Merilni sistem za merjenje mikrovalovnih dielektričnih lastnosti mora biti prilagojen raziskovalnemu ter razvojnemu delu, pri katerem so vzorci velikokrat, zaradi še neoptimiziranih pogojev termične obdelave, neidealnih oblik ter zelo različnih dielektričnosti. Merilni sistem mora omogočati tudi hitre rutinske kontrole mikrovalovnih lastnosti. Ker še ni izdelana potrebna standardizacija merilnih sistemov za določevanje mikrovalovnih lastnosti, je pomembno, da so rezultati čim manj obremenjeni z merilnim sklopom oziroma, da so čim bliže absolutnim vrednostim.

Metoda votlinskega resonatorja ("resonant cavity method") postaja vse bolj popularna za določevanje mikrovalovnih dielektričnih lastnosti keramičnih materialov, tako v industrijskih kot tudi v razvojnih in raziskovalnih laboratorijih. Napake meritev, ki se pojavljajo pri drugih metodah, so v tem primeru minimizirane oziroma jih je mogoče odpraviti z naknadno matematično obdelavo rezultatov.

V testni votlinski resonator cilindrične oblike je na nosilec nameščen dielektričen resonator iz preiskovanega materiala (Slika 2). Preko transmisijskih linij in sklopitvene zanke dielektričnemu resonatorju vzbujamo $TE_{01}\delta$ rod. Z analizo resonančnega odziva mu določimo resonančno frekvenco ter faktor kvalitete. Matematično takšno konfiguracijo opisuje Itoh-Rudokasov model /8/, na osnovi katerega lahko iz resonančne frekvence izračunamo dielektričnost preiskovanega materiala.

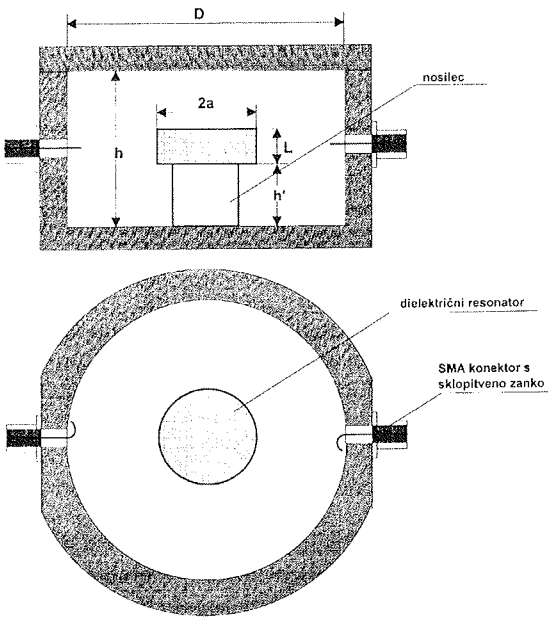

Slika 2: Merilni sklop pri metodi votlinskega resonatorja

Izbrana metoda votlinskega resonatorja je prilagojena meritvam vzorcev cilindrične oblike, vendar omogoča tudi dokaj natančne meritve vzorcev z nekoliko popačeno geometrijo, saj niso potrebni tesni stiki med merilnim sklopom in vzorcem. Z refleksijskim načinom merjenja lahko zelo natančno določimo faktor kvalitete ter resonančno frekvenco iz Smithove karte, za hitre rutinske meritve pa je primernejši transmisijski način, pri

katerem se faktor kvalitete določuje le iz širine resonančnega odziva.

Za generiranje in analizo elektromagnetnega valovanja uporabljamo mrežni analizator (HP8719C). Deluje v frekvenčnem območju med 50 MHz in 13.5 GHz. Standardno resolucijo mrežnega analizatorja (100 kHz) smo z vgradnjo opcijske enote 001 (HP86381A) izboljšali na 1 Hz. Takšna resolucija omogoča natančno analizo zelo ozkih resonančnih odzivov vzorcev z visokimi faktorji kvalitete (nad približno 5000 pri merjeni frekvenci). Mrežni analizator ima dva neodvisna kanala, preko katerih lahko opravljamo analize refleksijskih (S_{11}) ter transmisijskih (S_{12}) parametrov v logaritemski ali Smithovi karti. Za kalibracijo se uporablja 7 mm kalibracijski set (HP 850500). Mrežni analizator je preko 7 mm mikrovalovnih koaksialnih kablov (HP 85132, Zo = 50 Ω) ter 7 mm/3.5 mm adapterjev (HP 85130A/B) povezan s testnim votlinskim resonatorjem, v katerem je na teflonski nosilec nameščen vzorec. Testni votlinski resonatorji so narejeni iz medenine, površina pa je pozlačena. 3 mm SMA konektor, ki je pritrjen na vsakega od testnih resonatorjev, je povezan s pozlačeno sklopitveno zanko. Meritve resonančne frekvence in faktorja kvalitete izvajamo v testnih votlinskih resonatorjih šestih različnih velikosti. Uporabljamo testne resonatorje s premerom 20 mm (A), 27 mm (B), 37 mm (C), 50 mm (D), 68 mm (E) in 95 mm (F). Razmerje med višino in premerom (h/D) je pri vseh 0.6. Za meritve τf je mrežni analizator preko mikrovalovnega koaksialnega preklopnika (RLC Microelectronics, RF 1P6T, Model SR-6C-H) in valovodov povezan s testnimi votlinskimi resonatorji, nameščenimi v temperaturni komori (LABO, model Ultra 2000). Komora omogoča meritve v temperaturnem območju od -20°C do 100°C. Merilni sistem krmilimo z računalnikom preko vmesnika (HP 82335 HP-IB Interface).

Za ponovljive ter primerljive meritve je pomembno, da so delovni parametri meritve v vseh primerih enaki. Meritve izvajamo s 1601 merilnimi točkami na delovno frekvenčno območje. Moč vzbujevalnega signala je -50 dBm. Tako dosežemo zelo nizke izgube na prevodnih stenah sklopa, hkrati pa tudi dovolj visoko razmerje med signalom in šumom. Dodatno nivo šuma znižamo z zvišanjem selektivnosti sprejemnega kanala. Pred vsako meritvijo je bil sistem kalibriran s členom z odprtimi sponkami, s členom s kratko staknjenimi sponkami in s členom s karakteristično impendanco.

Izboljšava merilne tehnike na osnovi analize napake

Pri določevanju faktorja kvalitete dielektričnih resonatorjev pri resonančnih pogojih se pojavi problem zaradi obstoja EM polja nezanemarljive jakosti zunaj dielektričnega resonatorja. Zunanje EM polje lahko prodira v stene testnega votlinskega resonatorja, hkrati pa dodatne motnje polja povzročajo tudi sklopitvene zanke ter teflonski nosilec. Matematični model tako motenega polja ne opiše natančno, posledica tega pa je napačna določitev faktorja kvalitete ter dielektričnosti. Izmerjeni obremenjeni faktor kvalitete je praviloma nižji od neobremenjenega. Prav tako izmerimo tudi višjo resonančno frekvenco oziroma nižjo dielektričnost od dejanske.

Napaka meritve je manjša, če uporabimo večji testni votlinski resonator, vendar so v tem primeru lastne frekvence takšnega votlinskega resonatorja že tako nizke, da lahko pride do njihove sklopitve s $TE_{01\delta}$ rodom dielektričnega resonatorja ali celo do zamenjave rodov in zaradi tega do analize napačnega rodu. Navadno se meritve opravljajo s testnimi votlinskimi resonatorji, ki so tri do štirikrat večji od dielektričnega resonatorja. Pri dielektričnosti, višji od približno 20, takšno razmerje med velikostjo votlinskega in dielektričnega resonatorja zagotavlja, da je $TE_{01\delta}$ rod frekvenčno nižje od najnižjega resonančnega rodu testnega votlinskega resonatorja. Takšen položaj rodov omogoča hitro in zanesljivo identifikacijo $TE_{01\delta}$ rodu, vendar je napaka merjenja mikrovalovnih lastnosti pri takšni konfiguraciji znatna. Pri analizi napake smo uporabljali dielektrične resonatorje različnih dielektričnosti ter dimenzij. Manjše dielektrične resonatorje smo označili z oznako α, večje z oznako β, nizkodielektričnim resonatorjem smo pripisali indeks "low", visokodielektričnim pa indeks "high".

Pri določitvi ustreznega razmerja med višino in premerom (h/D) smo upoštevali položaje prvih dveh rodov votlinskega resonatorja (TM_{010} in TE_{111}). Prenizki testni votlinski resonatorji imajo lastne frekvence tako zgoščene, da je analiza $TE_{01\delta}$ rodu dielektričnega resonatorja pri frekvencah, višjih od resonančne frekvence TM_{010} rodu, onemogočena. Z višanjem razmerja h/D se frekvenčni interval med rodovoma zmanjšuje, hkrati pa, ob konstantni višini, postaja testni votlinski resonator primernejših dimenzij za praktično izvedbo meritev. Motnje v radialni smeri (ρ) so zanemarljive, saj se EM polje v tej smeri obnaša kot eksponentno upadajoča funkcija, ki jo najbližje ponazarja modificirana Besselova funkcija $K_1(k\rho)$ ($k \approx$ konstanta 2.404). Izračun na osnovi takšnega približka je pokazal, da je za vsa razmerja h/D od 0.4 do 0.8 EM polje na radialnih stenah vsaj za 106-krat nižje od tistega na površini dielektričnega resonatorja. Za meritve smo izbrali testne votlinske resonatorje z razmerjem h/D = 0,6. Pri takšnem razmerju je tudi pri velikih votlinskih resonatorjih frekvenčni interval med TM_{010} in TE_{111} rodovoma okoli 1 GHz širok, kar je dovolj za natančno analizo $TE_{01\delta}$ rodu dielektričnega resonatorja.

Faktor kvalitete in resonančno frekvenco vzorca α_{high} smo izmerili z uporabo testnih votlinskih resonatorjev A, B, C, D in E. Pri testnih votlinskih resonatorjih A, B, in C je bil $TE_{01\delta}$ rod dielektričnega resonatorja najnižja resonanca, pri nadaljnjem zvišanju velikosti votlinskega resonatorja (D in E) pa so bile nekatere lastne frekvence votlinskih resonatorjev nižje (Slika 3). V vseh primerih je bil $TE_{01\delta}$ dobro izoliran oziroma neskloplјen z ostalimi rodovi, kar je omogočilo njegovo natančno analizo. Pri votlinskem resonatorju F se je sklopitev pojavila, zato v tem primeru meritve ni bilo mogoče izvesti.

Sistematične meritve vzorca α_{high} so dokazale, da so izmerjene mikrovalovne dielektrične lastnosti odvisne od dimenzij testnega votlinskega resonatorja (Slika 4).

Pri večjih votlinskih resonatorjih so izmerjene resonančne frekvence znatno nižje kot pri manjših. Istočasno lahko opazimo tudi nižanje izmerjenega faktorja kvalitete. V primerjevi s faktorjem kvalitete izmerjenim v votlinskem resonatorju E, je faktor kvalitete, izmerjen v votlinskem resonatorju C (največjem, kjer je

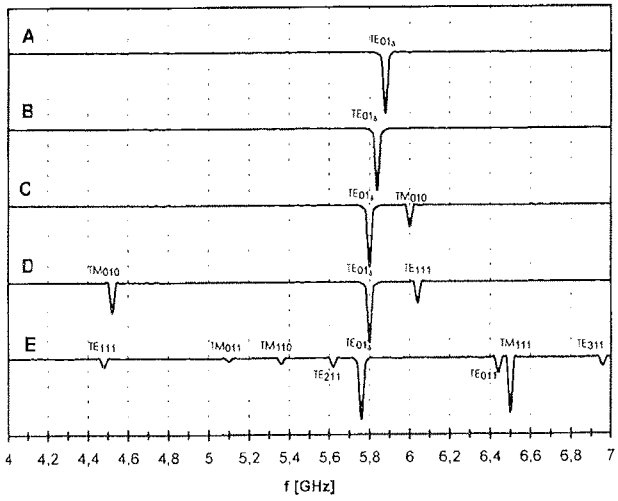

Slika 3: Shematski prikaz resonančnih rodov pri merjenju mikrovalovnih lastnosti vzorca α_{high} z različno velikimi testnimi votlinskimi resonatorji

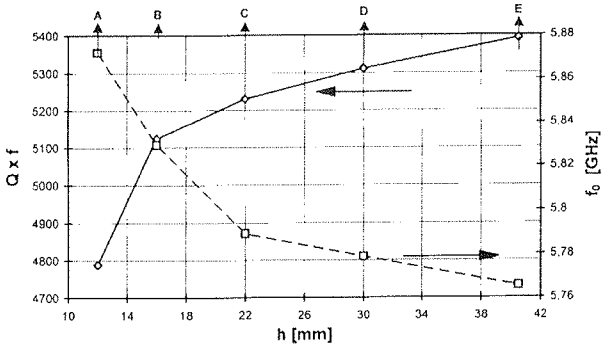

Slika 4: Izmerjene mikrovalovne dielektrične lastnosti vzorca α_{high} v odvisnosti od velikosti votlinskega resonatorja

resonančna frekvenca$TE_{01\delta}$ rodu še nižja od resonančne frekvence TM_{111} rodu), za približno 5% manjši. Dielektričnost je v tem primeru nižja za eno enoto.

Izmerjene mikrovalovne lastnosti vzorcev α_{low}, β_{high} in β_{low}, kažejo podobno odvisnost od velikosti testnega votlinskega resonatorja kot lastnosti vzorca α_{high}. Pri ovrednotenju $TE_{01\delta}$ rodu v primerih, ko je le-ta predstavljal najnižjo resonanco sistema, smo praviloma določili eno do dve enoti nižjo dielektričnost v primerjavi z meritvami, pri katerih je bila resonančna frekvenca $TE_{01\delta}$ rodu višja od najnižjih resonanc testnega votlinskega resonatorja. Hkrati smo izmerili tudi do 10% nižje vrednosti faktorja kvalitete.

Iz izmerjenih podatkov je razvidno, da je napaka pri meritvi mikrovalovnih dielektričnih lastnosti manjša, če uporabljamo večje testne votlinske resonatorje. Pri običajnem razmerju med velikostjo dielektričnega resonatorja in velikostjo testnega votlinskega resonatorja, takrat ko je resonančna frekvenca $TE_{01\delta}$ rodu nižja od resonančne frekvence TM_{010} rodu, je napaka meritve še vedno velika (cca. 10%). Potrebno je uporabiti še večje votlinske resonatorje, vendar pa je v tem primeru za zanesljivo identifikacijo $TE_{01\delta}$ rodu potreben natančen izračun lastnih frekvenc testnega votlinskega resonatorja z vstavljenim dielektričnim resonantorjem.

Izračun lastnih frekvenc testnega votlinskega resonatorja z vstavljenim dielektričnim resonatorjem

Lastne frekvence votlinskega resonatorja, homogeno zapolnjenega z medijem dielektričnosti ε in permeabilnosti μ, lahko izračunamo iz enačb:

$$\text{za } TM_{mnp} \text{ rodove } \omega_{mnp} = \frac{c}{\sqrt{\mu\varepsilon}}\sqrt{\frac{x_{mn}^2}{R^2}+\frac{p^2\pi^2}{d^2}} \qquad (1)$$

$$\text{za } TE_{mnp} \text{ rodove } \omega_{mnp} = \frac{c}{\sqrt{\mu\varepsilon}}\sqrt{\frac{x'^2_{mn}}{R^2}+\frac{p^2\pi^2}{d^2}} \qquad (2)$$

kjer je R polmer in h višina votlinskega resonatorja, c hitrost svetlobe, x_{mn} n-ti koren, x'_{mn} pa odvod n-tega korena Besselove funkcije m-tega reda /9/.

V primeru elektromagnetno nehomogenega testnega votlinskega resonatorja, ko so v resonančnem prostoru prisotni še sklopitvena zanka, teflonski nosilec in dielektrični resonator, enačbi (1) in (2) lastnih frekvenc ne opisujeta dovolj natančno. V primerjavi z izračuni so lastne frekvence takšnega testnega resonatorja premaknjene k nižjim vrednostim. Analitičen pristop k izračunu lastnih frekvenc testnega votlinskega resonatorja z vstavljenim dielektričnim resonatorjem bi lahko bil, ob upoštevanju vseh motenj EM polja, prezahteven in neprimeren za rutinsko uporabo med merjenjem. Da bi lahko vseeno izračunali lastne frekvence, smo razvili empirično metodo, ki je dovolj enostavna in natančna za uporabo.

Osnova za izračun sta enačbi (1) in (2), ki smo ju z dvema korekcijskima dodatkoma priredili obstoječemu problemu. Zaradi prisotnosti dielektričnega resonatorja, sklopitvene zanke ter teflonskega nosilca v resonančnem prostoru, le-ta ni več elektromagnetno homogen in zato konstanta ($\mu\varepsilon$) ne opisuje natančno njegovih elektromagnetnih lastnosti. Pri prvi korekciji smo konstanto ($\mu\varepsilon$) zamenjali s konstanto ($\mu'\varepsilon'$), ki opisuje elektromagnetne lastnosti nehomogenega medija. V enačbo smo uvedli še korekcijski faktor ν. Odvisen je od razmerja med volumnom testnega votlinskega resonatorja (V_{votl}) in volumnom vstavljenega dielektričnega resonatorja (V_{diel}).

Tabela I: Izmerjene in izračunane lastne frekvence testnih votlinskih resonatorjev z vstavljenim dielektričnim resonatorjem

	TM_{010} (GHz)			TE_{111} (GHz)			TM_{110} (GHz)		
	izmerjen	izračunan	rel.nap. (%)	izmerjen	izračunan	rel.nap. (%)	izmerjen	izračunan	rel.nap. (%)
$B\alpha_{low}$	8,035	8,094	0,73	10,487	10,411	-0,72	12,654	12,803	1,18
$C\alpha_{low}$	6,096	6,122	0,43	8,067	8,033	-0,42	9,539	9,713	1,82
$D\alpha_{low}$	4,541	4,568	0,59	6,034	5,998	-0,57	7,184	7,235	0,71
$E\alpha_{low}$	3,362	3,334	-0,83	4,481	4,518	0,83	5,374	5,357	-0,32
$C\alpha_{high}$	5,987	5,976	-0,18	7,875	7,889	0,18			
$D\beta_{low}$	4,171	4,164	-0,17	5,285	5,294	0,17			
$D\beta_{high}$	3,938	3,941	0,08	5,002	4,998	-0,08			

Enačbi za izračun lastnih frekvenc testnega votlinskega resonatorja z vstavljenim dielektričnim resonatorjem je z upoštevanjem obeh korekcij mogoče zapisati:

za TM_{mnp} rodove

$$\omega_{mnp} = \frac{c}{\sqrt{\mu'\varepsilon'}}\sqrt{\frac{x_{mn}^2}{R^2}+\frac{p^2\pi^2}{d^2}}\times(1+\nu) \qquad (3)$$

za TE_{mnp} rodove

$$\omega_{mnp} = \frac{c}{\sqrt{\mu'\varepsilon'}}\sqrt{\frac{x'^2_{mn}}{R^2}+\frac{p^2\pi^2}{d^2}}\times(1-\nu) \qquad (4)$$

Konstanta $(\mu'\varepsilon')^{1/2}$ ima navadno vrednosti med 1 in 1,4. Njene vrednosti nismo poskušali izračunati neposredno, temveč posredno s pomočjo znane ω_{mnp} iz enačb (3) oziroma (4). Med merjenjem lahko namreč zanesljivo identificiramo vsaj enega od prvih dveh rodov testnega votlinskega resonatorja. Če je $TE_{01}\delta$ v bližini TM_{010} rodu, uporabimo za izračun konstante $(\mu'\varepsilon')^{1/2}$ resonančno frekvenco TE_{111} rodu, če je $TE_{01}\delta$ rod v bližini TE_{111} rodu, pa resonančno frekvenco TM_{010} rodu.

Velikost korekcijskega faktorja ν smo določili empirično:

$$\nu = \left(\frac{V_{diel}}{V_{votl}}\right)^{0,83} \qquad (5)$$

Napaka takšnega empiričnega izračuna lastnih frekvenc testnega votlinskega resonatorja z vstavljenim dielektričnim resonatorjem je pri vseh preverjenih resonančnih konfiguracijah za TM_{010} in TE_{111} rodove manjša od ±101% (Tabela I). Pri višjih rodovih je napaka nekoliko večja, vendar takšen matematični postopek vseeno omogoča nedvoumno identifikacijo vseh rodov. Ta postopek smo uporabili med drugim tudi za identifikacijo rodov pri meritvi vzorca α_{high}, kar je prikazano na sliki 3.

Zaključek

Celoten postopek merjenja mikrovalovnih dielektričnih lastnosti z metodo votlinskega resonatorja lahko razdelimo na posamezne stopnje. Če ne poznamo približne vrednosti resonančne frekvence merjenega vzorca, začnemo meritev z majhnim testnim votlinskim resonatorjem, pri katerem so lastne frekvence dovolj visoko, da je $TE_{01}\delta$ rod nedvoumno najnižja resonanca. Ko je približna resonančna frekvenca znana, lahko uporabimo testni votlinski resonator, pri katerem je $TM_{010} < TE_{01}\delta$. Za zanesljivo identifikacijo $TE_{01}\delta$ rodu z opisanim postopkom izračunamo lastne frekvence takšne resonančne konfiguracije ter nato iz $TE_{01}\delta$ rodu dielektričnega resonatorja določimo faktor kvalitete in dielektričnost vzorca. Opisan pristop k analizi mikrovalovnih dielektričnih lastnosti omogoča meritev faktorja kvalitete z natančnostjo ±2% in dielektričnostjo ±0.5%.

Literatura

/1/ D. KAJFEZ, P. GUILLON, "Dielectric Resonator", Artech House, Inc., Dedham, 1986

/2/ W.E. COURTNEY, "Analysis and Evaluation of a Method of Measuring Complex Permittivity and Permeability of Microwave Insulators", IEEE Trans. MTT, MTT-18, 1970, 476-485

/3/ D. KAJFEZ, W.P. WHELEES, Jr, R.T. WARD, "Influence of an Air Gap on the Measurement of Dielectric Constant by a Parallel Plate Dielectric Resonator", IRE Proc., 133, (4), 1986, 211-218

/4/ B. W. HAKKI, P.D. COLEMAN, "A Dielectric Resonator Method of Measuring Inductive Capacities in the Millimeter Range", IEEE Trans. MTT, MTT-8, 1960, 402-410

/5/ Y. KOBAYASHI, M. KATOH, "Microwave Measurement of Dielectric Properties of Low-Loss Materials by the Dielectric Rod Resonator Method", IEEE Trans. MTT, MTT-33, 1985, 586-592

/6/ S.B. COHN, K.C. KELLY, "Microwave Measurement of High Dielectric Constant Materials", IEEE Trans. MTT, MTT-14, 1966, 406-410

/7/ G. KENT, "A New Method for Measuring the Properties of Dielectric Substrates", Int. Microwave Symposium Digest, 1987, 751-755

/8/ T. ITOH, R.S. RUDOKAS, "New Method for Computing the Resonant Frequencies of Dielectric Resonator", IEEE Trans. MTT, MTT-8, (1), 1977, 52-54

/9/ J.D. JACKSON, "Classical Electrodynamics", John Wiley & Sons, New York, ZDA, 1975, 334-389

Dr. M. Valant, dipl. ing.
Dr. D. Suvorov, dipl. ing.
S. Maček
Institut "Jožef Stefan"
Jamova 39, 1000 Ljubljana, Slovenija
tel.: +386 (0)61 177 39 00
fax: +386 (0)61 219 385

Prispelo (Arrived): 10.03.1996 *Sprejeto (Accepted): 24.03.1996*

AES CHARACTERIZATION AND ANALYTICAL DESCRIPTION OF POTASSIUM MIGRATION IN MICROCHANNEL PLATES MULTILAYERS

Prepared from poster presentation on the 4th European Vacuum Conference (EVC-4) and 1st Swedish Vacuum Meeting (SVM) in Sweden, Uppsala, 13-17 june 1994

B. Praček, M. Mozetič and M. Drobnič*
Institute of Surface Engineering and Optoelectronics, Ljubljana, Slovenia
* J. Stefan Institute, Ljubljana, Slovenia

Keywords: optoelectronics, MCP, microchannel plates, AES depth profiling, Auger electron microscopy, electrodiffusion migration, electrodiffusion, Goldhorn software packages, potassium chemical elements, multilayer structures, analytical descriptions

Abstract: The nature of potassium migration through the active multilayers structure of microchannel plates (MCP) was determined. Comparing the variation of Auger signal for K (252 eV) through a fresh and aged sample showed that a few surface monolayers of the aged sample are relatively rich in potassium what is indicative of K migration from the underlying layers to the surface. Data on the potassium migration onto active intrachannel surface and migration of K through the underlying layers were obtained with the AES method and analyzed using the Goldhorn software package. The analyses with the Goldhorn software package gave us the analytical description of AES measurements.

AES karakterizacija in analitičen opis gibanja kalija skozi plasti mikrokanalnih ploščic

Pripravljeno po posterski predstavitvi na 4. Evropski vakuumski konferenci (EVC-4) in 1. švedskem vakuumskem srečanju (SVM) na Švedskem, Uppsala, 13-17 junij 1994

Ključne besede: optoelektronika, MCP ploščice mikrokanalske, AES Auger spektroskopija elektronska - profiliranje globinsko, selitev elektrodifuzijska, elektrodifuzija, Goldhorn paketi opreme programske, K kalij elementi kemični, strukture večplastne, opisi analitični

Povzetek: Določana je bila narava gibanja kalija skozi večplastno strukturo mikrokanalnih ploščic (MKP). Primerjava spreminjanja intenzitete Augerjevega vrha K (252 eV) v plasteh svežega in staranega vzorca pokaže, da se v nekaj monoplasti površine staranega vzorca nahaja povečana vsebnost K. Primerjava nazorno nakaže, da gibanje K poteka iz spodaj ležečih plasti proti površini. Podatke o gibanju K iz globine proti površini notranjih sten kanalov smo dobili z AES profilno analizo. Obdelava tako dobljenih podatkov s pomočjo Goldhorn programske opreme je podala analitičen opis AES meritev.

1. INTRODUCTION

The active intrachannel surfaces in MCP s' or the surfaces lining the walls of the channel are composed of a few surface monolayers, the superficial about 20 nm thick silica-rich emitting layer, about 10 nm thick buffer layer and the underlying about 100-1000 nm thick semiconducting layer. The MCP layers composition is presented in Figure 1. All these layers are formed during the final stages of the manufacturing. Normally characterized by a decrease in channel gain, the ageing process is necessary to ensure a stable operation and minimum outgassing. The ionic migration on the active glassy surface and silica-rich emitting layer changed the elemental distribution of these layers during the ageing process (electron scrubbing). To characterize the essential differences in the elemental distribution of the glassy layers of the fresh and aged MCP s', AES sputter depth profiling through the 60 nm thick channel wall was applied. Comparing the variation of Auger signal for K (252 eV) through a fresh and aged sample shows that a few surface monolayers of the aged sample are relatively rich in potassium what is indicative of potassium migration from the underlying layers to the surface. Data on the potassium migration onto the active intrachannel surface in MCP s' and migration of K through the underlying layers were obtained with the AES method and analyzed using the Goldhorn software package. The analysis gave us the analytical description of the measurements.

2. EXPERIMENTAL

Two microchannel plates were investigated. The first was examined before and the second after ageing (electron scrubbing). Both samples were analyzed with a Scanning Auger Microprobe (Physical Electronics Industries SAM 545 A). A static primary electron beam of 5 keV energy, 0.3 μA beam current and a 10 μm diameter was used. The electron beam incidence angle with respect to the normal to the average surface plane was 30°. The both samples were ion sputtered with two symmetrically inclined beams of 1 keV Ar^+ ions, rastered over a surface area larger than 5 mm x 5 mm at

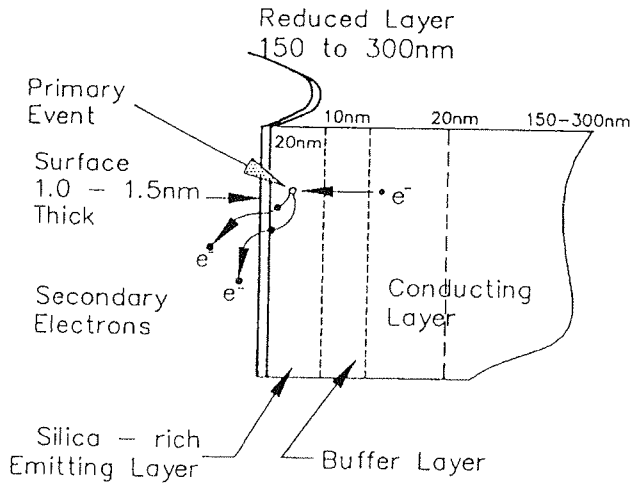

Fig.1: Microchannel wall cross-section

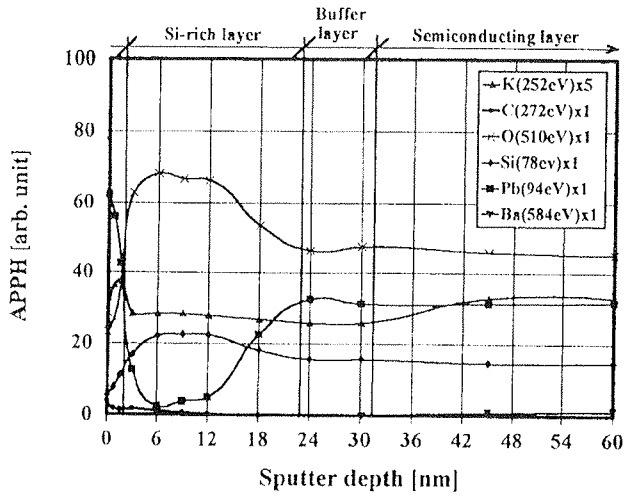

Fig. 2: AES sputter depth profiles of the important elements in the active surface of the channel before ageing of the MCP. The measured peak-to-peak intensity is normalized to the corresponding pure elemental target value which is set at 100.

an incidence angle of 47°. The sputter rate of about 3 nm/min for the MCP glass is assumed to be equal to that for SiO_2 and was determined on a standard multilayer Ni/Cr/SiO_2/Ni/Cr/<Si>. During simultaneous AES analysis and ion sputtering the Auger peak-to-peak intensities of Si(78 eV), Pb(94 eV), K(252 eV), C(272 eV), O(510 eV) and Ba(584 eV) were recorded against the sputtering time. In the depth profiles the peak-to-peak intensities of the corresponding Auger transition are normalized to the pure elemental sample value which was equated to 100 units.

3. RESULTS AND DISCUSSION

3.1. AES sputter depth profiles of intrachannel glassy layers

Fresh and aged microchannel plates were investigated by AES sputter depth profiling. Depth profiles of the elemental composition of both investigated active intrachannel glassy layers are similar and reveal the presence of the glass constituent elements: Si, O, K, Pb, Ba and C. The depth distribution of six main constituents of the unexposed sample is shown in Figure 2. The surface is composed of Pb, O, Si, K and C namely. The concentration of Pb is very high on the surface, while in a layer about 10 nm under surface the Pb concentration is considerably reduced. Deliberately and consequently this layer is enriched with Si and O. On the surface and in the underlying conducting layer the K concentration is almost the same, except for 1.5 nm beneath the surface, where a sudden increase of K concentration was observed. The quantity of C on the surface presents a relatively low contamination and its concentration decreases quickly to negligible amounts. The presence of Ba was observed in a depth of about 35 nm beneath the surface, and its content increases slowly in the bulk material. The distribution of the present element versus sputter depth of the exposed sample (Figure 3) shows that on the surface K concentration is rather increased, while the Pb concentration is significantly reduced, and C contamination seems to be higher in comparison to the unexposed sample. The thin silica-rich layer beneath the surface of the aged sample is enriched with Pb, and in the same layer the decrease concentration of K, Si, and O was observed. We found out that particles migration through the active glassy layers changed the elemental distribution, especially for K and Pb of these layers during the ageing process. The comparison of AES depth profiles shows a great increase in content of K, significantly reduced content of Pb and a minor reduction in that of Si and O on the intrachannel surface of the aged MCP. In the silica-rich emitting layer the empty places left by K, Si, and O, are replenished with Pb.

3.2. The variation in potassium Auger signal with ageing process

After the ageing process the concentration of potassium on the surface increased substantially, while the concentration in underlying about 20 nm thick silica rich layer decreased to about half of the original value compared to the unexposed sample. The concentration of potassium in the semiconducting layer of the intrachannel wall remained practically unchanged. We were interested in the major process occuring on during the ageing. To that end, the AES data were analyzed by the use of the Goldhorn software package, which has been developed recently /3/. One of the unique package features is not only to fit a curve through points, but also to finds a differential equations governing the process under investigation. The AES data shown in Figure 4, together with those of lead (Pb), were therefore processed with a computer. After an extensive computation

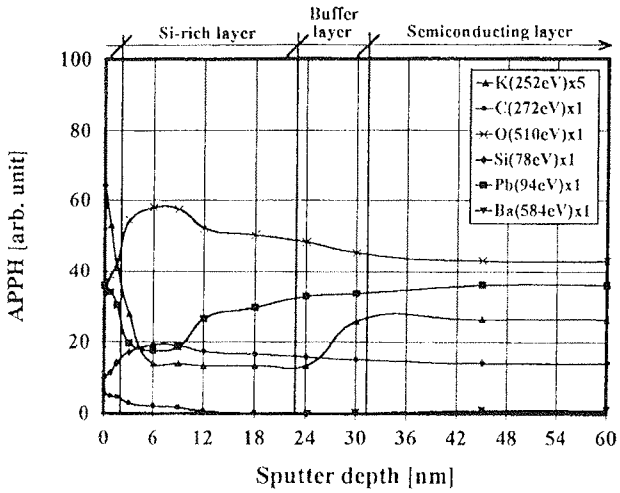

Fig. 3: As figure 2, but now after ageing of the MCP

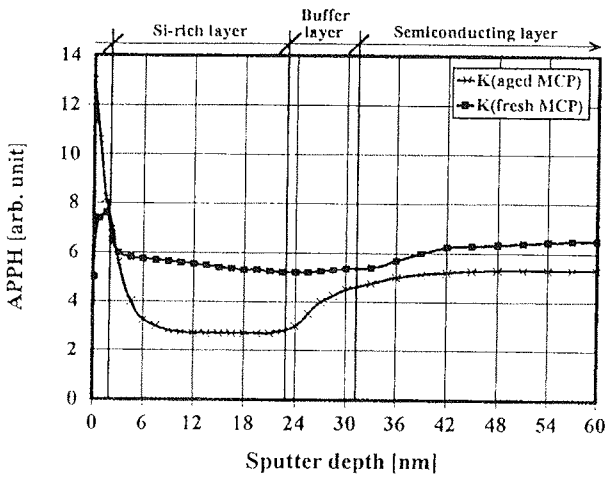

Fig.4: The variation in Auger peak-to-peak intensity for potassium without and with ageing process

it was found that the final distribution of potassium an lead follows differential equation

$$\nabla^2 C_K \left(a \frac{dC_K}{dx} + bC_K + cC_{Pb} + d \right) = e$$

Here, C_K and C_{Pb} are concentration of potassium and lead, respectively, ∇ is the nabla operator, $\frac{dC_K}{dx}$ is the gradient of the potassium concentration, a,b,c,d and e are constants, which were also computed by the Goldhorn package, and have the values -0.51, +1.38, -1.00, +15.31, and +0.48, respectively. The degree at which the equation fits the observed distribution of potassium is excellent, since the R factor is less than 0.01.

4. CONCLUSION

The differential equation computed by the Goldhorn software package has the same form as the theoretical equation for the distribution of particles suffering of electrodiffusion migration. Therefore, it can be concluded that the only process going on during the ageing procedure is pure electrodiffusion, since if any other machanisms of migration of potassium were presented the diffferential equation computed by the Goldhorn software package would have consisted of additional terms of a higher order.

5. REFERENCES

/1/ W B Feller, Proc SPIE 1243 (1990) 149

/2/ B N Laprade, S T Reinhart and M Wheeler, Proc. SPIE 1243 (1990) 162

/3/ V Kri'man, M Sc Thesis, University of Ljubljana, Ljubljana (1993)

B. Praček, dipl. ing.
mag. M. Mozetič, dipl. ing.
Institute of Surface Engineering and Optoelectronics
Teslova 30, 1000, Ljubljana, Slovenia
Tel.: +386 (0)61 126 45 92
Fax: +386 (0)61 126 45 93
Mag. M. Drobnič
Jozef Stefan Institute
Jamova 39, 1000 Ljubljana, Slovenia

Prispelo (Arrived): 19.03.1996 Sprejeto (Accepted): 24.03.1996

UPORABA PLAZME V ELEKTRONIKI
APPLICATION OF PLASMA IN ELECTRONICS

PLASMA PROCESSES

PART I: PLASMA BASICS, PLASMA GENERATION

I. Šorli*, W. Petasch, B. Kegel, H. Schmid, G. Liebl
*MIKROIKS d.o.o., Ljubljana, Slovenia
Technics Plasma GmbH, Kirchheim, Germany

Applications of plasma processes are becoming increasingly popular in many industrial and research communities. Electronics, microelectronics, automotive, aircraft, and food industry are among the most frequent plasma users. This is not surprising if we consider e.g. the field of cleaning applications. There, plasma cleaning or plasma combined with some suitable wet precleaning technique can totally replace CFC and some other toxic cleaning agents.

The first article describes basic plasma physics and plasma generation while the second focuses mainly on application of plasma in R&D and industrial processes.

Technics Plasma GmbH in Kirchheim, Germany is among the pioneers and leaders in plasma technology and its application in academic and industrial environments. We will focus mainly on their systems and give an overview of successful applications of their machines and processes in different environments.

1.0 INTRODUCTION

A plasma is a gas containing charged and neutral species, including some or all of the following: electrons, positive ions, negative ions, neutral atoms in ground and excited states, neutral molecules in ground and excited states, radicals and photons. On average a plasma is electrically neutral, because any charge imbalance would result in electric fields that would tend to move the charges in such a way as to eliminate the imbalance.

An important parameter of a plasma is the degree of ionization, which is the fraction of the original neutral species (atoms and/or molecules) which have been ionized. In weakly ionized plasmas the degree of ionization is much smaller than unity and the presence of large population of neutral species governs its behaviour. Most of the plasmas that we will be dealing with are weakly ionized.

To form and sustain a plasma some energy source is necessary to produce the required ionization. In steady state, the rate of ionization must balance the losses of ions and electrons from the plasma volume by recombination and diffusion or convection to the boundary of the plasma and the surrounding walls.

Plasmas are usually initiated and sustained by electric fields which are produced either by direct current (DC) or alternating current (AC) power supplies. Typical AC frequencies of excitation are 100 kHz, at the low end of the spectrum, 13.56 MHz in the radio frequency (RF) portion of the spectrum, and 2.45 GHz in the microwave region. These plasmas are also referred to as electric discharges, gaseous discharges, or glow discharges (the latter because they emit light).

In figure 1, a generic plasma reactor for thin film etching and deposition is depicted. A power source supplies energy to the main plasma discharge where reactive species and ions are generated. These species are transported to the substrate for etching or deposition. In many configurations, depending also on the excitation freguency, there is an electric field in the vicinity of the substrate which accelerates the ions.

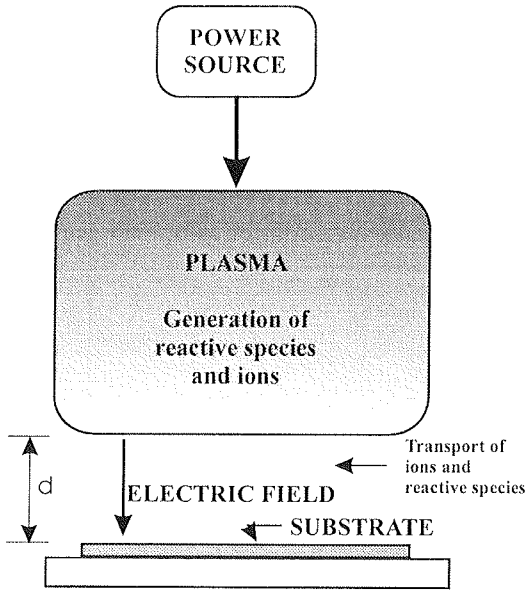

Figure 1: Generic plasma reactor

As we shall see later, electrons play the most important role in plasmas. It is useful to characterize plasma in terms of electron densities and electron energies. In a number of cases electrons have Maxwellian energy distribution if they are in thermodynamic equilibrium:

$$f(\varepsilon) = \frac{2\varepsilon^{1/2}}{\pi^{1/2}(kT)^{3/2}} \exp\left(-\frac{\varepsilon}{kT}\right) \quad (1)$$

$f(\varepsilon)$ is the electron energy distribution function (EEDF) and T the electron temperature

Average electron energy is related to the temperature and is calculated as

$$\int \varepsilon f(\varepsilon) d\varepsilon = \langle \varepsilon \rangle = \frac{3}{2} kT \quad (2)$$

Electron energies are usually expressed in eV. 1 eV is equivalent to the temperature of approximately 11600 K while energy of 0.025 eV corresponds to the electron average temperature of 300 K.

In figure 2, typical values of electron densities and temperatures are shown for a variety of plasmas. They range from the very rarified and cold interstellar plasmas up to the dense and hot plasmas used for controlled fusion. The plasmas of interest here are the process plasmas, which have electron densities in the range of 10^9 to 10^{12} cm^{-3} and average electron energies between 1 and 10 eV. The degree of ionization for these plasmas varies from about 10^{-6} up to 0.1. At the lower end of the density, energy, and ionization scale are the discharges that are formed between planar electrodes, while the upper end of this scale applies to discharges sustained at a frequency that corresponds to some natural frequency for the plasma (such as electron cyclotron resonance (ECR) plasmas).

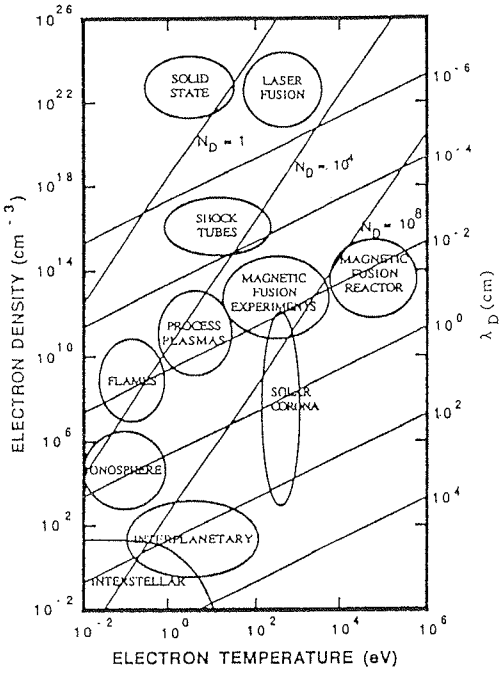

Figure 2: Electron density and temperature ranges for a variety of natural and man made plasmas.

The extensive use of plasmas for the deposition and etching of thin films derives from two salient features. Firstly, plasmas are capable of efficiently generating chemically active species.This is initiated by the bombardment of molecules and atoms by the plasma electrons, which have sufficient energy to break chemical bonds. The products of the electron bombardment processes which include radicals and ions, can undergo further reactions often at high rates, to form additional chemically reactive species. Radicals are very important for processes to be performed in plasmas. A radical is an atom, or electrically neutral molecule which is in a state of incomplete chemical bonding with highly increased reactivity. Some typical examples of radicals include F, Cl, O, H and CF_x,where x= 1,2 or 3. In general, radicals are thought to exist in plasmas in much higher concentration than ions, because they are generated at a faster rate, and they exist longer than ions in the plasma. The radicals, in fact, are responsible for most of the actual chemical etching phenomena that occur at the surface of the material being treated.

The second feature that makes plasma discharges so useful is their ability to generate ions and to accelerate these ions to energies of 50-1000 eV in the vicinity of the deposition or etching substrate.Energetic ions are useful for sputtering, as well as play sinergetic role in the deposition or etching of thin films.

To summarize, the gas in a plasma chamber when there is a plasma generated, generally consists of the following species, in order of decreasing concentration, and estimated concentration ranges:

- (etch) neutral gas molecules: 70-98 % of the total species in the chamber
- product molecules: 2-20 %
- radicals: 0.1-20 %
- charged species including positive ions, electrons and negative ions: 0.001-10 %

2.0 COLLISION PROCESSES

Collision processes among different types of particles are responsible for forming and sustaining plasma. Through collisions the particle kinetic energy is used up to create radicals, ions, excited atoms/molecules and photons.

2.1 ELASTIC AND INELASTIC COLLISIONS

Collision processes can be broadly divided into elastic and inelastic types according to whether the internal energies of the colliding bodies are maintained. Single particles usually have two types of energy: kinetic due to their motion and equal to 1/2 mv^2 for translational motion and internal or potential energy which may be in the form of electronic excitation and/or ionization, etc. (and in the case of molecules also in the form of vibrational as well as rotational internal energies).

An elastic collision is one in which there is an interchange of kinetic energy only. An inelastic collision has no such restriction, and internal energies can also change.

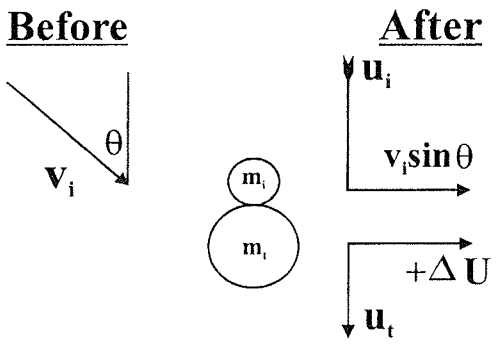

Figure 3: Collision between two particles

Refering to the figure 3, we can write the following GENERAL equation for energy transfer from incoming particle to the target particle:

$$\frac{1/2\, m_t u_t^2}{1/2 m_i v_i^2} = \frac{m_t u_t^2}{m_i}\left(\frac{2m_t u_t}{\frac{m_t}{m_i}(m_t + m_i)u_t^2 + 2\Delta U}\right)^2 \qquad (3)$$

and inelastic energy transfer function, which measures the portion of kinetic energy of the incoming particle transferred to the internal energy of the target atom (ΔU) is defined as

$$\frac{\Delta U}{1/2 m_i v_i^2} = \frac{m_t}{m_t + m_i}\cos^2\theta \qquad (4)$$

m_i, m_t: masses of incoming and target particles

v_i, u_t: velocities of incoming and target particles

ΔU: gained internal energy by target particle

Putting ΔU = 0 brings us to the elastic collision case where maximum energy transfer for head on collision is given by the equation:

$$\frac{1/2 m_t u_t^2}{1/2 m_i v_i^2} = \frac{4 m_i m_t}{(m_i + m_t)^2} \qquad (5)$$

We see that light impact particles (like electrons, $m_i << m_t$) can transfer only very small portion of kinetic energy to the kinetic energy of heavy ion, atom or a gas molecule. However in this case electron's momentum changes very much. On the other side elastic collisions of heavy ions, atoms or gas molecules among themselves always lead to overall equalization of kinetic energies, since having $m_i \approx m_t$, elastic energy transfer function is equal to 1!

In case of inelastic collision the situation is quiet different. Equation (4) predicts that a light particle striking much heavier particle ($m_i \approx m_t$) can transfer almost all of its kinetic energy into particle's internal energy and inelastic energy transfer function tends to 1!

2.2 THE MAIN COLLISION PROCESSES

As already mentioned a glow discharge contains many different particles. In principle we should consider collisions between all possible pair permutations, but fortunately some collisions are more important than others. Collisions involving electrons are dominant in determining the macroscopic behaviour of the glow discharge that is why we will describe them in more detail.

Electron - atom elastic collisions

The simplest collisions are elastic so that kinetic energy is conserved. But since the electron and any atom (molecule) have such different masses, we know that the transfer of energy is negligible, so electron just changes direction without significantly changing its speed, figure 4. If an electron is moving in an electric field, elastic collisions generally have the effect of restricting its velocity in the direction of the field. In both cases, the colliding atom is virtually unaffected.

As an example cross section for elastic scattering of electron in argon at 15 eV is about $2.5 \cdot 10^{-15}$ cm^2. So at 10 mtorr (0.013 mbar) when there are $3.54 \cdot 10^{14}$ atoms/cm^3 , the probability of elastic collision of a 15 eV electron is about 0.9/cm.

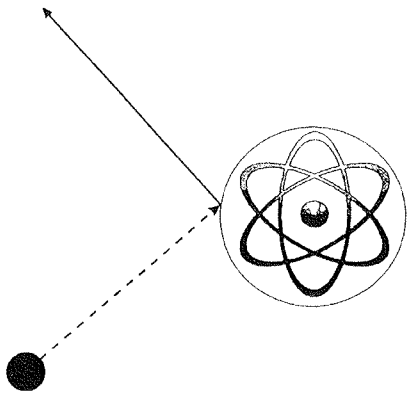

Figure 4: electron - atom elastic collision: no energy transfer - only electron momentum changes

Ionization

All other types of electron collisions are inelastic. The most important of these in sustaining the glow discharge is *electron impact ionization*, figure 5 in which the primary electron removes an electron from the atom, producing a positive ion and two electrons, for example

$$e + Ar \rightarrow 2e + Ar^+ \qquad (6)$$

The two electrons produced by the ionization collision can then be accelerated by an electric field until they, too, can produce ionization. **It is by this multiplication process that a glow discharge is maintained.**

There is minimum energy requirement for this ionization process to occur, equal to the energy to remove the most weakly bound electron from the atom, and this is

known as the ionization potential. For xenon this has a value of 12.08 eV, and for argon 15.8 eV. However, it is not only by electron impact that ionization is produced. In principle, ionization could be due to any suitable energy input, and the possibilities in the discharge must therefore include thermal and photon activation. Thermal activation means energy received by impact with neutral ground state atoms or with the atoms of the walls. For our "cold" plasmas, the temperature does not greatly exceed ambient so thermal activation is very unlikely.

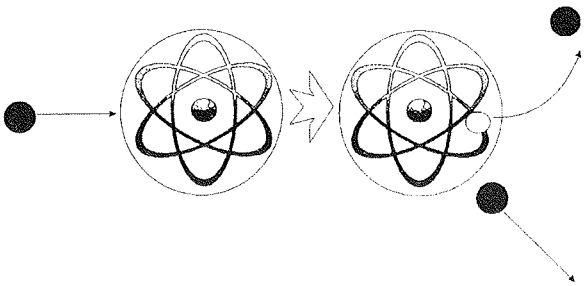

Figure 5: electron - atom inelastic collision causing ionization

Photoionization can be significant, however. Argon photoionization cross section rises to maximum of $2.6 \cdot 10^{-16}$ cm^2 and then falls down with energy. But at higher energies this does not necessarily mean that there is very little ionization since after photoionization the free electron receives excess photon energy in the form of kinetic energy and is capable of further ionization by itself; as well the hole left in the atom electron shell after ionization will be filled with another electron transition from a higher level and the accompanying photon emission usually causes more ionization - and hence the ejection of more electrons - on its way out of the atom (the Auger effect is an example). Similar arguments can be used to explain photoelectron emission from chamber walls and all internal surfaces, including electrodes. As a result one would expect a large proportion of photon energy to lead ultimately to ionization.

Excitation

In the ionization process, a bound electron in an atom is ejected from that atom. A less dramatic transfer of energy to the bound electron would enable the electron to jump to a higher energy level within the atom with a corresponding quantum absorption of energy. This process is known as an *excitation*, and as with ionization, can result from electron impact excitation, photoexcitation, or thermal excitation, although the latter is rare in our "cold" plasmas, figure 6.

The excited state is conventionally represented by an asterisk superscript, e.g. Ar*. As with ionization, there is minimum energy for excitation to occur. The value of the excitation potential for argon is 11.56 eV, somewhat less than the ionization potential, as would be expected since excitation raises an electron to a higher (less bound) shell, and ionization completely removes the electron from the atom. In an exciting collision the primary electron loses kinetic energy equal to the excitation potential and will also be deflected.

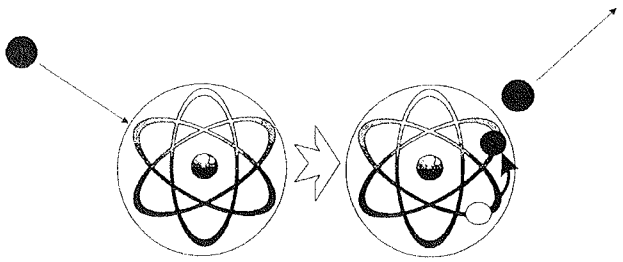

Figure 6: inelastic collision process that results in excitation of an atom

Atomic hydrogen excitation potential threshold is 10.2 eV, while molecular hydrogen excitation potential threshold is much lower - below 0.5 eV - due to the possibilities of vibrational and rotational excitations as discussed earlier.

Relaxation

One of the immediately self-evident features of the glow discharge is that it glows! This glow is due to the relaxation or de-excitation of electronically excited atoms and molecules - the inverse of the excitation process just discussed.

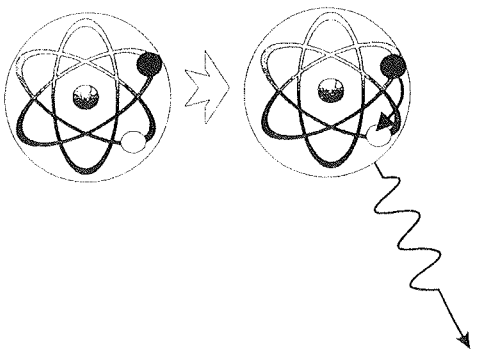

Figure 7: Relaxation (or de-excitation)

These excited states are rather unstable and the electron configuration soon returns to its original (ground) state in one or several transitions, with lifetimes varying enormously from nanoseconds to seconds, figure 7.

Each transition is accompanied by the emission of a photon of very specific energy, equal to the difference ΔE in energy between the relevant quantum levels. Our eyes are sensitive only to wavelengths between about 4100 Å (violet) and 7200 Å (red), corresponding to

electron transitions of 3.0 eV and 1.7 eV respectively, but with suitable detection equipment, photons from deep UV (atomic transitions) to far infra red (molecular vibrational and rotational transitions) can be detected.

As an example, in table 2, we present a list of light wavelengths emitted by excited reactants or products in plasmas typically used for etching and cleaning. Atoms and molecules emit a series of spectral lines which are unique to each species and thus can be used for end point detection purposes or plasma characterization.

Table 2: Species and emission wavelengths when etching different films

FILM	SPECIES	WAVELENGTH (nm)
Resist	CO	297.7, 483.5, 519.8
	OH	308.9
	H	656.3
Silicon, Polysilicon	F	704
	SiF	777
Silicon Nitride	F	704
	CN	387
	N	674
Aluminum	AlCl	261.4
	Al	396

Dissociation

The process of dissociation is the breaking apart of a molecule. An oxygen molecule can be dissociated into two oxygen atoms, but an atomic gas such as argon cannot be dissociated at all.

As with the other inelastic processes we have been studying, dissociation can in principle be accomplished with any energy in excess of the dissociation threshold, i.e. the relevant bond strength in the molecule. In glow discharges, electron impact dissociation is common:

$$e + O_2 \rightarrow e + O + O \qquad (7)$$

A normal result of dissociation is an enhancement of chemical activity since the products are usually more reactive than the parent molecule.

Dissociation may or may not be accompanied with ionization:

$$e + CF_4 \rightarrow e + CF_3 + F \text{ (dissociation)} \qquad (8)$$

$$e + CF_4 \rightarrow 2e + CF_3^+ + F \text{ (dissociative ionization)} \qquad (9)$$

There are different probabilities and hence different cross sections, for each of these processes.

Electron attachment

There is a possibility that an electron colliding with an atom may join on to the atom to form a negative ion. This process is known as electron attachment. The noble gases, including argon, already have filled outer electron shells and so have little or no propensity to form negative ions. Halogen atoms, however, have an unfilled state in their outer electron shells; they have high electron affinities and so readily form negative ions.

2.3 ION - NEUTRAL COLLISIONS

Charge transfer

The probability of a collision leading to the exchange of charge, generically known as charge transfer, is usually greater for atomic ions moving in parent atoms (symmetrical resonant charge transfer), e.g.

$$A + A^+ \rightarrow A^+ + A \qquad (10)$$

or similarly for molecular ions moving in parent molecular gases, than in charge exchange between unlike systems, e.g.:

$$B^+ + C \rightarrow B + C^+ \qquad (11)$$

which is known as assymetric charge transfer and tends to be less efficient.

Ionization by ion impact

Just as ionization can be produced by photon bombardment, so it can also be produced by fast ion or fast atom bombardment, provided the incident particles have enough energy.

3.0 PLASMA GENERATION

In the introduction we have briefly mentioned that plasma is usually produced by DC or AC electric field from which charged particles absorb energy in the form of kinetic energy. Then by inelastic collision processes they transform it into internal energy of neutral atoms or molecules finally producing plasma consisting of different neutral, excited, charged particles, radicals and photons.

The energetic electrons are responsible for most of the ionization, which produces additional electrons and ions to sustain the discharge against the various loss processes.

Since charged particle - electric, or magnetic field interaction is so important, we will describe it in more detail having always in mind their influence on macroscopic plasma behaviour.

Interaction of electrons with a static electric field

In a static electric field an electron experiences the following force which causes change of its momentum:

$$\vec{F} = -e\vec{E} = \frac{d}{dt}(m\vec{u}) \qquad (12)$$

For example, in argon at 30 mtorr (0.04 mbar) there are 10^{15} cm^{-3} atoms, and average mean free path is about $\lambda \approx 1$ cm. If we assume only elastic electron-neutral collisions (cross section is about 10^{-15} cm^2) electron gains in the average $eE\lambda\cos\theta$ energy between two collisions (θ is the angle between electron trajectory and electric field). We have already seen that after making elastic collision with heavy neutral, electron looses only $2 \cdot 10^{-4}$ fraction of its initial energy while its momentum change is large, as shown in the figure 8. Thus, the elastic collisions effectively transform the directed energy which electrons acquire from the electric field into random energy. This begins to establish the electron energy distribution function, and the electrons "heat up".

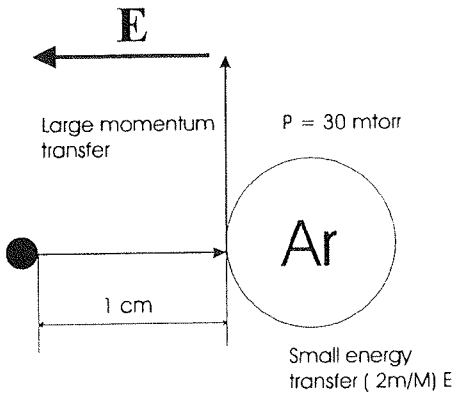

Figure 8: Elastic collision between electron and Ar atom

To be more precise, we can rewrite equation (12) to include the effect of collisions in the form of Langevin equation as:

$$(d / dt)(mu) = -eE - mu\, \nu_e \qquad (13)$$

where u is average drift (directed) velocity due to the electric field, and ve is the electron - neutral collision frequency. Steady state solution is:

$$u = \mu E \qquad (14)$$

where μ is electron mobility defined as $\mu = e/(m\nu_e)$.

Electron current density is:

$$J = enu = \sigma E = ne^2/(m\nu_e)E \qquad (15)$$

and finally we can calculate the rate at which the external power source inputs energy into electrons as

$$P_{in} = JE = \sigma E^2 = ne^2E^2/(m\nu_e) \qquad (16)$$

The rate at which the energy is lost due to collisions is:

$$P_{OUT} = n\delta W \nu_e + n\Sigma W_i \nu_i \qquad (17)$$

where the first term is energy lost due to elastic collisions and the second term is the sum over all inelastic processes, with energy loss Wi and collision frequency ν_i.

For the simplicity let us assume that only elastic collisions dominate. In this case if we equate $P_{in} = P_{OUT}$, we get expression for W, energy gained per electron:

$$W = \frac{E^2e^2}{4m\nu_e^2}\frac{M}{m} \qquad (18)$$

As an example, let us consider He at 0.5 torr (0.66 mbar) in a typical electric field of 1V/cm (100 V/m). Then, the equation (18) predicts an electron energy of approximately 5eV. The energy lost per collision is only 0.00125 eV, which in steady state is just equal to the energy which an electron gains from the electric field between collisions. Since such a small fraction of the electron's energy is lost in a collision, the electron must heat up to 5 eV to provide the energy balance. The small energy transfer results in negligible heating of the neutrals, which therefore usually remain at the room temperature.

The inclusion of inelastic processes will modify the energy balance because, in those processes, an electron can lose a large fraction of its energy. This will result in a lower electron energy than predicted by equation (18). However, the cross sections for inelastic processes are usually smaller than for elastic processes, so that the electrons will still have a higher temparture than the neutrals.

Interaction of electrons with a time dependent electric field

We will now consider the particle motion that results from using an AC power source at frequency ω, with no magnetic field present. It is convenient to write the electric field as a complex quantity:

$$\vec{E} = \vec{E}_0 \exp(i\omega t) \qquad (19)$$

Due to changing electric field the motion of the particles will be oscillatory, as will be the particle drift velocity. Solving the Langevin equation for such a case gives the following particle mobility:

$$\mu = \frac{e}{m(\nu_e + i\omega)} \qquad (20)$$

and

$$\sigma = \frac{ne^2}{m(\nu_e + i\omega)} \qquad (21)$$

Power input to the electrons is now

$$P_{IN} = Re(JE) = \frac{ne^2 E_0^2}{m\nu_e\left(1+(\omega/\nu_e)^2\right)} \qquad (22)$$

Let us examine some special cases. If $\omega = 0$, we recover the DC case. If there were no collisions ($\nu_e = 0$), we find that Pin averages to zero. The reason for that is that the drift velocity and electric field would be 90° out of phase, and thus no power could be transferred. As in the DC case, the collisions transform the directed energy that the electrons gain from the oscillating electric field to the random energy that represents electron heating.

If $\omega >> \nu_e$, then the mobility and conductivity are similar to the DC case with ν replaced by ω^2/ν_e. The power input would therefore decrease with increasing frequency.

Although it is not obvious from our derivations here, a more detailed calculation would reveal the fact that the maximum power input occurs when $\omega = \nu_e$. This can be seen qualitatively by the following argument. If the AC power frequency is much lower than the collision frequency, then the particle makes numerous collisions during each AC cycle which prevents the particles from reaching maximum energy during the AC oscillations. On the other hand, if $\omega >> \nu_e$, then the particles undergo many oscillations between collisions, but this does not increase their energy. When $\omega = \nu_e$, the electrons make approximately one collision for every cycle of the AC power, and that represents the optimum for transforming energy from the electric field to the electron energy distribution.

We are particularly interested in microwave spectrum of AC power input. Its specifics can be understood by examining the process in a simple example gas such as helium. The effective electron - neutral collision frequency at 300 K for helium is given by:

$$\nu_e = 2.3 \cdot 10^9 \cdot P, \quad P = \text{pressure in torr} \qquad (23)$$

For optimum power absorption we need $\omega = \nu$ condition and consequently we can see that good microwave energy coupling depends on the discharge pressure. For a 2.45 GHz excitation frequency maximum power absorption in helium occurs at approximately 7 torr (9.2 mbar) and discharge pressures of 5-10 torr (6.6-13 mbar) provide efficient coupling of microwave energy into a helium discharge. Generalizing this result to other gases with different elastic cross sections and accounting for the influence of the discharge walls, the optimum pressure range for efficient discharge breakdown and maintenance with 2.45 GHz microwave energy usually occurs between 0.5-10 torr (0.6-13 mbar). In practice, an optimum pressure range is found between 0.1 mbar and about 10 mbar.

Interaction of electrons with a time dependent electric field in the presence of a static magnetic field

We know that the total force exerted on a charged particle in an electric and magnetic field is:

$$\vec{F} = q\vec{E} + q\vec{v} \times \vec{B} \qquad (24)$$

However, having present only a static magnetic field charged particles will oscillate around the direction of magnetic field. Their gyration frequency and radius are determined by:

$$\omega_c = \frac{eB}{m}, \quad \rho_c = \frac{mv_\perp}{qB} \qquad (25)$$

Obviously, lighter particles will oscillate with higher frequency having shorter radius of oscillation.

If we introduce a perpendicular AC electric field of freguency ω which is resonant with ω_c, then we will be able to accelerate electrons synchronously. This effect we call ECR - Electron Cyclotron Resonance - AC energy is coupled to natural resonance plasma frequency.

As electron's perpendicular energy increases, the gyration radius will increase, but the cyclotron frequency will remain constant, and therefore the particles will remain in phase with the applied field, figure 9. As in all the previous cases if we want to heat the electrons, we will need collisions to transform this directed energy to random thermal energy. However one big difference here is that the electron energy is increasing with each cycle, so that there is no need to have the collision frequency equal to the applied frequency. This facilitates the operation at lower pressures. However, if the collision frequency becomes of the order of ω_c or larger, then the electrons will not be able to undergo the complete cyclotron orbit. If the resonance is sufficiently broad, then there is little advantage to have a magnetic field at all.

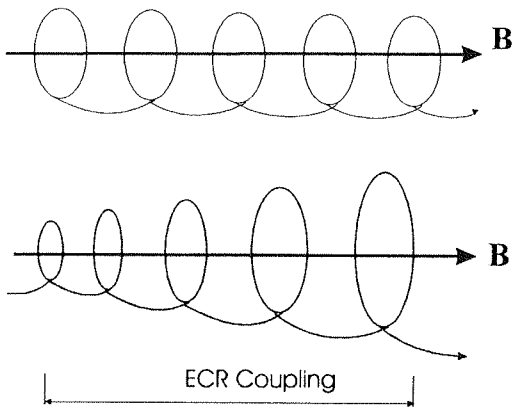

Figure 9: Electron motion in a static magnetic field
a) zero electric field
b) alternating electric field with $\omega = \omega_c$ and $E \perp B$

However, rewriting equation (22) taking into account ECR resonance, we obtain:

$$P_{IN} = Re(JE) = \frac{ne^2E_0^2\nu_e}{2m}\left(\frac{1}{\nu_e^2+(\omega-\omega_c)^2}+\frac{1}{\nu_e^2+(\omega+\omega_c)^2}\right) \quad (26)$$

ECR effect actually becomes very important at very low pressures (≤100 mtorr (0.13 mbar)). That is when the mean free path of electron-neutral and electron-ion collisions becomes very long ($\nu_e << \omega_c$). In such a case, using only MW radiation for plasma excitation, we need high electric fields to sustain the discharge at low pressures. This can be seen from equation (22) which becomes proportional to

$$P_{IN} = Re(JE) = \frac{ne^2E_0^2}{m\nu_e}\left(\frac{\nu_e}{\omega}\right)^2 \quad (27)$$

However, the presence of an ECR static magnetic field simplifies discharge maintenance below pressures of 20 mtorr (0.025 mbar). This can easily be observed by studying equation (26). When $\nu_e << \omega_c$, and at the $\omega = \omega_c$ resonant frequency, electron velocity perpendicular to the static magnetic field increases, resulting in an outward, spiralling motion along a magnetic field line. The electron gains energy proportional to the square of time and in a typical discharge the radius of the electron orbit is limited by an elastic or inelastic collision, a collision with the walls or the electron moving out of the ECR region.

However, at higher pressures, when pressure is such that $\nu e \rightarrow \omega = \omega_c$, magnetic field has little influence on heating the electron gas. Thus it is clear that ECR is a coupling technique for low pressure discharges where the electrons can orbit many times between elastic and inelastic collisions.

In practice, MW energy at 2.45 GHz is usually applied to generate plasma. From equation (25) by putting ω_c = 2.45 GHz and m = m_e we can calculate B, needed magnetic field strength to create ECR at the stated frequency. This value is 875 Gauss.

4.0 WHY MICROWAVE PLASMA?

In figure 10 we show a comparison of Electron Energy Distribution Function (EEDF) for plasmas generated with frequencies below and above 100 MHz. For electron energies above 15 eV, when gas atoms ionization begins, as well as for energies below 7 eV, when dissociation of most commonly used gases takes place, the number of electrons generated with microwave (MW) frequencies is larger than the number of electrons generated with RF. This helps to explain why the degree of ionization, as well as the degree of dissociation are higher in the case of MW plasma generation. This means higher plasma densities per unit volume and faster creation of reactive chemical radicals. But, the electron density per unit volume is mainly determined by the limits of wave propagation leading to a so called cut-off electron density which is strongly different for RF and MW frequencies.

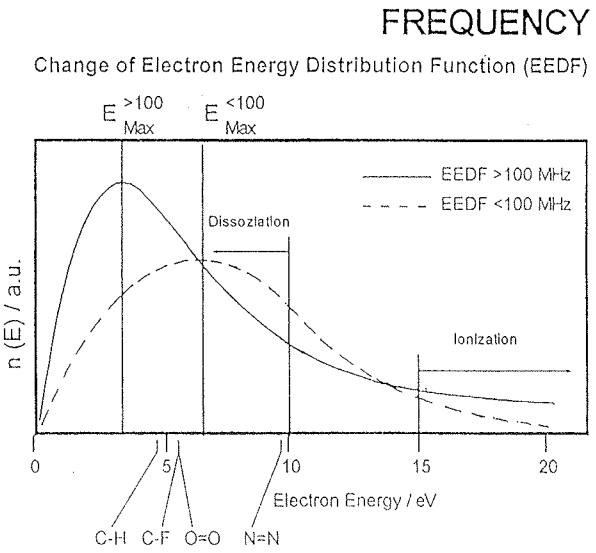

Figure 10: EEDF as a function of plasma excitation frequency

Another beautiful feature of the MW plasma can be seen in the figure 11, where substrate "floating potential", or selfbias, is shown as a function of frequency. In the region of MW frequencies, there is no, or very little selfbias which means "gentle" processing due to lower ion energies which assure minimum damage to sensitive substrates.

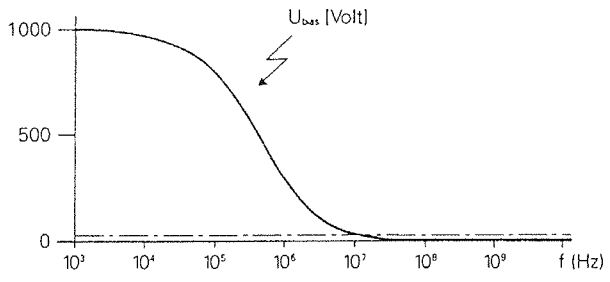

Prof. S. Vepřek, International Sommer School on Plasma Chemistry, Technical University Munich, 1992

Figure 11: Substrate selfbias potential as a function of plasma excitation frequency

We have already seen in section 3 that MW and MW/ECR plasmas are effectively generated at quiet low pressures. That is when electrons gain enough kinetic energy due to motion in AC electric field before making collisions with neutrals. ECR effect further pumps en-

ergy into electrons and keeps them longer within plasma volume preventing their recombination with reactor walls. This is not demonstrated only in the EEDF but also in electron temperature, which increases with decreasing pressure, as seen in the figure 12.

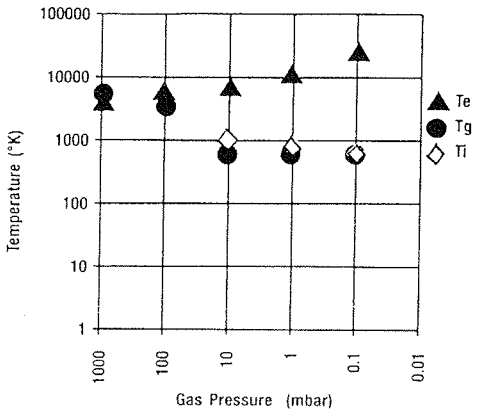

Figure 12: Electron (T_e), ion (T_i) and gas atom (T_g) temperatures versus total pressure

As well, MW plasma processors are compact, simple, reliable systems which require nearly no maintenace. MW radiation which is produced by commercially available magnetrons is coupled to the plasma via special applicators which are mounted on the wall of the vacuum chamber. So, there is no need for special electrodes for RF coupling, as well as none, or very little impedance matching is required. However, special MW/ECR sources have more components than their MW counterparts due to the presence of magnetic coils and - in some cases - collimation optics.

In table 2 we summarize and compare plasma characteristics generated at different frequencies.

	DC=	RF 13.56 MHz	MW 2.45 GHz	MW/ECR 2.45 GHz
Operating pressure, mbar	10^{-2}-10^{-3}	2-10^{-1}	2-10^{-1}	10^{-1}-10^{-4}
Ion density, cm^{-3}	10^{9}	10^{9}-10^{10}	10^{10}-10^{11}	10^{10}-10^{11}
Degree of ionization	10^{-7}	10^{-5}	10^{-4}-10^{-3}	10^{-2}-10^{-1}
Electron temperature, K		$5{\cdot}10^{4}$		$10{\cdot}10^{4}$
Level of dissociation	low	low	high	high
Self bias or plasma potential,V	>100	>100	<20	<20

5.0 MW PLASMA GENERATION

Microwave discharges are often required to operate with different gases, variable gas mixtures and flow rates over a wide range of operating pressures. Thus the MW discharge system should be able to efficiently produce a stable, repeatable and controllable discharge for many experimental conditions including discharge start up and adjustment for final processing operation. As well, application of such systems in industrial environments require certain level of automatic control without the need of a highly trained microwave engineer.

A generic MW plasma processing system together with its equivalent circuit is depicted in figure 13. It consists of several components such as:

- a power source, usually a constant frequency but variable power MW oscillator
- transmission line, often a waveguide or coaxial cable
- a MW applicator
- the MW plasma load

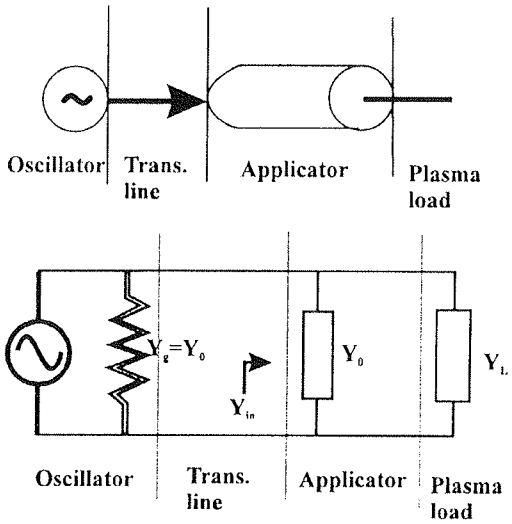

Figure 13: MW processing system and its equivalent circuit

An efficient plasma processing system is designed for maximum power transfer between the MW oscillator and the plasma - loaded applicator. This happens when the output admittance of the MW oscillator Y_g and the input admittance of the plasma loaded applicator Yin are equal to the transmission line characteristic admittance Y_0.

A major difficulty in the design of a MW or MW/ECR system is the variable, nonlinear often reactive discharge load. However, careful design of the applicator and the chamber can lead to the overall system construction which is robust enough to successfully transmit MW energy to varying plasma loads. Nevertheless, minor tuning is still required and is often performed via simple tuning stubs at the initial start up of the machine or after overhaul maintenance.

A typical industrial MW plasma barrel system is depicted in figure 14. It consists of:

- a plasma chamber where the substrates are placed during the process
- a roughing pump which is needed to evacuate the chamber
- several gas inlets distributed around the plasma chamber
- MW source/applicator usually on the wall of the chamber

Plasma is generated in the volume in the vicinity of the quartz or ceramic window and its species diffuse throughout the chamber volume and react with the substrates and chamber walls. Large reactor designs use several plasma sources to obtain high plasma densities and good uniformity within the chamber. Typically, two gas channels are sufficient (normally for O_2 and CF_4 gases) but several additional gas channels can be added for more exotic processes if required (air, He, Ar and their mixtures).

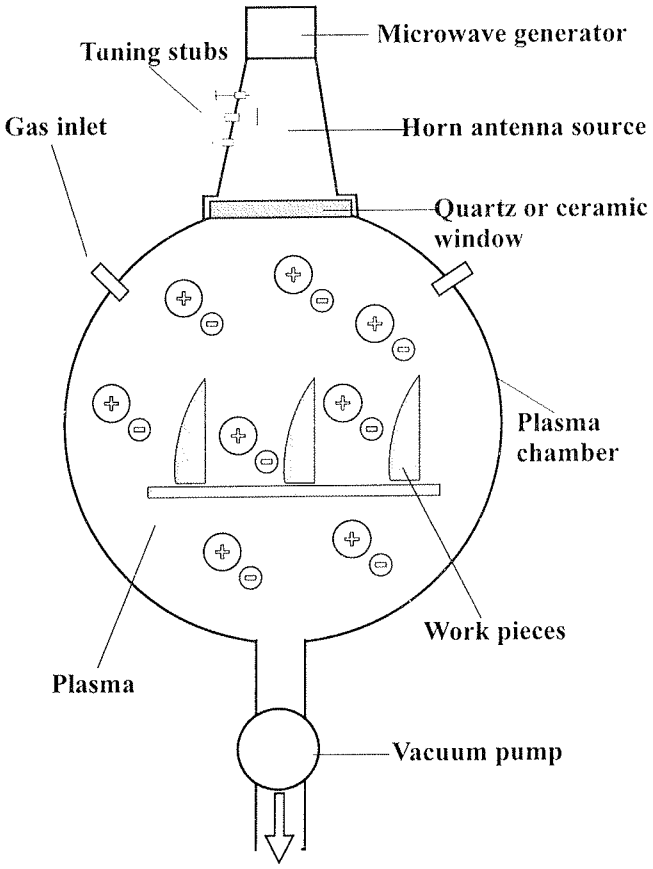

Figure 14: MW plasma barrel system

A schematic diagram of an ECR microwave plasma source is depicted in figure 15. As in normal MW plasma source designs, MW power of 2.45 GHz is transmitted to the plasma via a waveguide and through a quartz or alumina window. However, due to added magnetic coils there is a magnetic field parallel to the MW propagation vector introduced. In the plasma dome a resonant field of 875 Gauss is formed needed to trigger the ECR effect.

ECR source depicted in figure 15 operates in so called PLASMA STREAM mode since the majority of ionized species are extracted through the slit from plasma zone using only existing magnetic field gradient while non-charged particles freely diffuse through the slit into the chamber.

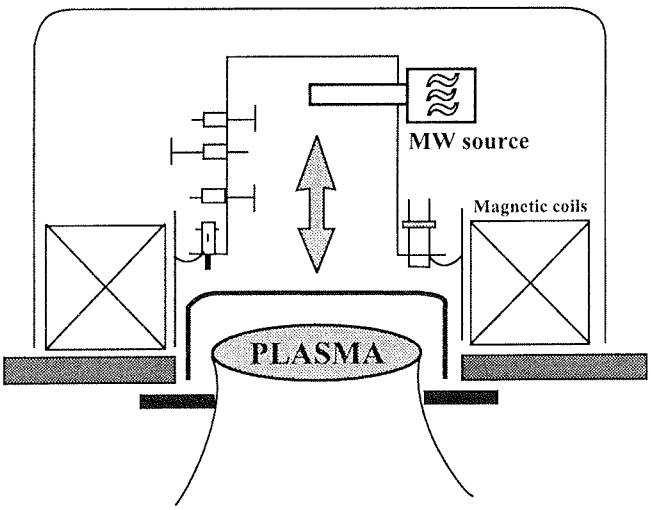

Figure 15: ECR plasma stream source

Slightly different mode of operation is achieved if biased extraction electrodes are added directly below the plasma dome. By varying the extraction voltage, beam of ions with controlled kinetic energy can be produced and directed to the substrate where suitable reactions take place. As well, current density varies with applied extraction voltage. This is so called ION BEAM mode of ECR source operation which is usually used for Reactive (RIBE) and Non-reactive (IBE) Ion Beam Etching of different thin films and substrates.

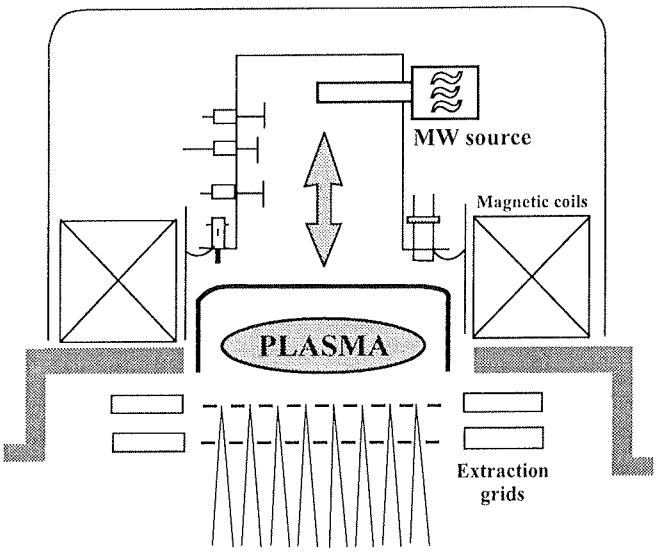

Figure 16: ECR ion beam source

Operating characteristics of a typical Technics Plasma ECR Ion Beam source (Model PLASMODULE ECR-160) are as follows:

- Extraction grids: two grids made of graphite (Mo if wanted)
- Extraction voltage: variable, 0 - 2000 V
- Ion current density: 1 - 2 mA/cm^2
- Ion beam area: 160 mm^2
- Ion beam uniformity: ±5% within 120 Φmm
- Beam divergence: 5°
- Working pressure: 10^{-4} to 10^{-5} mbar

6.0 LITERATURE

/1/ S.Wolf, R.N.Tauber, SILICON PROCESSING FOR THE VLSI ERA, Volume1: Process Technology, Lattice Press 1986, ISBN 0-961672-3-7

/2/ B.Chapman, GLOW DISCHARGE PROCESSES, John Wiley&Sons 1980, ISBN 0-471-07828-X

/3/ S.M.Rossnagel, J.J.Cuomo, W.D.Westwood editors, HANDBOOK OF PLASMA PROCESSING TECHNOLOGY, Noyes Publications 1990, ISBN 0-8155-1220-1

/4/ Technics Plasma GmbH, Application Reports

COMMENT: For more information about Technics Plasma systems and their applications, please call:

MIKROIKS d.o.o., Mr.Iztok Šorli
Dunajska 5, 1000 Ljubljana, Slovenia
tel. +386 (0)61 312 898,
fax.+386 (0)61 319 170

PREDSTAVLJAMO PODJETJE Z NASLOVNICE
REPESENT OF COMPANY FROM FRONT PAGE

INŠTITUT ZA ELEKTRONIKO IN VAKUUMSKO TEHNIKO - IEVT

IEVT deluje kot samostojna raziskovalno-razvojna organizacija že od leta 1954. Ker so osnovo takratne elektronike predstavljale elektronske cevi, te pa so bile povezane z vakuumsko tehniko, so glavne dejavnosti potekale prav na teh dveh področjih. Poznejši razvoj podjetja je potekal skladno z razvojem tehnike v svetu ter potrebami in možnostmi v takratni Jugoslaviji. To so bili časi zaprtega tržišča, lačnega zlasti tehnično zahtevnih izdelkov. Temu je IEVT znal prisluhniti in kaj hitro je poleg programsko izredno razvejane raziskovalno - razvojne dejavnosti zrasla tudi maloserijska proizvodnja kot zadnja faza razvoja. Nekateri od programov so se s programsko in kadrovsko izdvojitvijo prenesli tudi v štiri nova podjetja, ki jih je osnoval IEVT.

Aktivnosti IEVT-ja danes so naslednje: raziskave, aplikativni razvoji izdelkov in tehnologij, maloserijska proizvodnja in storitve na področjih:

- vakuumski sistemi in komponente
- oprema za medicino
- hermetično zaprti stikalni elementi
- posebna svetila
- elektronska oprema in sklopi

Skoraj vsa omenjena področja so tesno povezana z vakuumsko tehniko, ki je izrazito interdisciplinarno področje, saj se v njem prepletajo fizika, strojništvo, elektronika, elektrotehnika, kemija in metalurgija. Danes je vakuumska tehnika nepogrešljiva v mikroelektroniki in

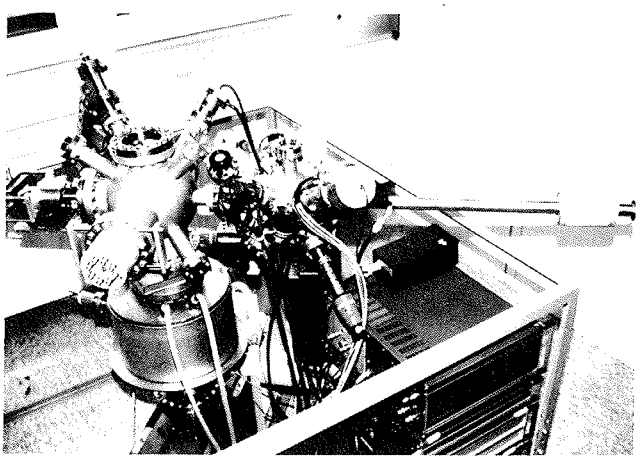

Slika 1: Visokovakuumski črpalni sistem z manipulatorjem, izdelek IEVT

celi vrsti tehnologij na področjih elektronike, kemije, metalurgije, v živilstvu, biologiji, farmaciji, medicini itd.

Večina bazičnih ter aplikativnih raziskav in razvojev na IEVT poteka na področjih ultra-visokega, visokega, srednjega in grobega vakuuma. Na IEVT deluje laboratorij za vakuumistiko in tehnologije (LVT) in Center za vakuumsko tehniko in tehnologije (CVTT). LVT je usmerjen izrazito raziskovalno, CVTT pa aplikativno; opravlja razvoje in storitve za zunanje naročnike. V svojo dejavnost vključuje tudi druge slovenske strokovnjake, ki se ukvarjajo z vakuumsko tehniko.

VAKUUM. TEHNIKA IN TEHNOLOGIJE	vak.črpalke	rotacijske oljne, membranske, difuzijske, ionske razprševalne
	merilniki	Pirani, Pirani - Penning, membranski (piezo)
	deli za vak. sisteme	ventili (ročni, elektropnevmatski, različne konstrukcije), vakuumske komore, povezovalni ter spojni elementi in drugo
	oprema	vakuumski črpalni sistemi
		druga tehnološka oprema
	storitve	kalibracija vakuumskih merilnikov
		preizkušanje vakuumskih elementov in sistemov n. pr. leak detekcija s He (tudi pri naročniku)
		toplotne obdelave v vakuumu, hermetični spoji: kovina - kovina (laser, TIG, mikroplazma, spajkanje), kovina - keramika, kovina - steklo nanašanje tankih plasti, razplinjevanje
MEDICINA	oprema	aspiratorji, inhalatorji, odvzemniki materinega mleka, aparati za uničevanje injekcijskih igel
ELEKTRO-TEHNIKA IN ELEKTRO-NIKA	hermetični stikalni elementi	miniaturni releji, reed releji, releji s Hg omočenimi kontakti
		magnetna položajna in nivojska stikala
	svetila	UV žarnice, neonske cevi, elektrode za neonske cevi
	oprema in sklopil	lokatorji napak na kablih in zračnih vodih lokatorji položaja kablov in kovinskih cevi v zemlji druga merilna oprema
		dajalniki za merjenje vlage in temperature
	storitve	kalibracija merilnikov in dajalnikov za merjenje vlage

V letu 1995 so razvojne in raziskovalne naloge tekle na naslednjih področjih: preiskave izbranih ultra visokovakuumskih pojavov, vodenje curka naelektrenih delcev, študij zmanjšanja prehodne upornosti in povečanja vzdržljivosti kontaktnih sistemov v miniaturnih relejih, študij tankoplastnih struktur kovina - polimer - kovina, razvoj visokovakuumske oljne frakcionirane in ionske razprševalne črpalke z veliko črpalno hitrostjo in razvoj respiratornih medicinskih naprav. Naloge so sofinansirali Ministrstvo za znanost in tehnologijo ter zunanji naročniki.

Sodelujemo z drugimi razvojno raziskovalnimi zavodi in fakultetami, zlasti mariborsko, na kateri se je in se še izobražuje večina naših postdiplomantov.

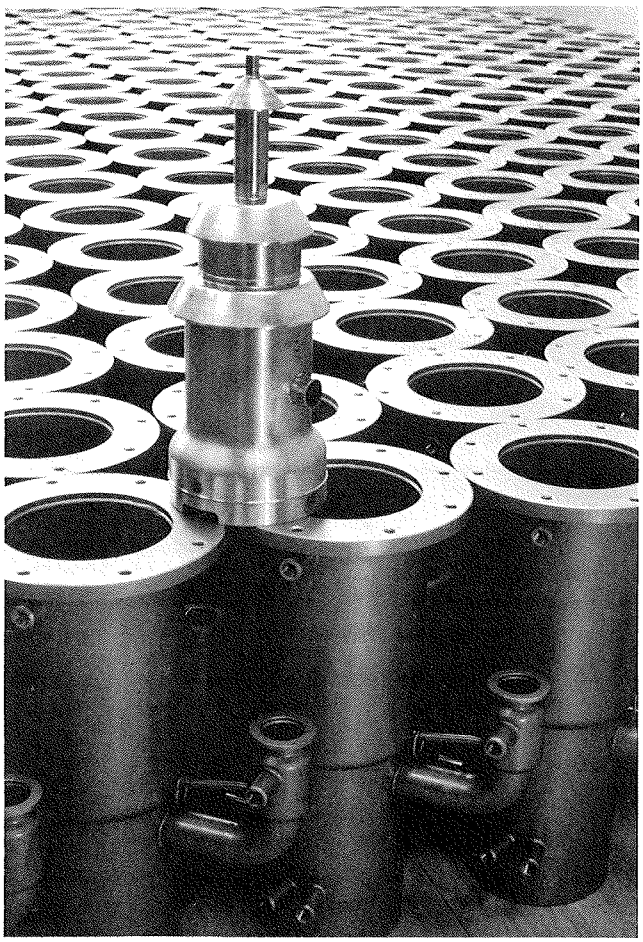

Slika 2: Oljne difuzijske črpalke, izdelek IEVT

V tabeli so predstavljeni naši najpomembnejši izdelki in storitve. Veliko novih izdelkov razvijemo in izdelamo po zahtevah posameznih kupcev po načelu custom design. Ker je Slovenija za našo dejavnost premajhno tržišče se skušamo čimbolj usmeriti v izvoz. V letu 1995 je bilo 40% prihodka ustvarjenega z izvozom, večinoma na zahodni trg. Najuspešnješi smo pri izvozu vakuumskih komponent iz nerjavnega jekla. Ena od teh je prikazana na sliki 2. Vključujemo se tudi v opremljanje slovenske žarkovne linije BOSS pri sinhrotronu ELETTRA v Trstu.

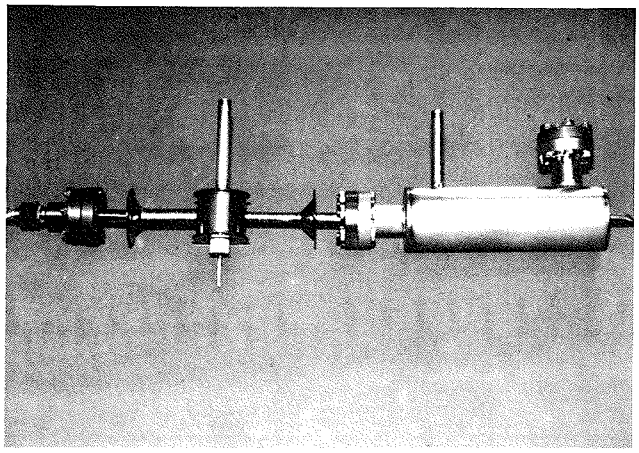

Slika 3: Kalibriran permeacijski leak, izdelek IEVT

Zavedamo se, da je kvaliteta izdelka eden od bistvenih pogojev, ki zagotavlja bodočnost podjetja. Pri tem ne mislimo samo fizičnega izdelka, ampak tudi raziskovalne ali razvojne naloge in storitve. Zato delno že uporabljamo postopke po standardu ISO 9001 in nameravamo čimprej pridobiti tudi certifikat.

INŠTITUT ZA ELEKTRONIKO IN VAKUUMSKO TEHNIKO
LJUBLJANA, Teslova 30
tel.: 061/126 45 84
fax : 061/126 45 78

KONFERENCE, POSVETOVANJA, SEMINARJI, POROČILA
CONFERENCES, COLLOQUYUMS, SEMINARS, REPORTS

SEMICON EUROPA 96
Palexpo, Geneva, March 27-29

Letošnja konferenca in razstava polprevodniške opreme in materialov Semicon Europe 96, ki je že 21. po vrsti, je bila po svojem obsegu večja in bogatejša od vseh predhodnih. Zbranih je bilo 800 razstavljalcev iz 22 držav, kar je odraz nezadržne rasti polprevodniške industrije (ta je znašala v letu 95 kar 25% po podatkih SEMI Europe).

Kot vsako leto je pripravil SEMI poleg razstave še posebna tehnična in izobraževalna srečanja, ki so se jih lahko udeležili obiskovalci ob predhodni registraciji.

Tehnični programi so ponudili letos sledeče zanimive teme:

- MEMS (mikro elektromehanski sistemi)-tretja okrogla miza o strategiji razvoja mikrosistemov
- Nove tehnologije montaže in zapiranja integriranih vezij
- Tehnična konferenca o treh ključnih zadevah pri izdelavi integriranih vezij:
  - obvladovanje izplena od materialov do proizvoda
  - CVD postopki v ekspanziji
  - opcije pri večnivojski metalizaciji
- Mikroelektronika in okolje - drugi letni forum
- Implementacija in integracija procesa kemijsko-mehanskega poliranja (CMP)
- Mikrolitografija in transfer vzorcev

Poleg tega so se odvijali tudi izobraževalni programi, kot na primer dvodnevni tečaj o tehnologiji procesiranja (cena 975 SFR!), nadalje o merilih za ovrednotenje zanesljivosti opreme in materialov ter o temi COO (cost of ownership).

Pod posebnimi programi so bila predstavljena srečanja proizvajalcev kemikalij in plinov pa forum o 300 mm Si rezinah kot nov standard, ki se že tretje leto usklajuje in še ni dokončen ter predstavitev razmer na trgu opreme in materialov.

Sam razstavni prostor z moderno opremljenimi stojnicami vzbuja obiskovalcu spoštovanje s svojo razsežnostjo. Že sam sprehod mimo stojnic brez prevelike radovednosti zahteva skoraj cel dopoldan. Poleg stalnih razstavljalcev, ki so proizvajalci procesne opreme, kemikalij, merilne opreme, osnovnih materialov, so bile tudi firme, ki ponujajo usluge s področja svetovanja in zagotavljanja kakovosti, s področja računalniško podprtega vodenja, zasledovanja in usklajevanja kompleksnih procesov v novih mikroelektronskih tovarnah. Osebni stiki med proizvajalci, ponudniki uslug, zastopniki ter uporabniki so bistvenega pomena pri razvijanju nadaljnjih sodelovanj, poslov ter vizij in na tem mestu pridejo do polnega izraza.

SEMI (Semiconductor Equipment and Materials International), kot organizator tega dogodka je s svojimi informacijami na voljo vsem zainteresiranim tudi na Internetu (http://www.semi.org.).

Obiskovalcem so bile tudi letos na voljo gratis brošure s seznamom in naslovi vseh udeleženih razstavljalcev po abecednem redu, kot tudi po panogah oziroma po proizvodih. Izvod brošure je na voljo za ogled v Laboratoriju za elektronske elemente.

Naslednje leto bo razstava ponovno v Ženevi in sicer od 15.-17. aprila, za leto 1998 pa so se razstavljalci odločali med Ženevo in Muenchnom ravno v teh dneh.

Drago Resnik
Laboratorij za elektronske elemente
Fakulteta za elektrotehniko
Tržaška 25, 1000 Ljubljana
Tel. 1768 303
Fax. 1264 630
E-mail: dragor@fer.uni-lj.si

PRIKAZI MAGISTRSKIH DEL IN DOKTORATOV V LETU 1995
M.S. and Ph. D. ABSTRACTS, YEAR 1995

MAGISTRSKA DELA

Naslov naloge: **Simulacija in določanje napak v aktivnih analognih filtrih**

Avtor: **Anton Biasizzo**, dipl. ing.

Mentor: **prof. dr. Franc Bratkovič**

Univerza v Ljubljani, Fakulteta za elektrotehniko in računalništvo

V magistrski nalogi so obdelani postopki za simulacijo in določanje napak v analognih vezjih z uporabo orodij umetne inteligence. Opisana je splošna problematika testiranja analognih vezij in podan je pregled stanja področja, ki vključuje klasifikacijo različnih diagnostičnih metod. Poseben poudarek je na problematiki modeliranja vezja in njegovih elementov. Razred aktivnih analognih filtrov je bil izbran kot problemska domena, v kateri je bil predstavljen postopek avtomatskega testiranja z uporabo CLP(R) sistema. Naloga vsebuje kratko predstavitev CLP(R) sistema in opisuje možnosti uporabe pri analizi analognih vezij. CLP(R) sistem omogoča tudi diagnosticiranje napak v vezju, kar smo uporabili pri zasnovi diagnostičnega postopka. Osrednji del naloge opisuje metode modeliranja vezja in elementov vezja ter metodo simulacije in diagnosticiranja aktivnih analognih filtrov z uporabo CLP(R) sistema. Podani so eksperimentalni rezultati ter nakazane smernice za nadaljne delo.

Naslov naloge: **Metode za iskanje optimalnih vektorjev za diagnostično testiranje digitalnih vezij s pomočjo modela napak**

Avtor: **Bogdan Dugonik**, dipl.ing.el.

Mentor: **red. prof. dr. Bogomir Horvat**

Komentor: **doc. dr. Zmago Brezočnik**

Univerza v Mariboru, Fakulteta za elektrotehniko, računalništvo in informatiko

Digitalna vezja so, enako kot vse druge naprave, izpostavljena vnosu napak. Naloga sodobnih testnih in diagnostičnih postopkov je, da morebitno napako v vezju čim prej ugotovijo. Kljub temu, da pozornost velja predvsem tehničnemu problemu testiranja, pa ne moremo zanemariti ekonomičnosti in stroškov testiranja. Znano je pravilo, da je napaka tem dražja, čim kasneje jo odkrijemo. Da bi se ekonomska računica izšla, nenehno iščemo nove poti in metode, kako bi bolje in ceneje testirali. V delu se ukvarjamo z iskanjem testnih vektorjev za enojne tehnološke napake v digitalnih kombinacijskih in sekvenčnih vezjih. Za to je najprimernejši strukturni način testiranja. Uporabljamo osnovni model zatičnih napak. Podanih je več metod, ki jih lahko uporabimo za generiranje testnih vektorjev. K tem smo dodali alternativni postopek, v katerem iščemo testne vektorje s simulacijo z modeli napak. V ta namen je izdelana knjižnica modelov napak za tiste logične elemente, ki se najpogosteje uporabljajo. Izdelano je programsko orodje za iskanje optimalnih testnih vektorjev za testiranje vezja in diagnostiko napak. Podan je primer, kako izbiramo testne vektorje, da ugotovimo maksimalno število napak v vezju z minimalnim številom testnih vektorjev, ali da dosežemo čim večjo ločljivost med napakami.

Naslov naloge:**Razvoj in analiza enosmernega napetostnega referenčnega vira in programske opreme za zagotavljanje metrološke avtonomnosti**

Avtor: **Primož Kranjec**, dipl.ing.

Mentor: **prof. dr. Dušan Fefer**

Univerza v Ljubljani, Fakulteta za elektrotehniko in računalništvo

Magistrsko delo predstavlja izvedbo in analizo polprevodniškega enosmernega skupinskega napetostnega vira z visoko izhodno stabilnostjo. Osnovni namen načrtovanja in izdelave napetostnega vira je njegova uporaba v funkciji enosmernega napetostnega etalona in s tem umestitev v metrološko piramido. Zasnovan je kot avtonomen sistem, ki je brez prisotnosti etalona višjega reda v medkalibracijskem obdobju sposoben definirati, če je referenčna napetost še znotraj specificiranih, ki so določene do sledljivosti vira natančno. S tem bi izboljšali dolgoročno stabilnost referenčne napetosti in absolutno točnost napetostnega vira. Pri tem nam pomaga izvedba napetostnega vira, ki temelji na upo-

rabi Zener diode LTZ1000 v napetostnih referenčnih elementih in vgrajenem merilnem sistemu za merjenje napetostnih razlik med napetostnimi referenčnimi elementi. Napetostne razlike meri sigma-delta (ΣΔ) analogno-digitalni pretvornik, ki ponuja zanimiv koncept pretvorbe analognega signala z dobrimi lastnostmi ob nizki ceni. Delovanje enosmernega napetostnega vira upravlja mikrokrmilnik PCB83C552. Skrbi za izvajanje merilno-kontrolnih funkcij, ki so implementirane, in za povezavo napetostnega vira z osebnim računalnikom preko RS232 vmesnika. Sposobnost določanja metroloških parametrov vira kot so funkcija gostote verjetnosti signala, srednja vrednost, standardna deviacija in meje zaupanja mu zagotavlja metrološko avtonomnost.

Uvod na kratko predstavi način zagotavljanja in reprodukcije električnih veličin glede na mednarodni sistem enot (SI). Opisane so splošne lastnosti napetostnih referenčnih virov, ki se danes uporabljajo v metrološke namene: Westonova celica, polprevodniški napetostni referenčni elementi in Josephsonov spoj. V drugem poglavju je prikazana izvedba polprevodniškega enosmernega napetostnega vira in osnovni princip delovanja in uporabe. Tretje poglavje obravnava postopke in ukrepe za stabilizacijo referenčne napetosti. Razloženi so postopki temperaturne kompenzacije, temperaturne regulacije napetostnih referenčnih elementov in temperaturna stabilizacija celotnega napetostnega vira. Predstavljeni so tudi vplivi motenj in navodila za njihovo zmanjšanje ali izločitev. To so predvsem za elektromagnetne in elektrostatične vplive okolice in elektronski šum, ki ga vnašajo elektronske komponente. Vgrajeni merilni sistem je tema četrtega poglavja. Bistveni del merilnega sistema je sigma-delta analogno-digitalni (AD) pretvornik. Razložen je princip delovanja, ki temelji na uporabi 1-bitnega kvantizatorja in nadvzorčenja. Matematična analiza modela AD pretvornika nudi vpogled v tehniko učinkovitega ločevanja signala od šuma in v tehniko decimacije, ki omogoča dosego visoke efektivne razločljivosti pretvornika. Pozornost je posvečena tudi stabilizaciji refrenčne napetosti za pretvornik in ostalim ukrepom za povečanje efektivne razločljivosti analogno-digitalnega pretvornika (ADC). Na koncu je podan izračun merilne negotovosti merilnega sistema. Peto poglavje govori o programski opremi, ki zagotavlja merilne in kontrolne funkcije napetostnega vira. Prvi del je posvečen testiranju in izbiri najučinkovitejšega merilnega algoritma, ki mora skrbeti za potek meritve in izračun merilnih vrednosti v realnem času. Drugi del predstavi protokol o kakovosti, pri katerem gre za izvedbo in uporabo statistične kontrole referenčne napetosti napetostnega referenčnega vira in določanje metroloških parametrov enosmernega napetostnega vira. Pri statistični kontroli gre za uporabo kontrolnih kart in določitev stanja referenčnega vira s pomočjo njihove analize. V šestem poglavju je izvedena analiza enosmernega napetostnega vira v vlogi etalona. Podane so specifikacije, ki jih dosega, vključno s postopkom določitve merilne negotovosti napetostnega vira. Opisana je tudi kalibracija napetostnega vira. Na koncu sta dodani tudi dve prilogi. V prilogi 1 so zbrani osnovni principi delovanja posameznih merilnih algoritmov ALG2, ALG3, ALG4, ALG5, ALG6. Priloga 2 vsebuje tabelo konstant za kontrolne karte.

Naslov naloge: **Večtočkovno povezovanje in usmerjanje v komunikacijskih omrežjih**

Avtor: **Roman Novak**, dipl.ing.

Mentor: **prof. dr. Ljubo Pipan**

Univerza v Ljubljani, Fakulteta za elektrotehniko in računalništvo

Delo obravnava problematiko večtočkovnega povezovanja in usmerjanja v komunikacijskih omrežjih z glavnim poudarkom na izračunu topologije prenosne poti. Definiran je problem večtočkovnega povezovanja in predstavljeno okolje za njegovo reševanje. Problem je preveden v teorijo grafov, kjer je praktično analogen že dolgo poznanemu Steinerjevemu problemu.

Ker problem večtočkovnega povezovanja ni neodvisen od višjenivojskih storitev, ki vključujejo komunikacijo znotraj grupe sodelujočih entitet, se je potrebno dotakniti tudi teh. Zato so po uvodni formalizaciji in klasifikaciji problema najprej obdelani modeli večtočkovne komunikacije. Poudarek je na preslikavi večtočkovne komunikacije na večtočkovne povezave, ki predstavljajo rešitev problema večtočkovnega povezovanja.

Jedro dela tvori pregled in primerjava algoritmov za izgradnjo večtočkovnih povezav z ilustracijami njihovega delovanja. Večtočkovno povezovanje za komunikacije v realnem času je obravnavano ločeno zaradi specifičnosti, ki nastopijo zaradi omejitve časa prenosa podatkov med izvornim in ponornimi vozlišči.

Delo je zaokroženo s poglavjem o večtočkovnem usmerjanju, problemu večtočkovnega povezovanja v nepovezavno orientiranih komunikacijah. Algoritmi za usmerjanje so predstavljeni v zaporedju, ki nakazuje potek njihovega razvoja.

Naslov naloge: **Metode za avtomatsko preverjanje pravilnosti mask integriranih vezij**

Avtor: **Robert Porenta**, dipl.ing.

Mentor: **prof. dr. Janez Trontelj**

Univerza v Ljubljani, Fakulteta za elektrotehniko in računalništvo

Primerjanje pravilnosti dveh električnih vezij je ena od variant problema izomorfizma grafov. Izomorfizem grafov je povezan z mnogimi praktičnimi problemi, zato je zelo dobro obdelan v strokovni literaturi. Uporabimo ga lahko, na primer v kemiji pri identifikaciji spojin, ali pri računalniški analizi slik, ter povsod tam, kjer primerjamo strukture, ki jih lahko predstavimo z grafom. Trenutno še ni učinkovitega splošnega algoritma, ki bi rešil problem v polinomskem času.

Osnova za primerjanje dveh vezij sta načrt in maska vezja. Načrt vezja je osnova za celoten postopek načrtovanja vezja. Maska vezja je končni rezultat načrtovanja vezja. Masko integriranega vezja lahko iz načrta zgeneriramo povsem avtomatsko, ali pa dovolimo tudi ročno izdelavo dela maske ali celotne maske vezja.

Preverjanje pravilnosti električnih vezij uporabljamo povsod tam, kjer pri načrtovanju vezja postopek ni povsem avtomatski. Ročni posegi v postopek načrtovanja vezja pa lahko povzročijo napake pri končni realizaciji vezja.

Če je maska vezja narejena z avtomatskim postopkom, potem predpostavljamo, da je tudi pravilna (pri tem se zanašamo na to, da program, ki generira masko vezja, deluje pravilno). Za avtomatsko generiranje maske so najbolj primerna digitalna vezja predvsem zaradi njihovih geometrijskih lastnosti in standardiziranih podvezij.

Po drugi strani pa zahteva načrtovanje vezij za posebne namene tudi možnost, da lahko načrtovalec vezja neposredno (s programom za načrtovanje maske) spreminja masko vezja. Posledica načrtovanja in spreminjanja maske vezja so napake v maski. Odkrivanje in popravljanje napak v vezju je zato nujno za vsako vezje, ki ni narejeno povsem avtomatsko.

V tekstu so najprej opisane metode za preverjanje pravilnosti električnih vezij. Poseben pomen imajo metode topološkega primerjanja vezij, ker lahko le na osnovi topološke enakosti dveh vezij zanesljivo sklepamo, da sta vezji načrtovani pravilno.

Topološko primerjanje temelji na ugotavljanju izomorfizma grafov, zato sledi kratek opis metod za ugotavljanje izomorfizma v povezavi s teorijo grafov.

Naslov naloge: **Trinivojski tranzistorski usmernik**

Avtor: **Rudolf Prosen**, dipl.ing.

Mentor: **izr. prof. dr. Miro Milanović**

Komentor: **red. prof. dr. Bogomir Horvat**

Univerza v Mariboru, Fakulteta za elektrotehniko, računalništvo in informatiko

Magistrska naloga predstavlja reguliran usmernik s korekcijo faktorja moči. Takšen usmernik optimira porabo električne energije in ne kvari oblike napetosti v omrežju. Lastnosti usmernika so predpisane s standardom IEC 555-2. Posebno pozornost smo posvetili faktorju moči, torej obliki vhodnega toka usmernika.

V delu je predstavljen matematični pristop za razvoj in analizo stikalnih usmernikov. Nadalje je prikazano modeliranje usmernika za simulacijska orodja in simuliranje stikalnega usmerika. V delu je tudi opis izdelanega usmernika, reguliranega z mikrokrmilnikom. Sledijo rezultati meritev in ocena faktorja moči pri simuliranju vezja ter pri delovanju izdelanega usmernika.

Teoretično razvito vezje usmernika je preverjeno s simulacijskimi orodji in tudi praktično izvedeno ter preizkušeno v delovanju.

Naslov naloge: **Raziskave metroloških lastnosti vakuumskega merilnika z lebdečo kroglico**

Avtor: **Janez Šetina**, dipl. ing. fizike

Mentor: **dr. Jože Gasperič**, znanstveni svetnik

Komentor: **red. prof. dr. Vitodrag Kumperščak**

Univerza v Mariboru, Fakulteta za elektrotehniko, računalništvo in informatiko

V prvem delu magistrske naloge sem predstavil osnove statistične obdelave merilnih rezultatov. Pri posredni meritvi neke fizikalne veličine opravimo več neposrednih meritev drugih veličin in nato z matematičnim izračunom določimo merjeno veličino. Pri meritvah moramo oceniti tudi verjetno napako merilnega rezultata. K napaki posredno merjene veličine prispevajo napake vseh neposrednih meritev. Opisal sem variančno metodo (Gaussov postopek) v kompaktni matrični obliki, ki povsem splošno in formalno obravnava negotovost merilnih rezultatov.

V nadaljevanju sem predstavil raziskave nekaterih meroslovnih lastnosti merilnika vakuuma z lebdečo kroglico (v tuji literaturi **S**pinning **R**otor **G**auge-**SRG**). Med vakuumskimi merilniki je to razmeroma nov merilnik, ki je bil razvit ob koncu 70. let in se je pojavil na tržišču po letu 1980. Zaradi odlične stabilnosti in točnosti se je uveljavil kot referenčni etalonski merilnik, zato raziskavam njegovih meroslovnih lastnosti posvečajo posebno pozornost v nacionalnih metroloških laboratorijih po vsem svetu. V te raziskave sem se vključil tudi sam, saj sem uporabljal SRG merilnik pri raziskovalno razvojnem delu na Inštitutu za elektroniko in vakuumsko tehniko (IEVT) v Ljubljani že od leta 1984. V obdobju 1991 do 1992 pa sem kot gostujoči raziskovalec sodeloval pri raziskavah lastnosti SRG merilnikov v Laboratoriju za vakuumske standarde Nacionalnega inštituta za standarde in tehnologijo (NIST) v ZDA. O rezultatih teh raziskav sem poročal v tuji strokovni literaturi in na raznih mednarodnih konferencah.

V magistrski nalogi sem podrobno predstavil princip delovanja SRG merilnika. Razčlenil sem vse pomembne vire naključnih in sistematskih napak v molekularnem in prehodnem področju. S pomočjo eksperimentalnih podatkov sem ocenil, kolikšne so te napake. Za oceno skupne merilne negotovosti sem sestavil matematični model SRG merilnika v matrični obliki $F(X,Y)=0$. Za reševanje modela sem napisal računalniški program. Z uporabo programa sem izračunal merilno negotovost SRG merilnika v celotnem delovnem področju pri nekaterih značilnih pogojih uporabe ter določil spodnjo in zgornjo merilno mejo. S predstavljenim modelom in programom je mogoče izračunati negotovost izmerjenega tlaka pri dejanskih razmerah, ki nastopajo pri neki meritvi. Mogoče ga je uporabiti tudi pri izračunu napake pri kalibraciji nekega vakuumskega merilnika, če pri tem uporabimo SRG merilnik kot referenčni etalon. V program sem vključil tudi izračun korelacijskih koeficientov med raznimi izhodnimi veličinami modela. Ti nam pokažejo, katere veličine največ prispevajo k skupni napaki, in jih je potrebno zmanjšati, če želimo izboljšati natančnost merjenja.

Naslov naloge: **Zvezni in stopničasti heterospoj v polprevodniku**

Avtor: **Monika Vidic**, dipl. ing.

Mentor: **prof. dr. Jože Furlan**

Univerza v Ljubljani, Fakulteta za elektrotehniko in računalništvo

Namen predloženega dela je bil prikazati možnost analitične obravnave notranjih dogajanj v polprevodniških strukturah s heterospoji.

V nalogo sem vključila tudi poglavje, v katerem so podane osnovne enačbe za opis polprevodniških struktur s krajevno spremenljivimi snovnimi parametri. Te

enačbe so mi služile kot izhodišče za obravnavo PN-heterostrukture, sestavljene iz polprevodniškega materiala p-tipa s široko energijsko režo ter iz polprevodniškega materiala n-tipa z ožjo energijsko režo. Strukturo sem obravnavala po segmentih z določenimi lastnostmi in poenostavitvami. Vsak segment sem opazovala ločeno in na koncu podala izraze za tokove gostote in gostote nosilcev naboja na levem in desnem robu segmenta. Izpeljane izraze sem uporabila za segmentno analizo P^+I a-Si/N c-Si sončne celice. V to analizo sem dodatno vključila efekt zmanjšanja injiciranega toka preko spoja, kjer ima nezveznost obliko špice. Z združitvijo posameznih segmentov oz. enačb na robovih segmentov sem prišla do celotne tokovno-napetostne karakteristike sončne celice.

Prednost podane segmentne analize je v tem, da nam da vpogled v notranja dogajanja na posameznih delih strukture. Fizikalna slika, ki si jo zgradimo ob opazovanju posameznih segmentov, je mnogo jasnejša, kot bi bila pri opazovanju strukture kot celote. Hkrati taka analiza omogoča dodajanje dodatnih efektov, modeliranih s samostojnim segmentom.

Za konec pa je treba poudariti, da vsaka analitična obravnava zahteva vrsto poenostavitev, ki omogočajo analitično rešljivost obravnavanega problema. Vpeljane poenostavitve morajo temeljiti na dobrem poznavanju dogajanj v obravnavani strukturi. V primeru obravnave heterospojnih polprevodniških struktur pa vsa dogajanja, povezana z neenakostjo materialov, ki tvorita strukturo, še niso povsem raziskana. Zaradi zanimivosti problema in predvsem zaradi uporabnosti takih struktur je v bodoče pričakovati nadaljevanje intenzivnega raziskovanja na tem področju. Nova spoznanja bo mogoče dodatno vključiti v analitične modele. Vendar pa, kot smo zapisali že v uvodu, pričakovanje nekega univerzalnega modela, ki bi zajemal vsa dogajanja na meji dveh snovi, verjetno ni realno.

Naslov naloge: **Numerične metode za analizo elementov integrirane optike**

Avtor: **Edi Vovk**, dipl.ing.

Mentor: **prof. dr. Joško Budin**

Univerza v Ljubljani, Fakulteta za elektrotehniko in računalništvo

V tem delu sta obdelani dve numerični metodi za analizo elementov integrirane optike: metoda končnih elementov (FEM) in vektorska metoda širjenja snopa (VBPM).

Metoda končnih elementov je primerna za analizo vseh struktur, ki se ne spreminjajo vzdolž smeri širjenja svetlobe (mikrovalovne strukture, optična vlakna). Uporaba vseh šestih komponent elektromagnetnega polja omogoča analizo problemov, v katerih lahko nastopajo linearne neizotropne snovi s poljubnim kompleksnim tenzorjem dielektričnosti in permeabilnosti. Analiza pravokotnega valovoda s homogenim izotropnim dielektričnim polnilom je pokazala, da so odstopanja numerično izračunanih vrednosti od analitično izračunanih vrednosti zelo majhna, še zlasti za nižje rodove.

Metoda širjenja snopa analizira širjenje elektromagnetnega valovanja skozi dano strukturo. Vektorska obravnava električnega polja omogoča analizo polarizacijskih lastnosti elementov, ki so občutljivi na smer polarizacije. Upoštevanje prestopnih pogojev na meji različnih dielektrikov pri izračunavanju parcialnih odvodov elektromagnetnega polja izboljša natančnost modeliranja problema. Prepustni robni pogoji, ki preprečujejo nefizikalne odboje izhajajočega elektromagnetnega polja nazaj v analizirano področje, dovoljujejo, da je področje analize majhno, s tem pa se zmanjša obsežnost problema. Program lahko reši sistem enačb po dveh metodah. Implicitna metoda izmenjajočega izbiranja smeri je bistveno hitrejša od iteracijskega reševanja sistema enačb. Zamenjava kazalcev nekaterih matrik pri računalniški realizaciji programa odpravi potrebo po kopiranju vektorjev iz take matrike in s tem pospeši izvajanje programa. Realizirani program je dovolj hiter za uporabo na osebnem računalniku. Kot primer uporabe programa so prikazani rezultati analiz optičnega sklopnika iz gradientnih valovodov, stopničastega vlakna ter simetričnih in nesimetričnih smernih sklopnikov. Primerjava rezultatov z analitično rešljivim problemom stopničastega vlakna je pokazala majhno relativno napako numerično izračunanega efektivnega lomnega količnika (pod 0.01% pri še razmeroma veliki diskretizacijski razdalji v prečni smeri). Rezultati izračunanih sklopnih dolžin simetričnega smernega sklopnika, dobljeni z vektorsko metodo širjenja snopa (VBPM), se dobro ujemajo z objavljenimi rezultati drugih metod, še zlasti z vektorsko metodo končnih elementov.

V dodatku so na majhnem zgledu prikazane vhodne in izhodne datoteke realiziranega programa za analizo po vektorski metodi širjenja snopa. Opisani so tudi dodatni programi za pripravo in obdelavo teh datotek.

DOKTORSKE DISERTACIJE

Naslov doktorske disertacije: **Optimizacija komutacijske in prenosne zmogljivosti širokopasovnega telekomunikacijskega omrežja**

Avtor: **mag. Janez Bešter**, dipl.ing.

Mentor: **prof. dr. Beno Pehani**

Univerza v Ljubljani, Fakulteta za elektrotehniko in računalništvo

Vsebina doktorske disertacije je razdeljena na deset poglavij, vsa pa odgovarjajo na nekaj temeljnih vprašanj, ki se postavljajo pri optimizaciji komutacijske in prenosne zmogljivosti širokopasovnega telekomunikacijskega omrežja.

Vsebina uvodnega poglavja odgovarja na vprašanje: kje smo danes in kam hočemo na področju telekomunikacij, kaj lahko prispeva to delo k razvoju?

Danes je področje telekomunikacij nedvomno na začetku novega obdobja, za katerega so značilni naslednji momenti: širokopasovne telekomunikacije, mobilne telekomunikacije, zlivanje "klasičnih" telekomunikacijskih storitev in računalniških komunikacij in novi načini kreiranja telekomunikacijskih storitev.

Logično je, da zlitje ni možno, če nimamo na razpolago tehnologije in sistemskih znanj, ki zaobjamejo ves spekter storitev in iz njih izvirajočega heterogenega telekomunikacijskega prometa. Sinteza ključnih tehnologij in znanj je združena v konceptu z imenom "Širokopasovno digitalno omrežje z integriranimi storitvami" (B-ISDN), ki temelji na asinhronem prenosnem načinu (ATM). S postavitvijo časovnega, tehnološkega in znanstveno raziskovalnega okvira, je v uvodnem poglavju, prikazano obstoječe stanje na obravnavanem področju. Predvsem je poudarjeno stanje raziskav, potek preizkusnih projektov in zrelost produktov, ki so temeljni gradniki omrežja. Navedena so bistvena odprta vprašanja pri raziskavah širokopasovnih telekomunikacijskih omrežij. Motivacija za poglobljene raziskave, ki so vodile v izdelavo doktorske disertacije, je v sooblikovanju komutacijskega elementa širokopasovnega omrežja, ki bo prometno zmogljiv, in definiranju ustreznih algoritmov upravljanja omrežja. Kljub zahtevni tehnologiji, ki se uporablja na tem področju, in upoštevanju standardov, so tako pri razvoju komutacijskih elementov kot pri upravljanju z omrežjem in storitvami možne in zaželene specifične rešitve. Z njimi proizvajalci opreme, ponudniki storitev in operaterji omrežij dosegajo večje izkoristke in s tem konkurenčnost. V zaključku prvega, uvodnega, poglavja so navedene teze, ki naj bi jih potrdili v nadaljnjih poglavjih.

Drugo poglavje obravnava bistvene značilnosti širokopasovnega digitalnega omrežja z integriranimi storitvami in s tem odgovarjamo na vprašanje: kakšne so potrebe uporabnikov in kakšen telekomunikacijski sistem jih je sposoben realizirati?

Celotna obravnava mora izhajati iz dejstva, da je namen vsakega telekomunikacijskega omrežja zagotavljanje storitev uporabnikom, ki so pripravljeni plačati določeno ceno za svoje uporabniške aplikacije. Aplikacije oziroma storitve pa so generator telekomunikacijskega prometa. Prav od pravilnega načrtovanja in upravljanja prometnih tokov je odvisna kvaliteta storitev. Različne storitve in aplikacije imajo specifične zahteve glede zanesljivosti, točnosti, zakasnitev, razpoložljivosti in drugih parametrov. Univerzalnost in prilagodljivost ATM telekomunikacijskih omrežij, ki so temelj za B-ISDN, pa zaradi heterogenosti prometnih tokov in velikih prenosnih hitrosti (reda 100 Mbit/s) zahteva bolj izpopolnjene prometne tehnike od današnjih. Drugo poglavje poleg definiranja storitev, ki naj jih bo sposobno realizirati širokopasovno omrežje z integriranimi storitvami (B-ISDN), obravnava tudi sorodna omrežja in proces ter stanje standardizacije ter protokolni referenčni model.

Vsebina tretjega poglavja podaja nekatere pomembne elemente ATM koncepta, kot odgovor na vprašanje: katera tehnika je osnova telekomunikacijskih omrežij bodočnosti?

Vsi znaki (raziskave, standardizacija, produkti, aplikacije) kažejo, da je asinhroni transportni način (ATM) tehnika, na kateri bodo temeljila telekomunikacijska omrežja bodočnosti. V tretjem poglavju tako obravnavamo bistvene značilnosti ATM, ki so pomembne za prometne analize in optimizacije v naslednjih poglavjih. Koncepta navideznih poti (VP) in navideznih povezav (VC) sta mehanizma komutacije, usmerjanja prometa in ločitve logične strukture omrežja od fizične. Ustrezna sta formata celice na uporabniškem (UNI) in omrežnem (NNI) nivoju, kot osnovnega elementa prenosa in komutacije. Vse aplikacije imajo dostop do ATM nivoja preko prilagoditvenega nivoja (AAL), ki je prav tako podan v tretjem poglavju.

Vsebina četrtega poglavja je namenjena definiranju gradnikov in sistemskih znanj, da bi odgovorili na vprašanje: kateri produkti so danes na voljo za realizacijo širokopasovnih omrežij z integriranimi storitvami in kakšno sistemsko znanje je za to potrebno?

V predhodnih poglavjih so definirana vsa bistvena izhodišča za obravnavanje širokopasovnih telekomunikacijskih omrežij, zato v četrtem poglavju preidemo na podrobnejšo obravnavo elementov omrežja. To so: fizične povezave in na njih realizirani transportni protokoli, posredovalni elementi (PE) in njihovi gradniki ter znanja za sistemsko integracijo in upravljanja omrežja. Podobno kot v nekaterih naslednjih poglavjih so najprej opredeljeni pojmi, saj na tem področju ni ustrezne domače literature. Tako se na podlagi pregleda obsežne literature iz angleškega in nemškega govornega področja smiselno uskladijo pojmi in oznake. Utemeljena je uporaba sinonima komutacijsko polje (SWA).

Komutacijska polja in njihovi gradniki so sistematsko predstavljeni razvojno, tehnološko in z bistvenimi značilnimi topologijami. Navedena je tudi obsežna literatura, ki obravnava področje ATM komutacijskih polj.

Izpostavljena je preganjena arhitektura SWA, kot primer realizacije posredovalnega elementa, ki ustreza razpoložljivi tehnologiji. Razdelan je primer modularne gradnje preganjanega komutacijskega polja s 16384 linki. Na podlagi analize prometnih tokov v preganjanem komutacijskem polju so utemeljene naslednje prednosti: porazdelitev telekomunikacijskega prometa, ekonomična realizacija oddaljenih komutacijskih modulov z upoštevanjem prometne optimizacije in statističnega multipleksiranja.

Dopolnjena obravnava prometnih tokov, ki kaže na prednosti izbrane arhitekture, pomeni avtorjev prispevek, saj je ni zaslediti v literaturi.

Kot podlaga za matematično obravnavo prometnih tokov v ATM omrežju, je v četrtem poglavju, z upoštevanjem navedb v literaturi, postavljen model posredovalnega elementa.

V zaključnem podpoglavju četrtega poglavja so navedena potrebna znanja za sistemsko integracijo, od teh so nekatera podrobno definirana v naslednjih poglavjih.

V petem poglavju je obravnavan model prometnih izvorov, kot odgovor na vprašanje: kako matematično opredeliti storitve, ki so cilj telekomunikacij in izhodišče optimizacije prenosnih in komutacijskih zmogljivosti?

Za teoretično obravnavo telekomunikacijskih prometnih tokov v ATM omrežju je potrebno poglobiti obravnavanje storitev in aplikacij iz drugege poglavja. V petem poglavju, ki pomeni uvod v nadaljnje prometne analize širokopasovnih telekomunikacijskih omrežij, je utemeljeno večnivojsko obravnavanje prometa. V primerjavi s klasičnim telefonskim omrežjem, kjer sta poznana

le nivo klica in nivo omrežja, so v ATM omrežju za celovito obravnavanje prometa nujni še dodatni nivoji: celice, izbruha in asimetričnosti. Dodatni nivoji zahtevajo ustrezne matematične modele prometnih izvorov za nivo celic in izbruhov. Za glavne vire (govor, video in podatki) je v drugem podpoglavju prikazan pregled modeliranja. Na podlagi sistematičnega študija so podani načini kodiranja, kompresije in modeli virov, ki iz tega izhajajo. Ker se v modelih pogosto pojavlja Poissonova porazdelitev, je podana izpeljava, ki dodatno opredeli matematične zapise modelov prometnih izvorov za nivo celic in izbruhov. Obravnavani so tako viri s konstantno bitno hitrostjo (CBR) in spremenljivo bitno hitrostjo (VBR). S stališča ATM so zanimivi predvsem VBR viri, kjer pride do izraza efekt statističnega multipleksiranja. Izbran je Markovski model prometnih virov z dvema stanjema, oziroma preklopni model. Predhodno so postavljeni kriteriji za izbiro. Preklopni model je izbran zaradi primernosti za aplikacije v realnem času, saj so z njim karakteristike vira podane s setom treh parametrov {CR, cm, b}, skladen pa je tudi s signalizacijskimi formati. Za preklopni model so v zaključku petega poglavja navedeni parametri za tipične govorne, video in podatkovne vire.

Šesto poglavje obravnava prometno analizo širokopasovnega omrežja in odgovarja na vprašanje: kako dimenzionirati prometne zmogljivosti širokopasovnega telekomunikacijskega omrežja?

Iz ekonomskih in organizacijskih razlogov se v telekomunikacijskem omrežju prenosne in komutacijske zmogljivosti časovno porazdeljujejo med uporabnike. Pravila in algoritmi za porazdeljevanje zmogljivosti omrežja morajo biti zasnovani tako, da uporabniki praviloma ne občutijo, da komunikacijske zmogljivosti delijo z ostalimi uporabniki omrežja, le tako imajo zagotovljeno predpisano kvaliteto storitev.

Kot izhodišče za prometne analize je v šestem poglavju najprej opredeljen telekomunikacijski prometni inženiring. V nadaljevanju so podani in kritično ocenjeni dosedanji klasični postopki prometne analize na nivoju klicev. Navedene so pomanjkljivost obstoječih modelov in matematičnih orodij za nivo klicev. Kljub pomanjkljivostim se v tej fazi razvoja uporablja Erlang-B formula za nivo klicev, saj bodo šele z razvojem širokopasovnih omrežij in opazovanjem realnih prometnih tokov dani realni pogoji za točno definiranje novih porazdelitev na nivoju klicev v B-ISDN.

Za celovito obravnavo ATM prometnih tokov na obeh glavnih nivojih (celica, klic), je v šestem poglavju postavljena definicija ekvivalentnega ponujanega prometa vira i $A_{C(i)} = c_i \phi_i$ [erl M], ki je produkt ekvivalentne kapacitete c_i [Mbit/s] izoliranega vira i in ponujanega prometa ϕ_i [erl]. Podobno je bilo zaradi sistematske in celovite obravnave prometnih tokov potrebno definirati efektivni dopustni promet elementa omrežja, ekvivalentni dopustni promet elementa omrežja in ekvivalentni ponujani promet skupine virov.

Postavitev navedenih definicij, ki jih ni zaslediti v literaturi, predstavlja avtorjev prispevek. Prometni nivo celic, za katerega je značilno statistično multipleksiranje, je obravnavan z metodo ekvivalentne kapacitete. Izbrana je bila po predhodnem študiju obsežne literature zaradi primernosti za izračune v realnem času in skladnosti s preklopnim ATM modelom vira. Izpeljava metode ekvivalentne kapacitete je podana v prilogi 1 doktorske disertacije.

Na podlagi izbrane metode ekvivalentne kapacitete je bil specificiran in realiziran računalniški program, z imenom CELICA. Ta program omogoča analizo značilnosti izbrane metode glede na parametre prometnih virov, dimenzioniranje linkov in dimenzioniranje VP. Z iterativno metodo je mogoče dimenzioniranje kapacitet na nivoju celice tudi obratni smeri (izračun števila virov, ki jih je možno multipleksirati v dano kapaciteto linka ali VP). Rezultati značilnih izračunov so podani v obliki diagramov.

Šesto poglavje je zaključeno z vpeljavo parametra prometne asimetričnosti χ, ki da celovit rezultat o dejanski ekvivalentni prometni kapaciteti širokopasovnega telekomunikacijskega omrežju. Parameter χ je upoštevan v nadaljevanju doktorske disertacije pri načrtovanju B-ISDN in raziskavah krmiljenja dopuščanja zveze (CAC).

Sedmo poglavje z vsebino, ki podaja specifičnosti upravljanja omrežja in krmiljenja prometa, odgovarja na vprašanje: katere so bistvene razlike v optimizaciji današnjih in bodočih širokopasovnih telekomunikacijskih omrežij?

B-ISDN, ki bazira na ATM tehniki, je načrtovan za posredovanje širokega spektra prometnih razredov (traffic classes). Heterogenost prometnih razredov, statistično multipleksiranje na nivoju VC in VP, kot poglavitnem načinu povečevanja izkoristka omrežnih elementov, skupaj z velikimi prenosnimi hitrostmi zahtevajo temu prilagojene mehanizme nadzora in krmiljenja prometa, ter upravljanja omrežja. Če ti mehanizmi ne delujejo, ali pa niso usklajeni, potem v delovanju omrežja pride do zamašitev ali drugih nepravilnosti v delovanju, kar ima za posledico zmanjšanja kvalitete storitev ali pa celo prenehanje funkcioniranja omrežja. Upravljanje omrežja pa ima tudi dolgoročnejšo funkcijo, saj na podlagi zbranih podatkov načrtujemo tudi investicije v prenosne in komutacijske kapacitete. Tako so v sedmem poglavju najprej definirani nivoji upravljanja omrežja. Pri tem je pomembna signalizacija tako na UNI kot NNI nivoju. Glede na tehnološke možnosti in velike zahteve širokopasovnega omrežja je predlagano porazdeljeno upravljanje, ki lahko zagotovi sprotne odzive. Prikazane so specifičnosti upravljanja konfiguracije ATM omrežja. Prav univerzalnost omrežja in fleksibilnost upravljanja sta prednosti ATM koncepta, ki ju nekateri avtorji uvrščajo med pomembnejše od statističnega multipleksiranja.

Temeljna značilnost upravljanja ATM omrežja je v velikem obsegu sprotnega (on-line) upravljanja, ki zajema tako nivo zvez (VC), kot nivo poti (VP), to pa zagotavlja visoke izkoristke elementov. Predlagan je koncept dinamičnega načrtovanja, izgradnje in upravljanja ATM omrežja, ki pomeni prehod iz obstoječega tehnološkega stanja v ATM tehnologijo, z upoštevanjem kratkoročnih in dolgoročnih ciljev ob čim manjših investicijah.

Koncept dinamičnega načrtovanja, izgradnje in upravljanja ATM omrežja predstavlja prispevek avtorja, ker pa celovita obravnava presega obseg tega dela, pomeni izziv za nadaljevanje raziskovalnega dela.

Upoštevanje parametra prometne asimetričnosti χ vpliva na strukturo B-ISDN. Podana je topologija asimetričnega omrežja, ki ga sestavljajo trije paralelni deli (za simetrične aplikacije, distribucijske aplikacije in asimetrične interaktivne aplikacije).

Mehanizmi krmiljenja prometnih tokov in preprečevanja zamašitev so obravnavani ob koncu sedmega poglavja. Izbrani algoritem krmiljenja dopuščanja zvez je poglobljeno prikazan v osmem poglavju.

Vsebina osmega poglavja prikaže dodeljevanje omrežnih zmogljivosti in odgovarja na vprašanje: kako v realnem času dodeljevati omrežne zmogljivosti?

Obširna vsebina predhodnih poglavij pomeni podlago za izbiro in celovit prikaz algoritma za krmiljenje dopuščanja zvez (CAC). Problem dodeljevanja omrežnih zmogljivosti v realnem času skriva v sebi še razumljivejše vprašanje: Koliko povezav J prometnih virov tipa j, ki zahtevajo kvaliteto storitev QoS_j lahko realiziramo po virtualni poti s kapaciteto K_{VP}, ki poteka po fizičnem linku K_L? Odgovor na to, na videz preprosto vprašanje zahteva poznavanje kvalitete storitev iz drugega poglavja, principa VP, VC in AAL nivoja iz tretjega poglavja, modela PE $\rightarrow$ link iz četrtega poglavja, modela virov iz petega poglavja, večnivojskega obravnavanja prometnih tokov (klic, izbruh, celica) iz šestega poglavja in mehanizma dopuščanja zveze iz sedmega poglavja. Z dopolnitvijo navedenega znanja iz predhodnih poglavij z določitvijo izgubnih mest v ATM prenosnem ali komutacijskem sistemu, uporabo metode ekvivalentne kapacitete v CAC algortimu in vpeljavo iteracijskega postopka za usklajevanje nivoja celic z nivojem klicev se J lahko izračuna in tako lahko odgovorimo na postavljeno vprašanje.

V osmem poglavju so najprej določena možna izgubna mesta telekomunikacijskega prometa na primeru linka. V nadaljevanju je metoda ekvivalentne kapacitete iz šestega poglavja dopolnjena za primer uporabe v CAC algoritmu. V tej točki je ponovno ugotovljena primernost za izvajanje v realnem času, saj obseg računskih operacij dovoljuje sprotni izračun ob vsaki zahtevi za novo zvezo. Izmed različnih, v literaturi navedenih, CAC algoritmov je izbran algoritem dvostopenjskega dopuščanja zvez. Prednost izbranega algoritma je v združevanju dveh nasprotujočih lastnosti: doseganje visokega izkoristka in primernosti za implementacijo v realnem času. Dobra lastnost izbranega algoritma je možnost postopne implementacije, glede na zahtevani izkoristek, tehnološke sposobnosti in sistemsko znanje.

Celoten postopek CAC je ponazorjen tudi z diagramom poteka. Posebej so obrazložene možnosti uveljavljanja eksplicitne ali implicitne prioritete dodeljevanja komutacijskih in prenosnih zmogljivosti. V tem poglavju predstavlja prispevek avtorja dopolnitev metode ekvivalentne kapacitete s prometnim nivojem klicev. Rezultat je bil specificiran in realiziran v obliki programa PRETOK, ki predstavlja z nivojem klicev dopolnjen program CELICA. Uporabljen je za izračune v osmem in devetem poglavju.

Osmo poglavje se konča z napovedjo trendov dimenzioniranja omrežnih zmogljivosti, ki predvideva veliko stabilnost fizične strukture ATM telekomunikacijskega omrežja, kljub naraščanju ponujanega prometa na nivoju klicev in uvajanju novih storitev.

Deveto poglavje obravnava optimiranje virtualnih poti, kot odgovor na vprašanje: kako povečati izkoristek omrežnih elementov?

Koncept virtualnih poti omogoči poenostavitev postopkov in algoritmov za komutacijo in usmerjanje in preglednejšo hierarhično strukturo omrežja.

Literatura in priporočila izhajajo iz omejitve determinističnega dodeljevanja VP. Deveto poglavje pa z vpeljavo prerazporejanja prometa med VP povečuje izkoristek omrežnih elementov. Nelogično je, da bi od dveh VP, ki potekata vzporedno (logično ali fizično), ena bila prometno preobremenjena, druga pa le delno izkoriščena. Prvo podpoglavje najprej obravnava funkcijske zveze med fizično strukturo omrežja in logično strukturo virtualnih poti. Razložene so različne teoretične možnosti maksimiranja multipleksiranega prometa, ki se preliva med VP. Efekt prerazporejanja prometnih tokov je računsko preverjen s programom PRETOK. Iz rezultatov, ki so za obravnavani primer govornih in podatkovnih izvorov prikazni v tabeli, lahko ugotovimo faktor povečanja ekvivalentne dopustne kapacitete 1.4 za govorne izvore, oz. 2.5 za podatkovne izvore. Prvi prispevek v tem poglavju je v metodi prerazporejanja prometa in izračunu posledičnega izkoristka.

Drugi prispevek je v uvedbi splošnega večstopenjskega algoritma krmiljenja dopuščanja zvez (CAC), ki upošteva asimetrične interaktivne aplikacije, distribucijske aplikacije, izbiro alternativne poti, prerazporeditve prometa med VP in delovanje v primeru izpada nadzornega centra. S predlaganim CAC pridobimo na prometni kapaciteti in izkoristku omrežja. Izračun s programom PRETOK za primer podatkovnih izvorov pokaže, da z prerazporejanjem prometa povečamo dopustno ekvivalentno kapaciteto za faktor 3.5.

Deseto, zaključno, poglavje je namenjeno vprašanju: ali so potrjene začetne teze, kako smo odgovorili na zastavljena vprašanja v posameznih poglavjih doktorske disertacije, kateri so izvirni prispevki k obravnavani tematiki in kakšni so novi raziskovalni izzivi?

Doktorska disertacija obravnava kompleksno področje prenosnih in komutacijskih zmogljivosti v širokopasovnem telekomunikacijskem omrežju, ki temelji na ATM tehniki. Kot je razvidno iz povzetka osmega poglavja, je tematika obsežna in razvejana, saj odgovor na navidez preprosto vprašanje, ali dopustimo še zvezo $n+1$, če imamo v sistemu že n zvez, zahteva predhodno obravnavo in pripravo dokaj zahtevnih modelov in orodij.

V ustvarjanju celotne podobe obravnavane tematike, ki v našem okolju praktično še ni prisotna, so bile tako skozi vsebino posameznih poglavij obdelane nekatere temeljne zakonitosti, gradniki in sistemska znanja.

Doktorska disertacija podaja širši in celovit pogled na obravnavano tematiko B-ISDN in ATM z naslednjimi rezultati:

- določitev tistih prometnih parametrov, ki so bistveni za prometno analizo,
- izbira algoritma za dodeljevanje komutacijskih in prenosnih zmogljivosti v realnem času na podlagi prometnih parametrov,
- kritična ocena klasične teorije telekomunikacijskega prometa in njena dopolnitev z večnivojskim pristopom,
- sistematski pristop k obširni tematiki in definiranje novih pojmov,
- predlagan je koncept dinamičnega načrtovanja, izgradnje in upravljanja ATM omrežja, ki temelji na dolgoročno stabilnem hrbteničnem in regionalnem omrežju, fleksibilnih uporabniških vmesnikih in ekonomičnem prehodu iz bakrenega naročniškega omrežja v optičnega.

Navedeni rezultati predstavljajo, skupaj s predlaganimi novimi raziskovalnimi izzivi, temelj za realizacijo optimiranih produktov in omrežij.

Izvirni prispevki te doktorske disertacije k znanosti so podani v Zahtevi za priznanje avtorstva.

Naslov doktorske disertacije: **Preiskava vloge cezija pri visokoobčutljivih multialkalijskih antimonidnih fotokatodah**

Avtor: **mag. Bojan Erjavec**, dipl. ing. fizike

Mentor: **dr. Jože Gasperič**, znanstveni svetnik

Komentor: **red. prof. dr. Vitodrag Kumperščak**

Univerza v Mariboru, Fakulteta za elektrotehniko, računalništvo in informatiko

Potek kemijskih reakcij med sintezo multialkalijskih antimonidnih fotokatod je odvisen od parnih tlakov alkalijskih kovin in njihovih medsebojnih razmerij. Pri tem pa na celotni čas sinteze vpliva predvsem dinamika par alkalijskih kovin v UVV komori. Najprej je bil izvršen študij porasta parnega tlaka izbrane alkalijske kovine in njegovega padca v modelni UVV komori za različna območja tlakov v režimu molekularnega pretoka, ki mu je sledila meritev spremembe parnega tlaka posameznih alkalijskih kovin z Langmuirjevo ionizacijsko sondo v slikovnem ojačevalniku. Primerjava dobljenih rezultatov je vodila k oceni geometrijskih (prostornina in notranja površina UVV komore, efektivna in površinska črpalna hitrost) in tehnoloških vakuumskih parametrov (koeficient lepljenja oziroma kondenzacijski koeficient ter povprečni rezidenčni čas alkalijskega atoma na notranji površini), ki vplivajo na prostorninsko časovno konstanto in podaljšano časovno konstanto za različna tlačna območja molekularnega pretoka, ter s tem omogočila izbiro optimalnih vakuumskih parametrov za sintezo visokoobčutljive fotokatode.

V tej nalogi je bil raziskan heterospojni model visokoobčutljive polprepustne multialkalijske antimonidne fotokatode $Na_2KSb(Cs,Sb)$ ki ga sestavljata homogena, polikristalna in močno *p*-dopirana osnovna plast Na_2KSb in površinska plast tipa *n* Cs_xSb.

Debela osnovna plast Na_2KSb je bila sintetizirana z zaporednimi adicijskimi in substitucijskimi reakcijami pri $T = 200^oC$ v ultravisokem vakuumu z optimiziranim standardnim postopkom. Potek parnih tlakov alkalijskih kovin je lahko odločilen pri formiranju osnovne plasti. Presežna Na in K, ki se nahajata v residualni atmosferi po vsakem naparevanju Sb, lahko nepričakovano reagirata z le-tem, kar vodi k nedopirani in nehomogeni osnovni plasti. Presežni Cs reagira podobno z naparevajočim Sb, kar najprej prepreči močno *p*-dopiranje osnovne plasti in nato vodi k neugodni polprevodniški spojini tipa *p* Cs_3Sb v površinski plasti.

Tanka plast Cs_xSb je bila nanesena na osnovno plast Na_2KSb z izmeničnimi uvajanji pare Cs in naparevanji Sb pri $T = 150^oC$ po dokaj spremenjenem standardnem postopku. Ocena debeline te površinske plasti s pomočjo enostavnega modela rasti je bila približno 30 Å za stehiometrično razmerje $x = 1.5$ in je bila narejena s fotoelektrično analizo "yo-yo" tehnike, ki je vodila k visokoobčutljivi fotokatodi. Termodinamski izračun sinteznih reakcij iz binarnega sistema Sb-Cs je bil izveden z uporabo dokaj zanesljivih ocen osnovnih termodinamskih podatkov in izbiro deljenih termodinamskih funkcij in njihovih zvez, ki pripadajo realnim trdnim raztopinam. Le-te so bile izbrane zaradi ionskega karakterja kemijske vezi, ki je značilen za alkalijske antimonidne spojine. Odločilna količina, na kateri temelji ves termodinamski izračun, je prenos valenčnega naboja med neenakima atomoma, ki je sorazmeren s standardno entalpijo tvorbe spojine Cs_xSb. Narejeni sta bili primerjavi izračunanih zvez disociacijskega parnega tlaka Cs_xSb-Cs z izmerjenimi izrazi $P_{Cs}(T)$ za desorpcijo Cs s površine fotokatod $Na_2KSb(Cs)$ ter asimetrije Augerjevega signala Sb MNN spojin Cs_xSb, ki je linearno odvisna od prenosa valenčnega naboja med neenakima atomoma, z izmerjeno obliko linije Sb MNN visokoobčutljivih fotokatod $Na_2KSb(Cs)$, ki obe vodita k stehiometričnemu razmerju $x = 1.5$.

Zaradi pomanjkanja izmerjenih podatkov je bila predpostavljena prevodnost tipa *n* za spojino $Cs_{1.5}Sb$, za katero sta ocenjeni tudi širina prepovedanega pasu, ki je enaka ali večja od 1.5 eV, in ugodna elektronska afiniteta, ki je približno 1.0 eV. Na koncu je bil skonstruiran idealni diagram energijskih pasov za heterospojni model, ki ga sestavljata močno *p*-dopirana osnovna plast Na_2KSb in površinska plast tipa *n* $Cs_{1.5}Sb$.

Termično izstopno delo $Cs_{11}O_3$ je znatno nižje od tistega, ki je značilno za kovinski Cs. Če je $Cs_{11}O_3$ nanesen kot tanka plast skupkov na masivni oksid tipa n Cs_2O, se termično izstopno delo slednjega zniža na približno 1.0 eV. Na osnovi raziskav heterospojnega modela fotokatode $Na_2KSb(Cs,Sb)$ je bil skonstruiran diagram energijskih pasov za heterospojni model fotokatode $Na_2KSb(Cs,O)$, ki ga sestavljata debela in močno p-dopirana osnovna plast Na_2KSb s širino prepovedanega pasu 1.0 eV in elektronsko afiniteto 1.0 eV ter tanka in močno *n*-dopirana površinska plast $Cs_2O/Cs_{11}O_3$ s termičnim izstopnim delom 1.0 eV. Ker se mora rezultirajoče fotoelektrično izstopno delo izenačiti s termičnim izstopnim delom površinske plasti ima tako skonstruirana fotokatoda $Na_2KSb(Cs,O)$ ničelno elektronsko afiniteto.

Homogena osnovna plast Na_2KSb z močno teksturo je bila sintetizirana *in situ* s standardnim postopkom, pri povišani temperaturi v UVV, na ukrivljeno površino vlaknaste optike, vgrajene v slikovni ojačevalnik druge generacije. Prevleka z nizkim termičnim izstopnim delom je bila nanesena pri sobni temperaturi na podlago Na_2KSb z izmeničnim izpostavljanjem njene površine ceziju in kisiku, dokler ni fototok dosegel maksimalne vrednosti, medtem ko se je slikovna elektronka črpala s pomožno ionsko-razprševalno črpalko. Zelo čist Cs se je napareval z uporovnim segrevanjem iz pomičnega izvira Cs. Ta je vseboval standardni dispenzer Cs, ki je bil vstavljen v zaprto kovinsko cev z majhno odprtino. Tako naparevajoč divergentni atomski curek Cs je prekril samo fotokatodno površino, ostala notranja površina slikovnega ojačevalnika pa je ostala pri tem neprizadeta. O_2 se je uvajal iz trdnega izvira O_2, temelječega na termičnem razgrajevanju CuO. Ta izvir je sestavljala uporovna žica s spiralno navito bakreno žičko, katere površina je bila oksidirana do CuO pri povišani temperaturi v residualni atmosferi O_2. Na poti do aktivacijskega mesta O_2 zelo rad reagira z residualnimi plini, kot sta H_2 in CH_4, ki so adsorbirani na notranjih stenah. Za preprečevanje kontaminacije je bil izvir O_2 vgrajen v dodatno ohišje, ki je bilo priključeno na slikovni ojačevalnik s kratko bakreno cevjo.

Narejenih je bilo več poskusov aktivacije podlage Na_2KSb s Cs in O_2 pri sobni temperaturi, ki so se končali neuspešno, tj. dobljene integralne in ustrezne spektralne svetlobne občutljivosti v bližnjem IR področju so bile dokaj skromne. Aktivacija ni uspela zaradi difuzije O v bližnje-površinsko območje Na_2KSb, kar je povzročilo oksidacijo gibljivih alkalijskih kovin v alkalijske subokside in okside ter negibljivih anionov Sb^{3-} preko elementarnega Sb^0 v katione Sb^{5+}, pri tem slednji tvorijo Sb_2O_5, in zaradi močne difuzije K iz notranjosti Na_2KSb v bližnje-površinsko območje le-tega, kar je povzročilo dodatno rast debele oksidne plasti z zaporedjem oksidnih plasti: K_3O/K_2O, ki je neugodno za potek fotoemisijskega procesa. Nizka foto občutljivost je bila posledica debele vmesne oksidne plasti, ki je povzročila nastanek visoke potencialne bariere, s tunelskim efektom neprehodne za fotoelektrone, in znaten primanjkljaj alkalijskih atomov v osnovni plasti Na_2KSb, le-ta je bil vzrok za zmanjšano izstopno globino vzbujenih elektronov zaradi dodatnih energijskih izgub pri interakciji s kationskimi vrzelmi.

Na koncu je bil za visokoobčutljivo fotokatodo Na_2KSb (Cs,O) predpostavljen model skupkov, ki ga sestavljata debela osnovna plast Na_2KSb in ena monoplast skupkov $Cs_{11}O_3$. Struktura $Cs_{11}O_3$ vsebuje atome O, ki zasedajo notranje pozicije, obdane z atomi Cs na različnih atomskih razdaljah. Najzunanjejša plast atomov Cs ima kvazi-kovinsko strukturo. Tako lahko nanos zelo tanke plasti $Cs_{11}O_3$ na podlago Na_2KSb izboljša njene fotoemisijske lastnosti z dvema mehanizmoma: a) površinska bariera se zmanjša zaradi dveh kombiniranih pojavov: kvantnega razsežnostnega pojava v skupkih $Cs_{11}O_3$ in vpliva električnega dipolnega polja, povzročenega z nastankom vmesne površine alkalijski antimonid/suboksid, b) antimonid postane bolj *p*-dopiran in območje upogiba energijskih pasov ožje zaradi povečane gostote alkalijskih vrzeli (akceptorskih centrov), nastalih z difuzijo alkalijskih atomov v tanko plast $Cs_{11}O_3$.

Nadaljnja aktivacija Na_2KSb s Cs in O_2 bo potekala pri temperaturah, znatno nižjih od sobne temperature, z namenom omogočiti adsorpcijo prevleke Cs, ki je sestavljena iz najmanj treh enoatomskih plasti, ter preprečiti škodljivo difuzijo kisika v bližnje-površinsko območje Na_2KSb in močno difuzijo K iz notranjosti Na_2KSb proti njeni površini.

Naslov doktorske disertacije: **Analiza in optimizacija prebojnih lastnosti poprevodniških planarnih struktur**

Avtor: **mag. Dejan Križaj**, dipl. ing.

Mentor: **prof. dr. Slavko Amon**

Univerza v Ljubljani, Fakulteta za elektrotehniko in računalništvo

Zaporne lastnosti polprevodniških struktur so omejene s pojavom plazovite ionizacije. Pri visokih poljih nosilci električnega naboja pridobijo dovolj energije, da s trki povzročijo nastanke novih parov elektron-vrzel. Mehanizem plazovite ionizacije je mogoče upoštevati pri analizi polprevodniških lastnosti s pomočjo numerične simulacije, ali pa z analitičnimi modeli. Zaradi različne kompleksnosti uporabljenih modelov se lahko rezultati analitične in numerične analize bistveno razlikujejo, kar je pokazala tudi v tem delu opravljena primerjava. Ujemanje med numeričnim in analitičnim izračunom prebojnih napetosti ravnih spojev s širokim razponom koncentracij dopiranja je bilo izboljšano s spremembo koeficientov v Fullopovi formuli za hitrost ionizacije.

Prebojne napetosti pri planarnih spojih so nižje, kot pri ravnih spojih zaradi pojava višjih polj na zaokrožitvah spojev. Matematična analiza je pokazala, da so normirane prebojne napetosti cilindričnih spojev z Gaussovim profilom dopiranja odvisne od razmerja med površinsko koncentracijo dopiranja in koncentracijo dopiranja substrata. Pri tem so prebojne napetosti cilindričnih spojev normirane s prebojno napetostjo ravnega spoja, globine spojev pa s širino osiromašenega področja ravnega spoja pri preboju. Numerična analiza je pokazala višje normirane prebojne napetosti za nižja razmerja med površinsko koncentracijo dopiranja in koncentracijo dopiranja substrata. Za planarne spoje z različno vertikalno in lateralno globino difuzije je namesto cilindrične predlagana eliptična oblika metalurškega spoja. S primerjavo prebojnih napetosti eliptičnih in cilindričnih spojev so bile določene efektivne globine cilindričnih spojev. Na ta način je omogočen enostaven analitični izračun prebojnih napetosti tudi za eliptične strukture.

Ena od uspešnejših metod zviševanja prebojnih napetosti planarnih spojev je zaključitev z zaščitno elektrodo preko oksidne plasti. Če zanemarimo možnost preboja na robu zaščitne elektrode, se idealnim prebojnim napetostim približamo le ob uporabi zelo tankih oksidov in plitvih spojev. Pri večanju globine spoja se namreč prebojna napetost zmanjšuje zaradi šibkejšega vpliva zaščitne elektrode, pri še večjih globinah spoja pa se

prebojna napetost zopet poveča zaradi manjšega radija ukrivitve spoja. Najnižje vrednosti prebojnih napetosti so ocenjene pri globinah spoja od 0.2 do 0.3-kratne širine osiromašenega področja pri preboju ravnega spoja.

Za izboljšanje prebojnih lastnosti visoko-napetostnih elementov znotraj visokonapetostnih integriranih vezij se kot izredno primeren izkaže RESURF LDMOS transistor. RESURF tehnika zaključitve, ki temelji na uporabi tanke epitaksijske plasti drift področja na substratu nasprotnega tipa dopiranja. Močneje dopirana epitaksijska plast omogoča nizke izgube pri prevajanju, šibkeje dopiran substrat pa visoke prebojne napetosti. V delu je predlagan analitični model za analizo in optimizacijo prebojnih lastnosti RESURF struktur. Pri tem sta ločeno obravnavana modela za prebojno napetost lateralnega in vertikalnega dela RESURF strukture, napetost preboja celotne strukture pa je določena kot manjša od obeh. Predlagani model se dobro ujema tako z rezultati numerične simulacije, kot tudi z rezultati iz literature. Model poleg določitve optimalnih načrtovalnih parametrov omogoča analizo občutljivosti parametrov na prebojne lastnosti struktur. Analiza je pokazala, da so optimalne prebojne napetosti težko dosegljive, če se koncentraciji dopiranja epitaksijske plasti in substrata bistveno razlikujeta. Tako vrata, kot tudi izvor in ponor RESURF LDMOS transistorja lahko delujejo kot zaščitna elektroda. Iz rezultatov numerične analize sledi, da lahko s pravilno načrtovanimi kontakti v obliki zaščitne elektrode preko ene ali več debelin oksida bistveno zmanjšamo občutljivost parametrov na prebojno napetost.

Zadnje poglavje podaja prvič prikazane eksperimentalne rezultate strukture z zaščitno spiralo. Numerična analiza je pokazala najvišje zaporne napetosti pri strukturah z majhnimi razmaki med "obroči" spirale. Vendar pa pri zelo majhni razdalji in dovolj velikem padcu napetosti med obroči lahko osiromašeno področje obroča z višjo napetostjo doseže obroč z nižjo napetostjo. Posledica je močno prevajanje med obročema in povečan tok skozi spiralo. Pri dovolj visokih zapornih napetostih lahko velik tok med dvema obročema povzroči povečano pomnoževanje nosilcev naboja (multiplikacijo) in s tem naraščanje toka substrata (katode). Rezultat je nekoliko zgodnejši preboj, predvsem pa neostra prebojna karakteristika. Strukture z zaščitno spiralo so bile načrtovane za rezine s 45 Ωcm upornostjo, ki v idealnem primeru (raven spoj) omogočajo 1420 voltov prebojne napetosti. Od struktur s konstantno razdaljo med obroči spirale so bili najboljši rezultati doseženi s spiralami z najmanjšo razdaljo med obroči (4 μm) in najslabši pri največjih razdaljah med obroči (22 μm), kar je v skladu z rezultati modeliranja. Prebojne napetosti struktur z zaščitno spiralo so bile več kot 10-krat višje od prebojnih napetosti testnih diod brez zaščitne spirale, vendar še vedno bistveno nižje od idealnih vrednosti. Boljše rezultate pa smo dosegli z zaščitnimi spiralami z neenakomerno širino spirale in spreminjajočo razdaljo med obroči spirale. Pri spiralah, ki so bile širše v okolici anode (glavni spoj) in so se ožale proti zunanjemu obroču (ravno nasprotno je veljalo za razdalje med obroči), je bilo mogoče doseči manjše padce napetosti v okolici anode. Poleg tega se je z večanjem razdalje med obroči z oddaljenostjo od anode zmanjšala tudi možnost lokalnega preboja med obroči spirale (reach-through). Čeravno smo pri tem načrtovanju naleteli na omejitve uporabljene tehnologije, so rezultati meritev pokazali, da lahko tako načrtovane strukture dosežejo do 1300 voltov zaporne napetosti, kar je več kot 90% idealne. Le nekoliko nižje zaporne napetosti so dosegle strukture z zaščitnimi "plavajočimi" obroči, ki pa so imele tudi nižje zaporne tokove v primerjavi s strukturami z zaščitno spiralo. Še nekoliko nižje zaporne napetosti, vendar še vedno preko 1000 voltov, so dosegle strukture z združenim pin/Schottky jedrom (anodo).

Prednosti struktur z zaščitno spiralo so predvsem nizka cena, visoke zaporne napetosti ter majhna občutljivost na različne neidealnosti procesa, glavni pomanjkljivosti pa možnost lokalnega preboja med obroči spirale in zvečan zaporni tok zaradi toka skozi spiralo. Ker je pomanjkljivosti mogoče s pravilnim načrtovanjem bistveno omejiti, lahko pričakujemo strukturo z zaščitno spiralo kot možno tehniko zaključitve bodočih visokonapetostnih in močnostnih elementov.

Naslov doktorske disertacije: **Izbira optimalnih podstruktur digitalnega sita s porazdeljeno aritmetiko**

Avtor: **mag. Mitja Solar**, dipl. ing. el.

Mentor: **red. prof. dr. Bruno Stiglic**

Komentor: **doc. dr. Rudi Babič**

Univerza v Mariboru, Fakulteta za elektrotehniko, računalništvo in informatiko

V delu smo opisali kombinirano realizacijsko obliko nerekurzivnega digitalnega sita. Obravnavali smo izvedbe digitalnih sit, ki delujejo v realnem času. Klasične izvedbene strukture digitalnih sit vsebujejo registre, seštevalnike in množilnike. V takšni izvedbi so množilniki najbolj kompleksne strukture in prispevajo največje zakasnitve. Množilnikom smo se izognili z uporabo porazdeljene aritmetike s stalno decimalno vejico. Pri porazdeljeni aritmetiki hranimo v pomnilniku delne vsote koeficientov impulznega odziva sita, rezultat pa dobimo po zaporedju seštevanj delnih vsot. Velikost pomnilnika je določena s številom koeficientov N impulznega odziva nerekurzivnega sita in znaša 2^N besed. Torej je uporaba porazdeljene aritmetike za nerekurzivna digitalna sita v osnovni realizacijski obliki omejena z velikostjo pomnilnika.
Na osnovi poznavanja problematike smo postavili originalno delovno hipotezo:

1. Z uporabo porazdeljene aritmetike lahko naredimo kombinirano strukturo nerekurzivnega digitalnega sita višje stopnje.
2. Z izbrano kombinirano strukturo se zelo zmanjša velikost potrebnih pomnilnikov, pri tem pa dušenje sita ni bistveno manjše od dušenja nekvantiziranega optimalnega digitalnega sita.
3. Pri omejeni amplitudi vhodnega signala $|x_{max}| \leq 1$ je amplituda izhodnega v enakem velikostnem razredu $|y_{max}| \leq 1$ ali najmanj $|y_{max}| \leq 0{,}5$, kar zadošča za praktične realizacije digitalnih sit.

4. Izvedba digitalnega sita v kombinirani strukturi je primerna za realizacijo v obliki tiskanega vezja s standarnimi integriranimi komponentami in omogoča realizacijo v obliki naročniškega integriranega vezja.

Z našim raziskovalnim delom smo potrdili vse točke delovne hipoteze.

Na osnovi že znanih struktur za zmanjšanje pomnilnika s paralelnimi in kaskadno vezanimi podstrukturami smo razvili dve originalni optimalni kombinirani strukturi sit.

Prva kombinirana struktura je posebej primerna za realizacijo v obliki tiskanega vezja. Zasnova strukture je splošna in omogoča uporabo poljubno velikih pomnilnikov. Izbira velikosti pomnilnika naj omogoča popolno kompatibilnost med statičnimi bralno-pisalnimi pomnilniki RAM in bralnimi pomnilniki tipa ROM, EPROM ali EEPROM. Izbrali smo pomnilnike velikosti 2k osembitnih besed, ki so ceneni, imajo enojno napajalno napetost in v osnovni strukturi omogočajo gradnjo digitalnih sit, katerih stopnja je enaka $N-1=10$.

Druga kombinirana struktura omogoča realizacijo v obliki naročniškega integriranega vezja. V tej strukturi so namesto pomnilnikov uporabljeni registri z vpisanimi koeficienti impulznega odziva. Ta oblika je zelo primerna za realizacije v adaptivnih sitih, kjer je potrebno sproti spreminjati koeficiente impulznega odziva sita.

Za dosego primernega dušenja sita smo naredili analizo kvantizacijskih pogreškov. Uporabili smo linearne modele za upoštevanje vpliva kvantizaciji in izpeljali originalni model za oceno izhodne šumne moči.

Razvili smo originalno programsko opremo za načrtovanje in simulacijo digitalnih sit v kombinirani realizacijski obliki.

Primerjali smo nerekurzivno nizkoprepustno digitalno sito stopnje 60 v različnih realizacijskih oblikah. Pokazali smo, da je v primerjavi z osnovno in kaskadno realizacijsko obliko digitalnih sit v porazdeljeni aritmetiki kombinirana struktura primernejša, ker z njo močno zmanjšamo potrebni pomnilnik, pri tem pa ohranimo dušenje, pasovno prepustno ojačenje in zaporno slabljenje digitalnega sita.

Originalni prispevki dela so:

- razviti sta kombinirani realizacijski obliki nerekurzivnega digitalnega sita, ki omogočata izvedbe sit višjih stopenj: prva kombinirana oblika omogoča gradnjo digitalnega sita s poljubno velikimi pomnilniki v obliki tiskanega vezja, druga pa omogoča realizacijo v obliki naročniškega integriranega vezja;
- izpeljava modela za izračun celotnega izhodnega šuma, ki nastane pri kvantizaciji besed v posameznih strukturah nerekurzivnega digitalnega sita v kombinirani realizacijski obliki;
- dopolnitev strukture digitalnega sita tako, da doseže sito v kombinirani realizacijski obliki podobno velik izhodni signal, kot ga ima digitalno sito v osnovni realizacijski obliki; pri tem smo optimirali normiranje v posameznih podstrukturah sita;
- določitev takšnih dolžin besed v vseh delih digitalnega sita, ki omogočajo podobna dušenja, kot ga ima referenčno optimalno nerekurzivno digitalno sito;
- razvita je programska oprema za načrtovanje in simulacijo digitalnih sit v kombinirani realizacijski obliki.

Naslov doktorske disertacije: **Teoretična zasnova univerzalnega odprtega programskega orodja za analizo vezij**

Avtor: **mag. Tadej Tuma**, dipl. ing.

Mentor: **prof. dr. Franc Bratkovič**

Univerza v Ljubljani, Fakulteta za elektrotehniko in računalništvo

Doktorska disertacija obravnava področje računalniškega načrtovanja analognih vezij. V grobem lahko razdelimo metode računalniškega načrtovanja na tri velike skupine. V prvo skupino sodijo postopki, ki pripeljejo do matematičnih modelov elektronskih komponent. V drugi skupini najdemo metode, ki zgradijo matematični model za celotno elektronsko vezje v obliki sistema enačb. Tretja skupina pa združuje postopke, ki pri danem vzbujanju rešijo sistem enačb ter tako pripeljejo do končnih rezultatov analize.

Jedro tega dela je predstavitev splošne redukcijske operatorske enačbe, iz katere se izpeljejo vse metode druge in tretje skupine. Obravnavano matematično orodje torej na enoten način popiše tako postopke za sestavljanje sistemov enačb (vozliščne enačbe, enačbe osnovnih zank, enačbe osnovnih prerezov ali celo enačbe stanja), kot tudi metode za njihovo reševanje (Gaussova eliminacija, vzvratna substitucija, trikotna dekompozicija, Gauss-Jordanova eliminacija, itd.). Splošna redukcijska operatorska enačba pravzaprav zabriše klasično ločnico med elektrotehniškimi postopki druge skupine in matematičnimi metodami tretje skupine.

Opisana teoretična dognanja imajo posledice tudi za praktične aplikacije. Prav vsako obstoječe programsko orodje je namreč zasnovano na vnaprej določeni kombinaciji iz druge in tretje skupine. Le izjemoma se najdejo primeri, ki omogočajo uporabniku izbiro med vsaj nekaj sorodnimi metodami. Redukcijska operatorska enačba pa obeta popolnoma splošno programsko orodje za analizo analognih vezij. Programska oprema, ki je zasnovana na redukcijski operatorski enačbi, vrh tega zlahka sprejme novo metodo ali neko posebno modifikacijo znane metode. Taka zasnova je torej poleg univerzalnosti tudi odprta.

Pričujoča disertacija je zgrajena iz štirih delov. Najprej je v drugem poglavju predstavljen redukcijski operator kot osnovni matematični gradnik. Tretje in četrto poglavje nato sistematsko obravnavata najbolj znane metode sestavljanja sistemov enačb oziroma metode za njegovo reševanje, medtem ko so v petem poglavju zbrani konkretni primeri uporabe.

VESTI-NEWS

News from AMS

Chips for the Year 2000

Together with the partners SGS-Thomson (France/Italy), GEC-Plessey (England), Matra-MHS (France), Mietec-Alcatel (Belgium), Philips (The Netherlands), Siemens (Germany) Austria Mikro Systeme International AG is participating in the SHAPE-Project "**Sub HA**lf Micron **P**rocess for **E**uropean Users".

The aim of SHAPE is the development of the next ASIC (Application Specific Integrated Circuit) generation of process structures of 0.35 micron (= Structures with a diameter of 0.00035 mm! - e.g. an area of 1 cm^2 contains more than 1 million functions!) that allow for completely new applications in the innovative segment of microelectronics and for mixed analogue/digital ICs which are becoming more and more sophisticated. This means a combination of the analogue world with the digital computer, all on one IC:

- Specifically, these smallest structures represent a revolution in the development of semiconductors for the year 2000 and beyond: In the segment of communications single chip mulimedia solutions for the transmission of video, voice and data (e.g. V-mail) will become a matter of fact in the networked world of tomorrow.
- Security electronics will profit from solutions such as recognition electronics and intelligent identification systems that are based on microelectronics.
- The whole segment of man/machine interaction, like computer, household and industry will experience a dramatic change with speaking/listening/thinking equipment.
- In the domain of medical microelectronics, like the artificial eye, chips that support body motorics due to damaged nerve cells, miniaturized heart pacemaker ICs, miniature factories and thinking robots that make carefully directed repairs of blood vessels in the human body.
- The new microelectronic generation will transform the car into a mobile computer including the new functions of communications and navigation.

AMS was invited to participate in this project because of the company's experience in the field of R & D and design of ASICs, the development and production of high performance analogue/digital ICs as well as the fact that AMS has become the most profiled independent European ASIC manufacturer.

Dr. Humbert Noll, Director of the Research and Development Department at AMS: "Through the participation in the SHAPE Project AMS is able to largely determine the development of the strategically important semiconductor technology for the turn of the century together with the most important European semiconductor manufacturers. Furthermore, AMS will be able to further expand and strengthen its leading position in the field of mixed analogue/digital integrated circuits regarding development methodology and process technology."

This project was founded by ESPRIT (**E**uropean **S**trategic **P**roject on the **R**esearch of **I**nformation **T**echnologies) in order to be able to participate in the foremost front of the worldwide semiconductor technology development.

Schloß Premstätten
A-8181 Unterpremstätten, Austria
Fax: +43 3136 52 501, 53 650
Tel.: 43 3136 500
Email: info @ ams.co.at
www: http://www.ams.co.at

News from European Semiconductor, 1995 and 1996

Top ten semiconductor equipment suppliers

A VLSI Research analysis reveals that the semiconductor equipment industry grew 65% in 1995, compared to 43.1% in 1994 and 23.4% in 1993. The top ten semiconductor equipment suppliers brought in collective sales revenues of $14.2 billion, an increase of 74.4% over 1994 figures. These ten companies have a combined market share of 43%, as opposed to 37% in 1994.

Semiconductors Equipment Manufacturers Top Ten

1995 Rank	1995 Sales ($M)	Company	Growth Rate	Rank 1994
1	3,500	Applied Materials	92%	1
2	2,872	Tokyio Electron	79%	2
3	1,820	Nikon	44%	3
4	1,215	Canon	62%	4
5	1,030	Lam Research	69%	5
6	1,027	Advantest	95%	6
7	791	Hitachi	62%	8
8	675	Teradyne	76%	9
9	617	Dainippon Screen	78%	10
10	606	Varian	50%	7

In terms of ranking, nothing has changed from position one through six in 1995.

Advantest, in sixth place, recorded the highest growth rate in 1995 at 95%, although its number six position

could still change according to VLSI Research, as the company's data were somewhat unclear.

Teradyne moved up to number eight. The figure of $675 million includes one month of Megatest sales, following Teradyne's merger with the company in December 1995. If Megatest's pre-merger revenues are included, Teradyne's sales total about $816 million for the year.

Varian's lost three places in the ranking, dropping to tenth position. However, VLSI Research excluded sales of Tokyo Electron joint venture equipment, accounting for $54.1 million in the US.

Second phase of the electronics revolution

Analyst Malcolm Penn sees a great future for European electronics, although a common European policy towards the industry is needed.

All industries today either depend on or use microelectronics in one way or another. New technologies, new rivals and fewer rules are creating opportunities and markets scarcely dreamed of a few years ago. Automobiles are rapidly becoming computers on wheels with integrated circuits now used in engine control, transmission, braking and air bags. It was not so long ago that telecommunications just meant phones. Today, cellular know-how and an aggressive, service based, market philosophy has made Europe a world leader in mobile communications. Booming personal computer sales are driving the high demand for microprocessors and memory with a substantial amount of these chips now produced in Europe from world beating plants. Finally, multi-media will spark robust growth in highly integrated boxes and, further out, the coming Information Super Highway promises huge new markets.

To survive in this environment, some of the production work that went offshore in the 1980s has returned to Europe in the 1990s as companies strive to become more agile in responding to market needs. Digital electronics is making all this possible; sub-micron VLSI is making it affordable. As the world moves into the second phase of electronics industrialization, two questions remain unanswered. Will Europe's world leadership in the automotive, consumer and communications industries prove to be a strategic advantage, and what are the correct strategies for future growth in Europe?

European Electronics

As with other world regions, the global semiconductor industry recovery that started in 1993 is accelerating at an unprecedented rate in Europe with the 1995 semiconductor market now set to reach close to $25 billion. Projections towards the year 2000 place Europe's market at $60 billion.

Though the overall market buoyancy obviously helps, the turnaround in Europe's fortunes cannot be rationalized away by market conditions alone. This significant turnaround in Europe's electronics industry is the direct result of a fundamental restructuring that started in the mid-1980s - an effort that was the combined result of company, government and European initiatives.

This effort has radically and sustainably changed the industry fundamentals and transformed several of Europe's electronics firms into world class players with leadership established in many key areas of the industry, in particular in communications, automotive electronics, consumer electronics and microelectronics. For the first time in the history of the semiconductor industry, Europe's semiconductor firms are rich in leading-edge, world-class products with the benefit of a strong local market demand from which to grow their global revenue base.

The change in Europe's fortunes has not been overlooked by the world's leading semiconductor manufacturers and, as a result, substantial investments have been made, or are in the process of being made, by Fujitsu, GEC-Plessey, Hitachi, IBM, Intel, Mietec Alcatel, Mitsubishi, Motorola, NEC, Philips, SGS-Thomson, Siemens, Temic and Texas Instruments.

AMD, Toshiba and Korea, led by Samsung, are also shortly expected to make significant investments in Europe.

Future outlook

The trends are inescapable. The circuit density of integrated circuits, and hence their computing power, is doubling every 18 months. Already the next generation $300 video game machines due out this year will put into schoolchildren's hands the graphics power of a 1980s vintage Cray supercomputer. At the same time, the unit cost of this computing power will continue to decline dramatically, distributing low cost, digital know-how to every corner of the globe, transforming corporations, redistributing wealth and remodeling institutions. In the digital age, product cycles are measured in months, not years.

Several governments have recognized the need to nurture and encourage this industry. They have also recognized that it requires supporting fiscal practices to encourage growth and investment. Such support, however, is fraught with difficulties in Europe. For example, national funding difficulties result in a general criticism of the various public authorities, with each country operating under different rules and regulations, diverse procedures, and national preferences, none of which can easily be standardized.

This problem is exacerbated by the lack of a common European policy towards the semiconductor industry, despite the fact that government policies have shaped the course of international competition in microelectronics since the inception of the industry, and the fact that the electronics industry will be the world's largest single industry by the turn of the century. Unfortunately, silicon chips do not yet grab the hearts and minds of most politicians; given the choice to vote for silicon chips vs. potato chips, the humble potato wins more often than not.

My personal view is that Europe's industrialists should tell their respective authorities what is needed by way of a common European policy on the semiconductor industry, perhaps utilizing the European Commission's resources and JESSI's proven diplomatic skills and

remarkable success in overcoming the varying degrees of nationalism and cultural differences among its members at the project level. Once consensus is reached, it ought to be relatively simple to establish a standardized form of funding.

Added to this issue is the fact that Europe has been notoriously poor at "blowing its own technological trumpet." For example, although the Eureka and other EU programs have been underway for a decade, very little has been published about their effects on the products, companies and markets. Europe needs a strong PR effort, both to ensure greater visibility of its successes and to promote a common European semiconductor policy. With this in mind, a leaf could be taken out of Intel's book, with a European "Jessi inside" logo on qualifying JESSI-enhanced products.

Smart worldwide

Europe is leading the way in smart cards. The rest of the world, however, is bracing itself to catch up.

Historically, France has been the forerunner in smart card applications due to its nationwide use of telephone cards. Until 1996, telecommunications will be the biggest market for smart cards, though not only in France, but increasingly in Germany, the United Kingdom and Switzerland. Germany, in fact, is catching up fast and has already reached a similar world status to France. This is largely due to the introduction of a health insurance card at the end of 1993. About 75% of the population is in possession of a card which stores the complete health record of every citizen. Health and security smart cards are currently growing at about 60% per year.

Europe as a whole is the largest regional market for smart card ICs, with 69% of global market share. It will probably remain in this position until the turn of the century, according to figures released by Siemens. French company Gemplus produces over 300 million smart cards per year - the largest quantity worldwide. In terms of turnover, Siemens is the biggest producer, with a market share of 33%, followed by Motorola and SGS-Thomson Microelectronics.

The world market for smart card ICs has increased from $14 million in 1987 to $315 million in 1995 (estimated), an annual increase of approximately 50%. Peter Bauer, Manager of Siemens' chipcard department now expects an annual market growth of 37%, reaching a figure of $1.12 billion in the year 2000.

The highest growth rates, however, come from the Asian/Pacific market with approximately 100% growth per annum, closely followed by the United States, which currently only plays a marginal role in the market. At the end of the century, these two regions together will account for nearly 50% of the worldwide market.

The Freedonia Group in Cleveland, Ohio, forecasts that the US market for complete smart card products, as opposed to ICs only, will increase eightfold to $1.8 billion by the year 2000.

The existing US credit and debit card system, for example, will be largely converted from magnetic stripe to smart card technology. Half the electronic transaction processing volume in the retailing and banking sector is forecast to be smart card-generated by the year 2005.

The Freedonia research analysts admit that so far the use of smart cards has been much more widespread in Europe, Japan, Canada and even numerous developing countries than in the United States. The cost to overhaul the magnetic stripe-based infrastructure in the country creates a problem. A bigger difficulty, however, is the decentralized and fragmented nature of potential smart card user sectors. To overcome the problem, multiple parties with different operating methods and information protocols have to collaborate.

Prices for smart cards with memory chips - about 80% of the market - for example in Germany, have plummeted from several Deutschmarks to less than one Deutschmark per card, due to advanced technologies and mass production.

One of the major problems in the manufacturing process is the packaging, particularly encapsulation, due to size restrictions. A typical smart card is approximately 800 microns thick, with the die and wire bonded chip on the leadframe accounting for about 560 microns. Once a cavity for the chip has been made, the back of the card is at the most 160 microns thick. When the module is encapsulated, thickness and viscosity of the epoxy should ideally be controlled in such a way that no subsequent milling or grinding is necessary

The industry is facing more cost and packaging problems again, as it starts to embed large microcontrollers into smart cards.

Encapsulation views

- A common process for the encapsulation of small memory chips is glob top technology, which is used by German company Mühlbauer. The modules are covered by epoxy which is dispersed out of eight units above the module. Temperature and viscosity of the epoxy are computer controlled to ensure that the encapsulant flows completely around the wire bonds, eliminating trapped air bubbles, and at the same time avoiding the need for any subsequent grinding. According to Dr. Savoy, Sales Manager in the chipcard department at Mühlbauer, the size of the chip is immaterial as far as the glob top technology is concerned. But large chips have a much bigger breakage risk, due to the small dimensions of the card, therefore the overall package is more fragile.
- Swiss company Sempac a subsidiary of Esec, is one of the first companies to use a different method of encapsulation for smart cards - multiplunger molding. The multiplunger mold is filled with epoxy, and acts as a press. The chip, wire bonded onto the metal leadframe, is put into the tool and left there for about 50 seconds until the epoxy dries and hardens. The mold configuration allows different chip sizes to be used without changing the tool. Willi Truckenbrod, Vice President of Marketing and Sales at Sempac, says "Multiplunger technology is mainly used to handle larger chips, i.e. up to 6 x 4 mm". Although most smart cards currently contain memory chips, Truck-

enbrod says, this will change soon because microcontrollers are more flexible and secure. He believes that multiplunger mold is the future technology for smart card production because microcontrollers are larger and generate more heat which cannot be absorbed by glob top materials.

News from Information CMP

CMP MICROMACHINES PROGRAM

INTRODUCTION

One of the main obstacles to start with microsystems is the fact that particular, and hence costly processes are needed. In order to get affordable prices and a high flexibility, thus be able to move microsystems from research prototypes to industrial development, low cost foundries facilities should be provided together with Computer-Aided-Design (CAD) tools. Microsystems should whenever possible be designed in such a way that they can be realized on existing production lines for micro-electronics, with an additional post-processing for micro-system specific 2D and 3D structures, e.g. through Multi-Project-Wafer services as proposed by CMP. Furthermore, this approach allows to integrate microelectronics, needed in most microsystems, on the same chip. This is the monolithic solution which should be considered as the normal evolution of ASIC-foundries to microsystem-foundries (foundries strategy). However, the service will address in the same way the hybrid solution to cover more applications and thus will introduce gradually new technologies such as LIGA UV and other particular silicon processes.

LOW-COST FOUNDRIES FOR MICROSYSTEMS

For more than one year, CMP has made experiments in view to extend its services to the domain of microsystems with the aim to offer an industrially oriented low cost prototyping and manufacturing service. CMP has used processes that have been developed for microelectronics and targeted them to microsystems. So works began on silicon compatible micromachining and similar works have started on gallium arsenide wafers.

Today, CMP provides services in fabrication of microsystems. The service will support micromachining technology to realize microsystems using the same principles applied to integrated circuits: to group projects together on a single wafer in order to fabricate them at a low cost. The present portfolio is as follows:

- 1.0 µ DLM/SLP (from ATMEL ES2) CMOS compatible front-side bulk micromachining. The post-processing operations (EDP or TMAH etching) are performed through the CMP service at dedicated laboratories (ESIEE or LAAS). Micro Electro Mechanical Systems (MEMS) such as cantilevers, membranes, microbridges, etc. ... may be processed together with the electronics. Figure 1 shows structures that have been manufactured through the CMP service. Such structures are used to perform piezoresistive sensors, thermopiles, gas sensors, gas flow sensors, thermal based sensors, thermal pixels, resonant sensors, electro-thermal actuators, and others.

  Other CMOS processes, such as CMOS 1.2 µ DLM/DLP (from AMS) compatible bulk micromachining is under final evaluation and will be introduced early 1996.
- Gallium arsenide test structures are under evaluation and have been performed using PML high electron mobility transistor (HEMT) and the Vitesse MESFET foundry processes followed by selective etching.
- Other techniques. such as silicon surface micromachining, LIGA (X and UV) and Quartz techniques will be introduced gradually.

Fig.1: SEM photograph of the main structures fabricated monolithically with ICs using front-side CMOS bulk micromachining

layer: 20
name: ACTIVE AREA

Rule Number	Parameter	min. dimension
M201	width of active area	3
M202	spacing between 2 active areas	5
M203	spacing to microstructure area	5
M204	margin to microstructure area	1
M205	active area must be covered with open contact	
M206	active area must be covered with open via	
M207	active area must enclose passivation opening	

The design rules for 1.0 µ CMOS compatible front-side bulk micromachining have been defined by the CMP and implemented into CAD environment. They are delivered to designers upon signature of a Confidentiality and Licence Agreement (CLA). Figure 2 shows a design rules example corresponding to the active area layer.

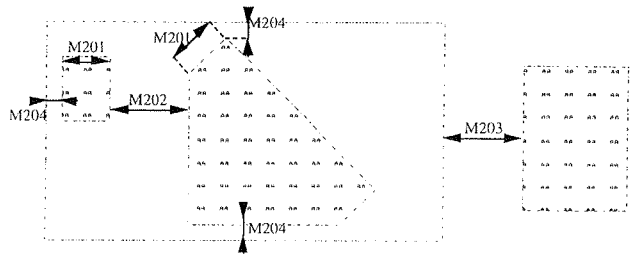

Fig. 2: Design rules example

The addressed technology could be illustrated by the figure 3 which shows a suspended microbridge with an inverter. The designer is restricted to use thin polysilicon layer, but can use thick glass and metal layers as free standing structural elements.

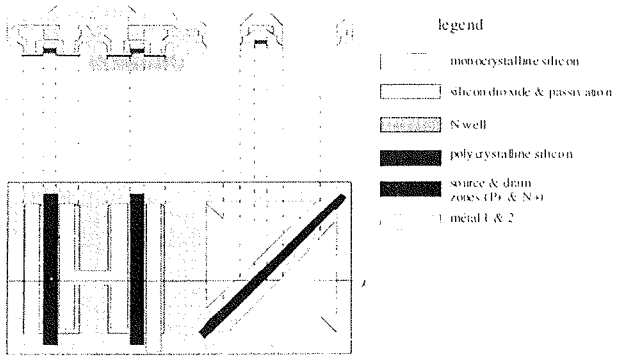

Fig. 3: Cross-sectional view of the microbridge with an inverter obtained by CMOS compatible front-side bulk micromachining

CAD TOOLS FOR *MICROSYSTEM DESIGN*

In addition, Computer-Aided-Design (CAD) software is needed to design microsystems without excessive complexity and design time. Currently available CAD tools, such as Cadence DFW2 or Mentor Falcon Framework, need modifications before they can be used for the automated design of micromachined devices.

Works at the CMP have extended the capabilities of Cadence OPUS to microsystem technology. The user is able to generate layout of a microsystem including electronic and non-electronic parts in a commonly used format (GDS2, CIF), run an extended DRC which submits the layout to design rules checks in process aspects and electrical aspects and, finally, extract parameters from the layout level to the netlist level. The extended extractor will recognize electronic components as well as microstructures, such as bridges, cantilevers and membranes. A netlist is generated and the simulation can be executed by the means of parametrized behavioural models of these microstructures. Finally, a parametrized cells library is also built.

The version 2.0 of CADENCE OPUS design kit has been distributed to more than 50 institutions.

The development of a Microsystem design kit for MENTOR GRAPHICS is in progress, and will be available end of Q2 96.

Figure 4 gives an example of a design rules checking and figure 5 illustrates the instantiation of a microbridge parametrized cell.

Fig. 4: Design rules checking

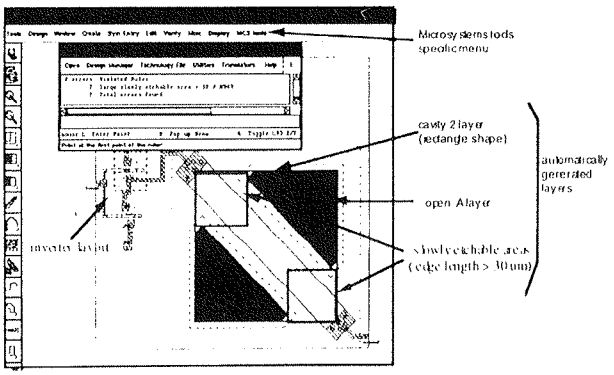

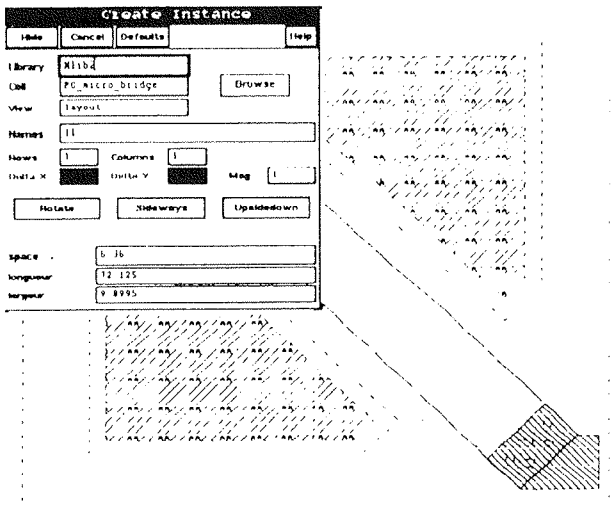

Fig. 5: Instanciation of a microbridge parametrized cell

VSE ČLANE DRUŠTVA MIDEM VLJUDNO PROSIMO, DA PORAVNAJO ČLANARINO ZA LETI 1995 IN 1996.

ALL MIDEM MEMBERS ARE KINDLY ASKED TO PAY MEMBERSHIP FEE FOR 1995 AND 1996.

HVALA LEPA!
THANK YOU VERY MUCH!

KOLEDAR PRIREDITEV 1996

APRIL

22.04.-25.04.1996
15th GENERAL CONFERENCE OF THE CONDENSED MATTER DIVISION
Baveno-Stresa, Lago Maggiore, Italy
Info.: + 39 382 302 859

22.04.-27.04.1996
THE HANOVER INDUSTRY FAIR
Hanover, Germany
Info.: + 44 1727 833 291

22.04.-28.04.1996
IEEE INTERNATIONAL CONFERENCE ON ROBOTICS & AUTOMATION
Minneapolis, Minesota
Info.: + 703 306 1318

28.04.-01.05.1996
VLSI TEST SYMPOSIUM
Princeton, New Jersey, USA
Info.: +1 814 941 4669

29.04.-03.05.1996
1996 IEEE INTERNATIONAL RELIABILITY PHYSICS SYMPOSIUM
Dallas, Texas, USA
Info.: + 315 339 3971

29.04.-03.05.1996
6th INTERNATIONAL CONFERENCE ON AC AND DC POWER TRANSMISSION
London, England
info.: +44 171 344 5472

30.04.-02.05.1996
ELECTRO 96 CONFERENCE AND EXIBITION
SOMERSET, NJ, USA
Info.: + 800 322 9332

MAY

05.05.-08.05.1996
CICC 96 - CUSTOM INTEGRATED CIRCUITS CONFERENCE
San Diego, CA, USA
Info.: + 1 301 527 0902

06.05.-09.05.1996
ICASSP 96 - INTTERNATIONAL CONFERENCE ON ACOUSTICS, SPEECH & SIGNAL PROCESSING
Atlanta, GA, USA
Info.: + 1 404 894 2958

12.05.-15.05.1996
4th ANNUAL EAST/WEST ELECTRONIC INDUSTRY EXECUTIVE FORUM
Moscow, Russia
Info.: + 44 1732 762 896

13.05.-15.05.1996
5th INTERNATIONAL CONFERENCE ON SATELLITE SYSTEMS FOR MOBILE COMMUNICATIONS & NAVIGATIONS
London, England
+ 44 171 344 5472

14.05.-16.05.1996
11th EUROPEAN MICROELECTRONICS CONFERENCE
Venice, Italy
Info.: + 39 382 27697

20.05.-24.05.1996
19th ANNUAL INTERNATIONAL CONFERENCE MIPRO '96
Opatija, Croatia
Info.: +385 1 6129 936

21.05.-23.05.1996
PCIM CONFERENCE & EXIBITION
Nurnberg, Germany
Info.: +49 911 981 7444

22.05.-23.05.1996
COMMUNICATIONS ENGINEERING 96 EXIBITION
Birmingham, England

25.05.-28.05.1996
ICS 96 - INTERNATIONAL CONFERENCE ON SUPERCOMPUTING
Philadelphia, PA, USA
Info.: +1 214 995 7957

JUNE

12.06.-14.06.1996
8th EUROMICRO WORKSHOP ON REAL TIME SYSTEMS
Oulu, Finland
Info.: +358 81 5 51 2111

17.06.- 19.06.1996
BASYS '96 - ARCHITECTURES & DESIGN METHODS FOR BALANCED AUTOMATION SYSTEMS
Info.: + 44 171 344 5472

19.06-21.06.1996
7th INTERNATIONAL WORKSHOP ON RAPID SYSTEMS PROTOTYPING
Thessaloniki, GREECE
Info.: + 1 919 541 7341

24.06.-26.06.1996
3 DAY COURSE ON ENCAPSULATION OF ELECTRONIC DEVICES & COMPONENTS
Amsterdam, Netherlands
Info.: + 31 20 638 2806

26.06.-28.06.1996
2nd EUROPEAN WORKSHOP ON LOW TEMPERATURE ELECTRONICS
Leuven, Belgium
Info.: Prof. C. Claeys, IMEC,
Kapeldreef 75, B-3001, Leuven, Belgium

DRUŠTVO MIDEM IN KONFERENCA MIEL-SD NA INTERNETU

Dragi člani društva in bralci revije!

Ob pomoči Dejana Križaja s Fakultete za elektrotehniko, Ljubljana, laboratorij za elektronske elemente, smo koncem meseca aprila 1996 postavili dve MIDEM strani na INTERNETU in sicer:

1. Predstavitev društva MIDEM in revije "Informacije MIDEM" na naslovu
   http://pollux.fer.uni-lj-si/MIEL/MIDEM.htm

2. Predstavitev konference MIEL-SD'96 na naslovu
   http://pollux.fer.uni-lj-si/MIEL/miel96.htm

3. Elektronsko pošto lahko pošiljate na naslov:
   Iztok.Sorli@guest.arnes.si

Pri vpisu pazite na velike in male črke!!

MIDEM SOCIETY AND MIEL-SD CONFERENCE IN INTERNET

Dear readers and Society members!
With the help of Mr. Dejan Križaj, Faculty for Electrical Engineering, Ljubljana, Laboratory for Electron Devices, MIDEM Society has, since end of April 1996, two pages on INTERNET:

1. Presentation of MIDEM Society and Journal "Informacije MIDEM", address
   http://pollux.fer.uni-lj-si/MIEL/MIDEM.htm

2. Presentation of the Conference MIEL-SD'96, address
   http://pollux.fer.uni-lj-si/MIEL/miel96.htm

3. Email can be sent to:
   Iztok.Sorli@guest.arnes.si

When inputting the address, please type in exact above address - lower and upper case letters make the difference.

DRUŠTVO ZA VAKUUMSKO TEHNIKO SLOVENIJE
SLOVENIAN SOCIETY FOR VACUUM TECHNIQUE

INŠTITUT ZA ELEKTRONIKO IN VAKUUMSKO TEHNIKO, Ljubljana, Teslova 30
INŠTITUT ZA TEHNOLOGIJO POVRŠIN IN OPTOELEKTRONIKO, Ljubljana, Teslova30

IZOBRAŽEVALNI TEČAJI v letu 1996

Vse uporabnike vakuumske tehnike obveščamo, da so v letu 1996 predvideni naslednji strokovno izobraževalni tečaji:

VZDRŽEVANJE VAKUUMSKIH NAPRAV - 16. in 17. april ter 15. in 16. oktober 1996

Pod tem naslovom se obravnava predvsem tematika, ki jo srečujemo v tehniki grobega vakuuma. To je: delovanje, vzdrževanje in popravila rotacijskih črpalk, pregled in uporaba različnih črpalk, ventilov in drugih elementov, meritve vakuuma, hermetičnost in odkrivanje netesnosti v vakuumskih sistemih, materiali za popravila, tehnike čiščenja in spajanja; skupno 20 šolskih ur, od tega tretjina praktičnih prikazov in vaj.

Cena tečaja je **30.000 SIT**. Vsak tečajnik bo prejel tudi brošuro "Vzdrževanje vakuumskih naprav" in potrdilo o opravljenem tečaju.

OSNOVE VAKUUMSKE TEHNIKE - 4., 5. in 6. junij ter 26., 27.in 28. november 1996

Pri tem tečaju je večji poudarek na teoretičnem razumevanju snovi. Obravnavana so vsa, že prej omenjena področja in poleg tega še: pomen in razvoj vakuumske tehnike, fizikalne osnove, črpalke za visoki vakuum, tankoplastne in druge vakuumske tehnologije, čisti postopki, analize površin ter doziranje, čiščenje in preiskave plinov - skupno 26 ur z vajami in ogledom Inštituta za elektroniko in vakuumsko tehniko, Inštituta za tehnologijo površin in optoelektroniko in Inštituta "Jožef Stefan".

Cena tečaja je **28.000 SIT**. Udeleženci prejmejo zbornik predavanj "Osnove vakuumske tehnike" in potrdilo o opravljenem tečaju.

Oba tečaja se pričneta ob 8.00 uri v knjižnici Inštituta za elektroniko in vakuumsko tehniko, Teslova 30, Ljubljana. Prosimo interesente, da se informativno javijo čimprej, za dokončno potrdilo udeležbe pa velja kopija položnice o plačilu - najkasneje tri dni pred pričetkom tečaja na naslov:

Društvo za vakuumsko tehniko Slovenije,
Teslova 30
1001 Ljubljana

(štev. žiro računa: 50101-678-52240).

Prijave sprejema organizacijski odbor (Koller, Spruk, Mozetič, Nemanič), ki daje tudi vse dodatne informacije (tel. 061-126 45 84 ali 126 45 92).